Draft version April 27, 2008
Preprint typeset using LaTeX style emulateapj v. 08/13/06

IMPROVED COSMOLOGICAL CONSTRAINTS FROM NEW, OLD AND COMBINED SUPERNOVA DATASETS

M. Kowalski[1], D. Rubin[2,3], G. Aldering[2], R. J. Agostinho[4], A. Amadon[5], R. Amanullah[6], C. Balland[7], K. Barbary[2,3], G. Blanc[8], P. J. Challis[9], A. Conley[10], N. V. Connolly[11], R. Covarrubias[12], K. S. Dawson[2], S. E. Deustua[13], R. Ellis[14], S. Fabbro[15], V. Fadeyev[16], X. Fan[17], B. Farris[18], G. Folatelli[12], B. L. Frye[19], G. Garavini[20], E. L. Gates[21], L. Germany[22], G. Goldhaber[2,3], B. Goldman[23], A. Goobar[20], D. E. Groom[2], J. Haissinski[24], D. Hardin[7], I. Hook[25], S. Kent[26], A. G. Kim[2], R. A. Knop[27], C. Lidman[28], E. V. Linder[6], J. Mendez[29,30], J. Meyers[2,3], G. J. Miller[31], M. Moniez[24], A. M. Mourão[15], H. Newberg[32], S. Nobili[20], P. E. Nugent[2], R. Pain[7], O. Perdereau[24], S. Perlmutter[2,3], M. M. Phillips[33], V. Prasad[2], R. Quimby[14], N. Regnault[7], J. Rich[5], E. P. Rubenstein[34], P. Ruiz-Lapuente[30], F. D. Santos[35], B. E. Schaefer[36], R. A. Schommer[37], R. C. Smith[38], A. M. Soderberg[14], A. L. Spadafora[2], L.-G. Strolger[39], M. Strovink[2,3], N. B. Suntzeff[40], N. Suzuki[2], R. C. Thomas[2], N. A. Walton[41], L. Wang[40], W. M. Wood-Vasey[9], J. L. Yun[4]
(The Supernova Cosmology Project)

Draft version April 27, 2008

ABSTRACT

We present a new compilation of Type Ia supernovae (SNe Ia), a new dataset of low-redshift nearby-Hubble-flow SNe and new analysis procedures to work with these heterogeneous compilations. This "Union" compilation of 414 SN Ia, which reduces to 307 SNe after selection cuts, includes the recent large samples of SNe Ia from the Supernova Legacy Survey and ESSENCE Survey, the older datasets, as well as the recently extended dataset of distant supernovae observed with HST. A single, consistent and blind analysis procedure is used for all the various SN Ia subsamples, and a new procedure is implemented that consistently weights the heterogeneous data sets and rejects outliers. We present the latest results from this Union compilation and discuss the cosmological constraints from this new compilation and its combination with other cosmological measurements (CMB and BAO). The constraint we obtain from supernovae on the dark energy density is $\Omega_\Lambda = 0.713^{+0.027}_{-0.029}(\mathrm{stat})^{+0.036}_{-0.039}(\mathrm{sys})$, for a flat, ΛCDM Universe. Assuming a constant equation of state parameter, w, the combined constraints from SNe, BAO and CMB give $w = -0.969^{+0.059}_{-0.063}(\mathrm{stat})^{+0.063}_{-0.066}(\mathrm{sys})$. While our results are consistent with a cosmological constant, we obtain only relatively weak constraints on a w that varies with redshift. In particular, the current SN data do not yet significantly constrain w at $z > 1$. With the addition of our new nearby Hubble-flow SNe Ia, these resulting cosmological constraints are currently the tightest available.

Subject headings: Supernovae: general — cosmology: observations—cosmological parameters

[1] Institut für Physik, Humboldt-Universität zu Berlin, Newtonstrasse 15, Berlin 12489, Germany
[2] E. O. Lawrence Berkeley National Laboratory, 1 Cyclotron Rd., Berkeley, CA 94720, USA
[3] Department of Physics, University of California Berkeley, Berkeley, 94720-7300 CA, USA
[4] Centro de Astronomia e Astrofísica da Universidade de Lisboa, Observatório Astronómico de Lisboa, Tapada da Ajuda, 1349-018 Lisbon, Portugal
[5] DSM/DAPNIA, CEA/Saclay, 91191 Gif-sur-Yvette Cedex, France
[6] Space Sciences Laboratory, University of California Berkeley, Berkeley, CA 94720, USA
[7] LPNHE, CNRS-IN2P3, University of Paris VI & VII, Paris, France
[8] APC, Université Paris 7, 10 rue Alice Domon et Léonie Duquet, 75205 Paris Cedex 13, France
[9] Center for Astrophysics, Harvard University, 60 Garden Street, Cambridge, MA 02138, USA
[10] Department of Astronomy and Astrophysics, University of Toronto, 60 St. George St., Toronto, Ontario M5S 3H8, Canada
[11] Department of Physics, Hamilton College, Clinton, NY 13323, USA
[12] Observatories of the Carnegie Institution of Washington, 813 Santa Barbara St., Pasadena, CA 9110, USA
[13] American Astronomical Society, 2000 Florida Ave, NW, Suite 400, Washington, DC, 20009 USA
[14] California Institute of Technology, E. California Blvd, Pasadena, CA 91125, USA
[15] CENTRA e Dep. de Fisica, IST, Avenida Rovisco Pais, 1049 Lisbon, Portugal
[16] Department of Physics, University of California Santa Cruz, Santa Cruz, CA 95064, USA
[17] Steward Observatory, the University of Arizona, Tucson , AZ 85721, USA
[18] Department of Physics, University of Illinois at Urbana-Champaign, 1110 West Green, Urbana, IL 61801-3080, USA
[19] Department of Physical Sciences, Dublin City University, Glasnevin, Dublin 9, Ireland
[20] Department of Physics, Stockholm University, Albanova University Center, S-106 91 Stockholm, Sweden
[21] Lick Observatory, P.O. Box 85, Mount Hamilton, CA 95140, USA
[22] Centre for Astrophysics and Supercomputing, Swinburne University of Technology, John St., Hawthorn, VIC, 3122, Australia
[23] M.P.I.A., Königstuhl 17, 69117 Heidelberg, Germany
[24] Laboratoire de l'Accélerateur Linéaire, IN2P3-CNRS, Université Paris Sud, B.P. 34, 91898 Orsay Cedex, France
[25] Sub-Department of Astrophysics, University of Oxford, Denys Wilkinson Building, Keble Road, Oxford OX1 3RH, UK
[26] Fermi National Accelerator Laboratory, P.O. Box 500, Batavia, IL 60510, USA
[27] Department of Physics and Astronomy, Vanderbilt University, Nashville, TN 37240, USA
[28] European Southern Observatory, Alonso de Cordova 3107, Vitacura, Casilla 19001, Santiago 19, Chile
[29] Isaac Newton Group, Apartado de Correos 321, 38780 Santa Cruz de La Palma, Islas Canarias, Spain
[30] Department of Astronomy, University of Barcelona,

1. INTRODUCTION

The evidence for dark energy has evolved from the first hints, for the case of a flat Universe (Perlmutter et al. 1998; Garnavich et al. 1998; Schmidt et al. 1998), through the more definite evidence for the general case of unconstrained curvature (Riess et al. 1998; Perlmutter et al. 1999), to the current work which aims to explore the properties of dark energy (for a review see Perlmutter & Schmidt 2003). Several new cosmological measurement techniques and several new Type Ia supernova (SN Ia) datasets have helped begin the laborious process of narrowing in on the parameters that describe the cosmological model. The SN Ia measurements remain a key ingredient in all current determinations of cosmological parameters (see, e.g., the recent CMB results (Dunkley et al. 2008)). It is therefore necessary to understand how the current world dataset of SN Ia measurements is constructed, and how it can be used coherently, particularly since no one SN Ia sample by itself provides an accurate cosmological measurement.

Until recently, the SN Ia compilations (e.g., Riess et al. 1998, Perlmutter et al. 1999, Tonry et al. 2003, Knop et al. 2003, Astier et al. 2006 and Wood-Vasey et al. 2007) primarily consisted of a relatively uniform high-redshift ($z \sim 0.5$) dataset from a single study put together with a low-redshift ($z \sim 0.05$) sample collected in a different study or studies. However, once there were several independent datasets at high redshift it became more important and interesting to see the cosmological constraints obtainable by combining several groups' work. Riess et al. (2004, 2007) provided a first compilation analysis of this kind, drawing on data chosen from Perlmutter et al. (1999); Riess et al. (1998); Schmidt et al. (1998); Knop et al. (2003); Tonry et al. (2003) and Barris et al. (2004). Many of the subsequent cosmology studies have used this compilation as the representation of the SN Ia sample, in particular the selection of supernovae that Riess et al. (2004, 2007) nicknamed the "Gold" sample. Other recent compilations that have been used are that of Wood-Vasey et al. (2007) and Davis et al. (2007).

At present a number of updates should be made to the SN Ia datasets, and a number of analysis issues should be addressed, including several that will recur with every future generation of SN compilations. These include the following major goals:

(1) It is important to add a new low-redshift SN Ia sample to complement the large and rapidly growing number of distant SNe. Especially valuable are the SNe in the smooth, nearby Hubble-flow (z above $\sim$ 0.02). Since this part of the Hubble diagram is currently not well constrained, new nearby SNe lead to a relatively large incremental improvement (Linder 2006). It is interesting to note, that the largest contribution in this redshift range still comes from the landmark Calan/Tololo survey (Hamuy et al, 1993).

(2) The analysis should reflect the heterogeneous nature of the data set. In particular, it is important that a sample of poorer quality will not degrade the impact of the higher quality data, such as the Supernova Legacy Survey (SNLS) and ESSENCE high-redshift datasets which have recently been published.

(3) The different supernova datasets should be analyzed with the same analysis procedure. The previous compilations combined measurements and peak-magnitude fits that were obtained with disparate lightcurve fitting functions and analysis procedures, particularly for handling the color correction for both extinction and any intrinsic color luminosity relation.

(4) A reproducible, well-characterized approach to selecting the good SNe Ia, and rejecting the questionable and outlier SNe, should be used. Previous compilations relied to a large extent on the heterogeneous classification information provided by the original authors. The selection process was somewhat subjective: The Gold compilation of Riess et al. (2004, 2007) excluded SNe that Knop et al. (2003) considered comparably well-confirmed SNe Ia.

(5) To the extent possible, the analysis should not introduce biases into the fit, including some that have only recently been recognized as being present in methods of determining extinction properties of SNe Ia.

To reach the goal of carrying out these improvements, we present in this paper a new SN compilation, a new nearby-Hubble-flow SN Ia dataset, and new analysis procedures. Several additional smaller enhancements are also presented.

With respect to Goal (1), it is important to note that both nearby and distant supernovae are needed to measure cosmological parameters. The brightness of nearby supernovae in the Hubble flow is compared to that of high redshift supernovae, which — following the dynamics of the Universe — might appear dimmer or brighter than expected for a reference cosmology. Nearby SNe lightcurves typically have better observational coverage and signal-to-noise ratio (SNR) than their high-redshift counterparts. However, they are significantly more difficult to discover since vast amounts of sky have to be searched to obtain a sizable number of supernovae,

Barcelona, Spain
[31] Southwestern College, Department of Astronomy, 900 Otay Lakes Road, Chula Vista, CA 91910
[32] Rensselaer Polytechnic Institute, Physics Dept., SC1C25, Troy NY 12180, USA
[33] Las Campanas Observatory, Carnegie Observatories, Casilla 601, La Serena, Chile
[34] Advanced Fuel Research, Inc., 87 Church Street, East Hartford, CT 06108
[35] Department of Physics, Faculty of Sciences, University of Lisbon, Ed. C8, Campo Grande, 1749-016 Lisbon, Portugal
[36] Louisiana State University, Department of Physics and Astronomy, Baton Rouge, LA, 70803, USA
[37] Deceased
[38] Cerro Tololo Inter-American Observatory, Casilla 603, La Serena, Chile
[39] Department of Physics and Astronomy, Western Kentucky University, Bowling Green, KY, USA
[40] Department of Physics, Texas A&M University, College Station, TX 77843, USA
[41] Institute of Astronomy, Madingley Road, Cambridge CB3 0HA, UK

due to the small volume of the low redshift Universe. We present lightcurves from the Supernova Cosmology Project (SCP) Spring 1999 Nearby Supernova Campaign (Aldering 2000), which consisted primarily of wide-field magnitude limited searches and extensive photometric and spectroscopic follow-up observations using a large number of ground-based telescopes. We provide BVRI lightcurves for 8 nearby supernovae in the Hubble flow.

We then address Goal (2) by combining the new data sample with published data of nearby and distant supernovae to construct the largest Hubble diagram to date (but presumably not for long). In this combination we adjust the weight of SNe belonging to a sample to reflect the dispersion we determine for the sample. With our prescription, SN samples with significant unaccounted-for statistical or systematic uncertainties are effectively deweighted.

All SN lightcurves are fitted consistently in the observer frame system using the spectral-template-based fit method of Guy et al. (2005) (also known as SALT). Where possible, the original band pass functions are used (Goal (3)).

To address Goal (4) we adopt a robust analysis technique based on outlier rejection which we show is resilient against contamination. The analysis strategy was developed to limit the influence of human subjectivity. Spectroscopic classification is arguably the most subjective component of SN cosmology (primarily because of the observational challenges associated with high redshift supernova spectroscopy) and we avoid decisions whether to include a specific SN that are based on spectroscopic features that go beyond that of the authors' classification.

Following Conley et al. (2006), the full analysis chain was developed in a blind fashion, that is, hiding the best fitting cosmological parameters until the analysis was finalized. This helps resist the impulse to stop searching for systematic effects once the "right" answer is obtained. We derive constraints on the cosmological parameters, taking care to test and remove possible sources of bias introduced in the fitting procedure (Goal (5)).

The paper is organized as follows. In Section 2 we methodically present the data reduction and photometric calibration of the lightcurves from the SCP Nearby 1999 Supernova Campaign: the reader more interested in Goals (2-5) and the subsequent cosmological analysis might want to only skim this section. In Section 3 we combine the new supernovae with a large set of nearby and high redshift supernovae from the literature and fit the full set of lightcurves in a consistent manner. We then proceed to determine stringent constraints on the dynamics of the Universe. Section 4 explains the methods employed for cosmological parameter estimation, which includes blinding the analysis and using robust statistics. We evaluate the systematic errors of the measurements in Section 5 and summarize the resulting constraints on $\Omega_{\rm M}$, Ω_Λ, w, and other parameters in Section 6.

2. A NEW SAMPLE OF NEARBY SUPERNOVAE

The SN lightcurve data presented in this paper were obtained as part of the SCP Nearby 1999 Supernova Campaign (Aldering 2000). The search portion of this campaign was designed to discover Type Ia supernovae in the smooth nearby Hubble flow, and was performed in collaboration with a number of wide-field CCD imaging teams: EROS-II (Blanc et al. 2004), NGSS (Strolger 2003), QUEST-I (Rengstorf et al. 2004), NEAT (Pravdo et al. 1999) and Spacewatch (Nugent et al. 1999b). In some cases the wide-field searches were focused entirely on supernova discovery (EROS-II and NGSS), while in other cases the primary data had different scientific goals, such as discovery of near-earth objects (NEAT, Spacewatch), quasars or micro-lenses (QUEST-I). The wide-field cameras operated in either point and track (NGSS, NEAT, EROS-II) or driftscan (QUEST-I, Spacewatch) modes, and in total covered hundreds of square degrees per night. Over a two month period beginning in February 1999, a total of more than 1300 square degrees was monitored for SNe. Since the search was magnitude limited—no specific galaxies where targeted—it resembles typical searches for high redshift supernovae. This is important because common systematics effects, such as Malmquist bias, are then expected to more nearly cancel when comparing low redshift with high redshift supernovae.

A total of 32 spectroscopically-confirmed SNe were discovered by the search component of this campaign. Of these, 22 were of Type Ia and 14 (of these) were discovered near maximum light, making them useful for cosmological studies. In addition, early alerts of potential SNe by LOTOSS (Filippenko et al. 2001) and similar galaxy-targeted searches, and the WOOTS-I (Gal-Yam & Maoz 2000) and MSACS (Germany et al. 2004) cluster-targeted searches, provided a supplement to the primary sample as the wide-area searches ramped up. Extensive spectroscopic screening and follow-up was obtained using guest observer time on the CTIO 4-m, KPNO 4-m, APO 3.5-m, Lick 3-m, NOT, INT, MDM 2.4-m, ESO 3.6m, and WHT 4.2-m telescopes. The results of these observations have been reported elsewhere: Kim et al. (1999b); Aldering et al. (1999); Strolger et al. (1999a); Gal-Yam et al. (1999); Strolger et al. (1999b); Nugent et al. (1999a,c); Kim et al. (1999a); Blanc et al. (2004); Strolger et al. (2002); Garavini et al. (2004, 2005); Folatelli (2004); Garavini et al. (2007). Photometric follow-up observations were obtained with the LICK 1-m, YALO 1-m, CTIO 0.9-m, CTIO 1.5-m, MARLY, Danish 1.5-m, ESO 3.6m, KPNO 2.1m, JKT 1-m, CFHT 3.6-m, KECK-I 10-m, WIYN 3.5-m and MLO 1-m telescopes. These consist of $UBVRI$ photometry with a nominal cadence of 3-7 days. The follow-up observations were performed between February and June 1999 and additional reference images to determine the contribution of host galaxy light contamination were obtained in spring 2000.

From this campaign we present $BVRI$ lightcurves for the eight Type Ia SNe, that fall into the redshift range $0.015 \lesssim z \lesssim 0.15$ and for which we where able to obtain enough photometric follow-up data: SN 1999aa (Armstrong & Schwartz 1999; Qiao et al. 1999), SN 1999ao (Reiss et al. 1999), SN 1999ar (Strolger et al. 1999a), SN 1999aw (Gal-Yam et al. 1999) and SN 1999bi, SN 1999bm, SN 1999bn, SN 1999bp Kim et al. (1999a). Further information on these SNe is summarized in Table 1. Photometric data on SN 1999aw have already been published by Strolger et al. (2002); here we present a self-consistent reanalysis of that photometry.

TABLE 1
Summary of SNe coordinates and redshifts. The heliocentric redshift was determined using narrow host-galaxy features for all but one SN. In case of SN 1999aw: due to the faintness of its host, the redshift was determined from the SN spectra.

Name	R.A. (J2000)	Decl. (J2000)	Redshift	IAUC
SN1999aa	08:27:42.03	+21°29'14"8	0.0142	7180,7109
SN1999ao	06:27:26.37	−35°50'24"2	0.0539	7124
SN1999aw	11:01:36.37	−06°06'31"6	0.038	7130
SN1999ar	09:20:16.00	+00°33'39"6	0.1548	7125
SN1999bi	11:01:15.76	−11°45'15"2	0.1227	7136
SN1999bm	12:45:00.84	−06°27'30"2	0.1428	7136
SN1999bn	11:57:00.40	−11°26'38"4	0.1285	7136
SN1999bp	11:39:46.42	−08°51'34"8	0.0770	7136

2.1. *Data reduction & photometric calibration*

The data were preprocessed using standard algorithms for bias and flat field correction. Additionally, images that showed significant fringing were corrected by subtracting the structured sky residuals obtained from the median of fringing-affected images. Reflecting an original goal of this program — to obtain data for nearby SNe Ia matching that of the high redshift data of Perlmutter et al. (1999) — we have employed aperture photometry to measure the SN lightcurves. For measurement of moderately bright point sources projected onto complex host galaxy backgrounds in fields sparsely covered by foreground stars, aperture photometry has higher systematic accuracy, but slightly lower statistical precision, than PSF fitting. We used an aperture radius equal to the FWHM of a point source, as determined from the field stars in the image. The aperture correction, which is defined as the fraction of total light which is outside the FWHM radius, is determined by approximating an infinite aperture by a 4×FWHM radius aperture. The aperture correction for a given image is then obtained by a weighted average for all the stars in the field.

In all, photometric observations employed a total of 12 different telescopes and 14 different detector/filter systems. This presented the opportunity to obtain a more accurate estimate of systematic errors induced by different instrumental setups — which might otherwise be masked by apparent internal consistency — and thereby come closer to achieving calibration on a system consistent with that of high-redshift SNe as required for accurate measurement of the cosmological parameters. Of course the need to account for the specific characteristics of these many different instruments, and their cross-calibration, made the calibration a particularly challenging component of this analysis, which we have addressed in a unique fashion.

Our photometric calibration procedure is subdivided into three parts:

1) Determination of zero points, color terms and atmospheric extinction for photometric nights on telescopes at high-quality sites, simultaneously employing observations of both Landolt (1992) standard stars and SN field tertiary standard stars.

2) Use of the tertiary standard stars to simultaneously determine color terms for all other instruments, and zero points for all other images.

3) Determination of SN magnitudes. This includes the SN host subtraction and photometric correction necessary for non-standard band passes.

In steps 1 and 2 the robustness of the fits was ensured by heavily de-weighting significant outliers, using an automated iterative prescription.

Elaborating further on step 1, the instrumental magnitudes were converted to magnitudes on the standard $BV(RI)_{KC}$ system using the relation:

$$m_x = \tilde{m}_x + m_{zp} + k_x\chi + c_x(m_x - m_y), \qquad (1)$$

where $\tilde{m}_x$ is the instrumental magnitude measured in band x, m_x and m_y are the apparent magnitudes in bands x and y, χ is the airmass, m_{zp} is the zero point and k_x and c_x are the atmospheric extinction and filter correction terms for band x. A simultaneous fit in two bands of standard stars cataloged by Landolt (1992) and our SN field stars allowed determination of m_{zp}, k_x, χ and c_x, as well as m_x and m_y for our tertiary standard stars. In total 125 Landolt standards, spread across 16 photometric nights, were used for calibration in B, V, R and I, respectively. Accordingly, the uncertainties on the night and telescope dependent terms k_x and c_x are typically very small. Their covariance with the other parameters is properly accounted for. The catalog of tertiary standard stars generated as a by-product of this procedure are reported in Appendix B.

Then, in step 2, the apparent magnitudes from the tertiary standard stars were used to determine color terms for all remaining instruments and zero points for all images. Since $BVRI$ do not require airmass-color cross terms over the range of airmasses covered by our observations, and since absorption by any clouds present would be grey, it was possible to absorb the atmospheric extinction into the zero point of each image. The catalog of tertiary standard stars includes both rather blue and red stars, therefore allowing reliable determination of the color terms. The color terms obtained for all instruments are summarized in Table A1 of Appendix A.

In order to determine the counts from the SN in a given aperture, the counts expected from the underlying host galaxy must be subtracted. In our approach, the image with the SN and the reference images without SN light are first convolved to have matching point-spread functions. Stars in the images are used to approximate the PSF as a Gaussian, which for the purposes of determining the convolution kernel needed to match one PSF to another is usually adequate. The instrumental magnitudes of objects (including galaxies) in the field are then used to determine the ratio of counts between the images. For a given image, the counts due to the SN are obtained by subtracting the counts from the reference image scaled by the ratio of counts averaged over all objects. Note that with this approach the images are never spatially translated, thereby minimizing pixel-pixel correlations due to resampling.

Several contributions to the uncertainty were evaluated, and added in quadrature: photon statistics, uncertainties in the image zero points and uncertainties in the scaling between reference and SN image. Additionally, possible systematic errors introduced during sky subtraction and flat-fielding are evaluated using field stars. The variance of field star residuals is used to rescale all uncertainties. Additionally, an error floor is determined for all

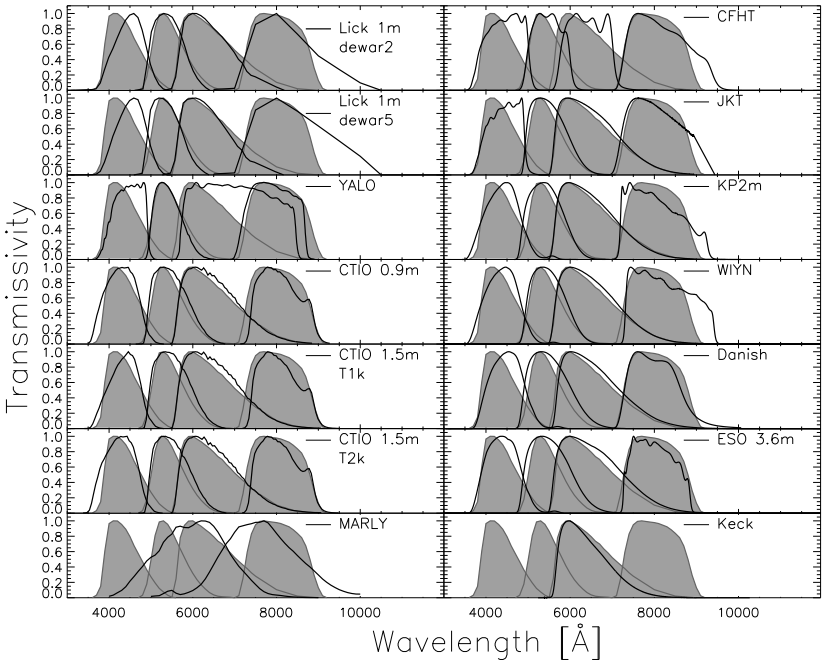

FIG. 1.— Band passes for the various instruments used in the Spring 1999 Nearby Supernova Campaign. For comparison, the filled regions represent the pass band transmission functions of the Bessell (1990) system.

instruments by investigation of the variance of the residuals as a function of the calculated uncertainty. Such an error might occur due to large scale variation in the flat-field. An appropriate error floor was found to be typically 1-2 % of the signal counts.

2.2. *Band pass determination*

The band passes for all telescopes have to be established in order to correct for potential mismatches to the Landolt/Bessell system (Landolt 1992; Bessell 1990).

The band pass is the product of the quantum efficiency of the CCD, the filter transmission curve, the atmospheric transmission and the reflectivity of the telescope mirrors. Figure 2.1 shows the band pass curves for the various instruments used in this work. The relevant data were obtained either from the instrument documentation or through private communication.

We test for consistency of the band passes using synthetic photometry (for a related study see Stritzinger et al. (2002)). For this, stellar spectra which best match the published $UBVRI$ colors of our standard stars are selected from the catalog of Gunn & Stryker (1983). The spectra that best match the published colors of the standard stars are further adjusted using cubic splines to exactly match the published colors. For instruments without standard star observations, a second catalog is generated using our determination of $BVRI$ magnitudes of field stars. With the spectra of standard and field stars at hand we perform synthetic photometry for the various band pass functions. The band pass functions are then shifted in central wavelength by $\Delta\lambda$ until they optimally reproduce the observed instrumental magnitudes. The change in color-term, c_x, when shifting the pass band is $\mathrm{d}c_x/\mathrm{d}\lambda \approx 0.001, 0.0008, 0.0005, 0.0003\,[1/\text{Å}]$ for B, V, R and I, respectively. An alternative procedure is to evaluate the color terms for a given band pass in an analogous way as for the observed magnitudes (see equation 1). We then determine the wavelength shift to apply to the band passes in order to reproduce the instrumental color terms. The two approaches agree on average to within 1 Å with an RMS of about 20 Å. The results are summarized in the Table A2 of Appendix A. The associated systematic uncertainty on the photometric zero point due to this shift depends on the color of the object and for $B - V \leq 1$ will remain below 0.02 mag.

3. LIGHTCURVES

3.1. *Lightcurves from the SCP Nearby 1999 Supernova Campaign*

Figure 2 shows the $BVRI$ lightcurves from the SCP Nearby 1999 campaign (the data are provided in Table C1). Different telescopes are marked by different symbols. Empty symbols represent uncorrected photometric data and filled symbols represent data corrected for non-standard band passes, the so called S-corrections (Suntzeff 2000). The S-corrections represent the magnitude shift needed to bring the data obtained with different band passes to a common standard system (in our case the Bessell system). The S-corrections are obtained from a synthetic photometry calculation using the "instrument dependent" band pass functions described above and a spectrophotometric lightcurve model. The spectrophotometric SN lightcurve model was adjusted using spline-functions to match the colors of the lightcurve models of our SNe. The lightcurve models are shown in Fig. 2 to guide the eye only. They are obtained in two different ways depending on the quality of the available photometric data. For the four SNe with $z < 0.1$, we have used the fit method explained in Wang et al. (2006) which has six parameters per band. This method allows effective fitting of R and I band data, which exhibits a second "bump" of variable strength appearing approximately 30 days after the maximum. However, since this fit method has six free parameters

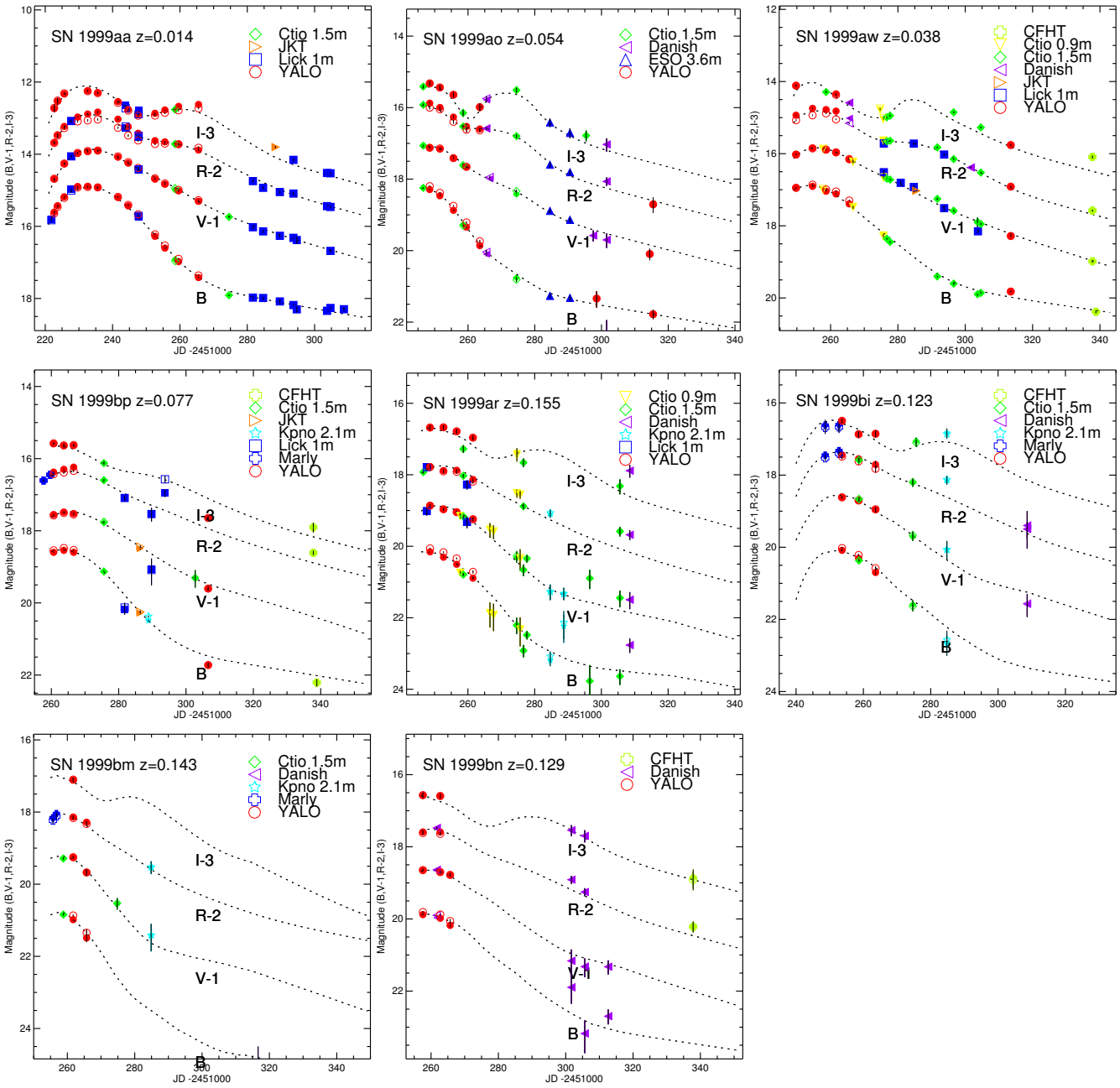

FIG. 2.— SNe lightcurves of the SCP Nearby 1999 campaign. The filled symbols represent the S-corrected data, the empty symbols the raw photometric data. Both the S-corrected data as well as the model parameterization (dashed line) are shown to guide the eye only and are not used any further in the remaining paper.

per fitted band one can use it only for lightcurves with dense temporal sampling with high signal-to-noise. For the more distant SNe 1999ar, 1999bi, 1999bm, 1999bn we use a more constrained lightcurve fitting method based on template matching. A library of template lightcurves obtained from well observed supernovae is K-corrected to the observed redshift. The best matching lightcurve is chosen as a model for the supernova. The lightcurve models along with the S-corrections shown in Figure 2 are meant to guide the eye and will not be used in the remainder of the paper; we continue with the concept of using instrumental magnitudes along with instrument-dependent passbands when fitting the lightcurve parameters.

The lightcurve parameters such as peak magnitude, stretch and color at maximum are obtained using the spectral template method of Guy et al. (2005) which is described in more detail in section 3.3. The method is well suited to this task since it uses telescope-specific band pass functions for modeling the observer-frame lightcurves. The B- (left) and V-band (right) observer-frame lightcurves are shown in Figure 3, along with the lightcurves predicted by the spectral template for the corresponding band pass. In the bottom part of the plots we show the residuals from the model prediction. In most cases the model describes the data reasonably well, with $\chi^2/\mathrm{DOF} \sim 1$. Systematic deviations, such as observed in the late-time behavior of the B-band lightcurve of SN 1999aw, are likely to be attributable to the limitations of the two-parameter spectral template model

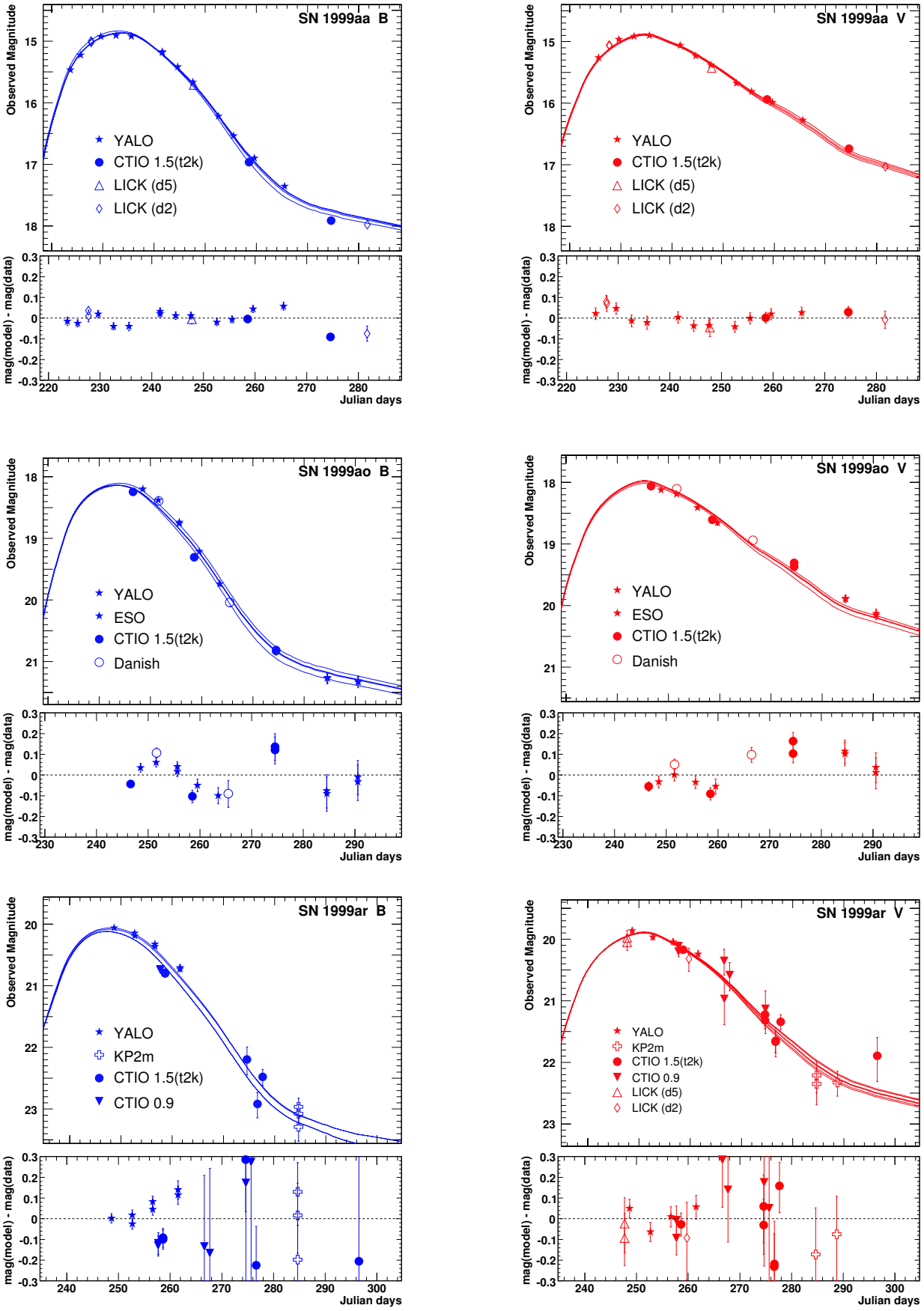

FIG. 3.— B and V lightcurves and residuals. The multiple curves represent the model predictions for the different band passes, and are obtained by integrating the product of passband and the redshifted spectral-template.

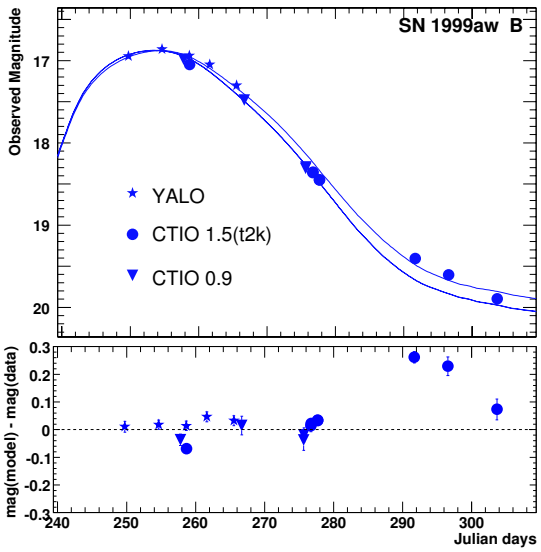

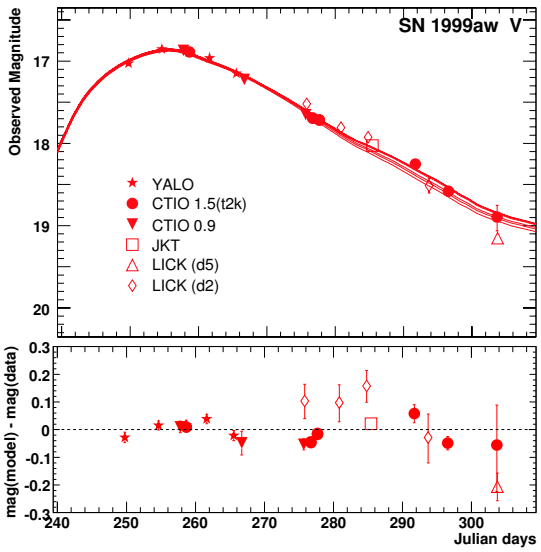

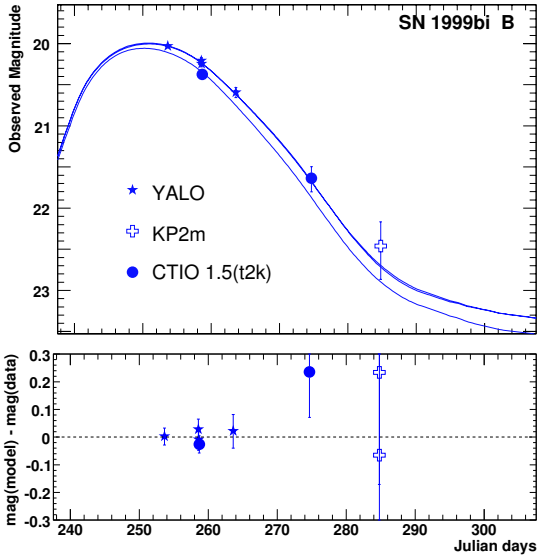

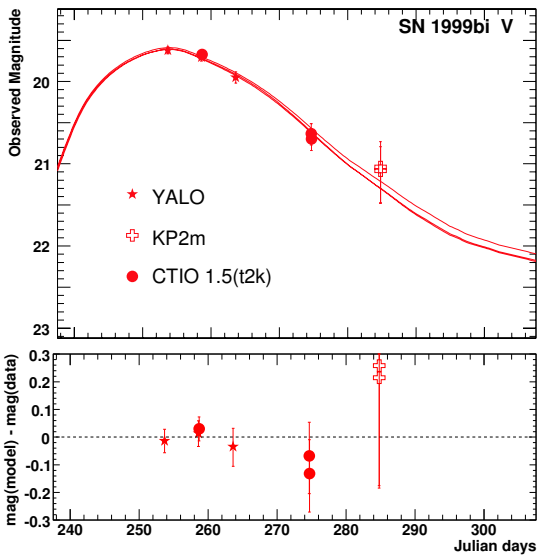

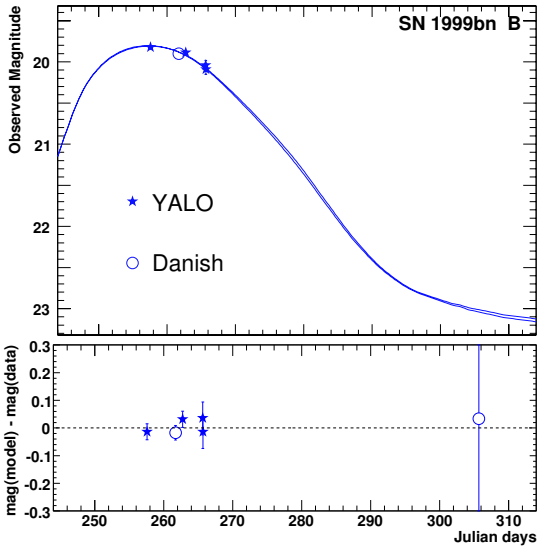

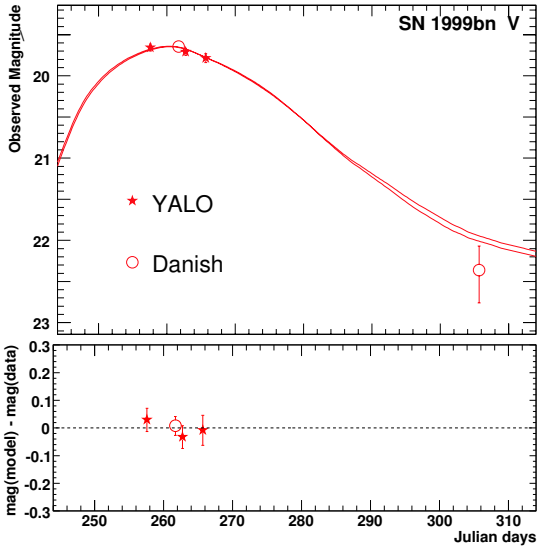

FIG. 3.— continued

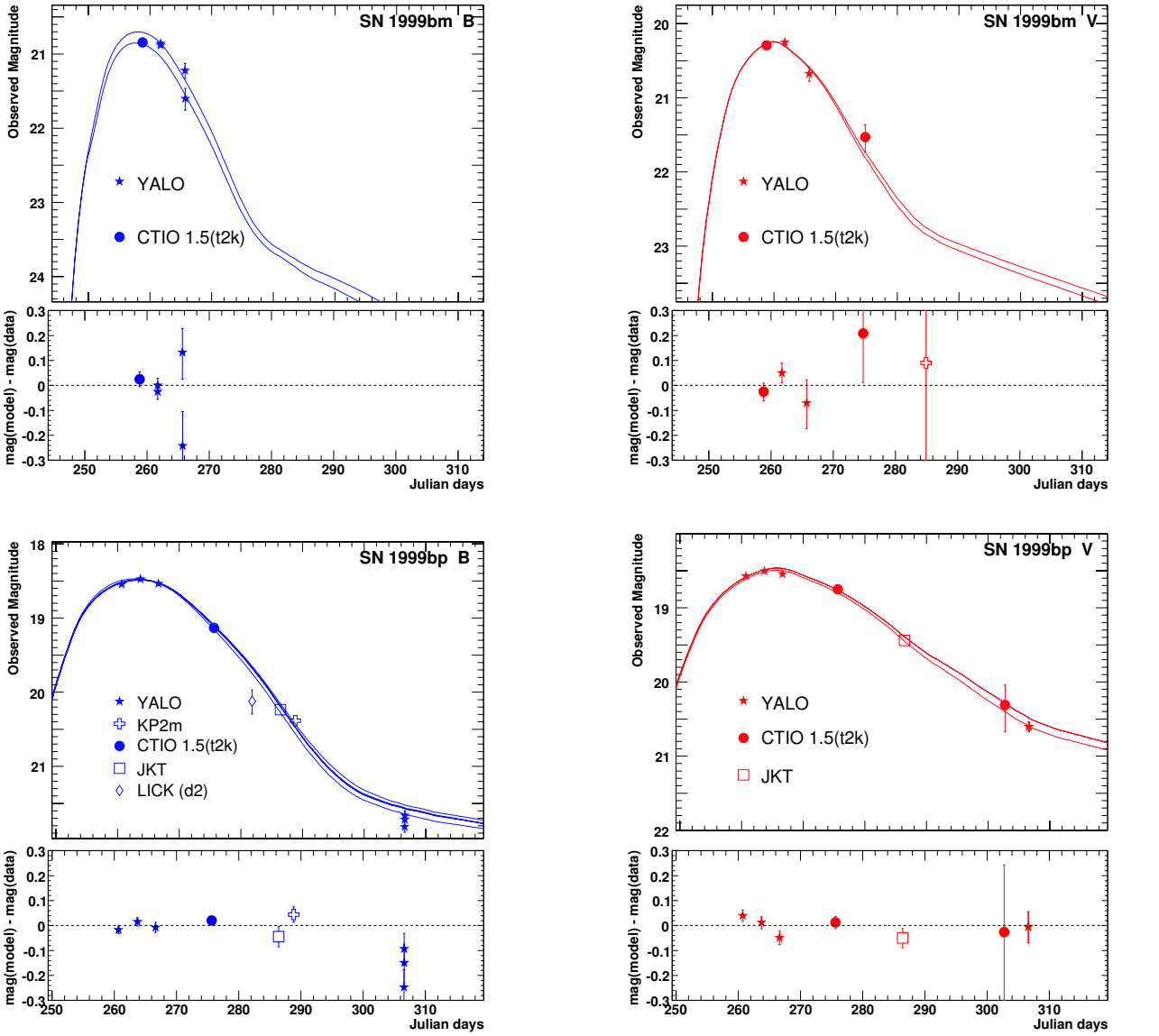

FIG. 3.— continued

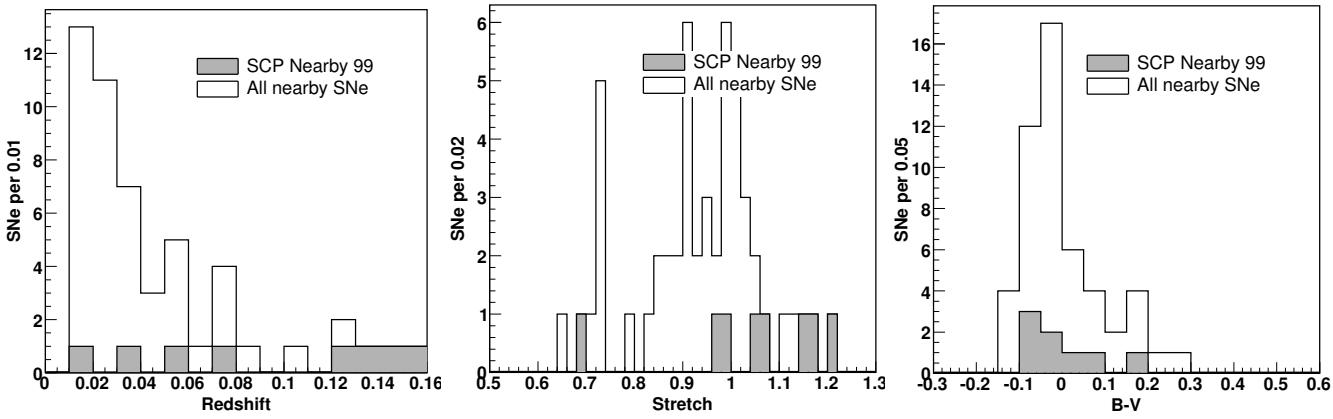

FIG. 4.— Left panel: redshift distribution; middle panel: stretch distribution; right panel: $B - V|_{t=B_{\max}}$ distribution.

in capturing the full diversity of Type Ia supernovae lightcurves.

Figure 4 (right and middle) shows the fitted $B-V$ color at maximum, as well as the stretch distribution. The stretch distribution has one low stretch supernova (SN 1999bm), but is otherwise dominated by supernovae with larger stretches. Two lower stretch SNe Ia were found in these searches, but are not presented here because of their faintness — in one case combined with proximity to the cuspy core of an elliptical host — prevented an analysis using the techniques described here. In any case, the larger number of high stretch supernovae is not very significant (a K-S test resulted in a 20% probability that the two distributions are consistent with each other).

For two of the eight supernovae, lightcurve data have previously been published. Jha et al. (2006); Krisciunas et al. (2000); Altavilla et al. (2004) present independent data on SN 1999aa. When comparing the fit results for SN 1999aa we find agreement to within 1% in maximum B-band luminosity, color and stretch. Spectroscopic and photometric data on SN 1999aw are previously reported by Strolger et al. (2002). While the raw data of Strolger et al. (2002) are largely the same as that presented here, the reduction pipelines used are independent. A main difference is the treatment of non-standard band passes. We report the original magnitudes and correct for non-standard band passes during the fit of the lightcurve, while in Strolger et al. (2002) corrections based on the color coefficient have been applied to the data. When fitting for peak B-band magnitude, color and stretch we obtain differences of $\Delta B = 0.04, \Delta(B-V) = 0.02$ and $\Delta s = 0.005$.

Figure 4 (left) shows the redshift distribution relative to the sample of other nearby supernovae (see 3.2 for a definition of that sample). As can be seen, the distribution extends to redshifts $z \sim 0.15$, an underpopulated region in the Hubble diagram.

3.2. *Literature supernovae*

Here we discuss the set of previously published nearby and distant supernovae included in the analysis. Not all SN lightcurves are of sufficiently good quality to allow their use in the following cosmological analysis. For all supernovae in the sample, we require that data from at least two bands with rest-frame central wavelength between 3470 Å (U-band) and 6600 Å (R-band) exist and that there are in total at least five data points available.

Further, we require that there is at least one observation existing between 15 days before and 6 days after the date of maximal B-band brightness, as obtained from an initial fit to the lightcurves (see section 3.3). The 6 day cut is scaled by stretch for consistency. In addition, we observed that for a smaller number of poorer lightcurves, the uncertainties resulting from the fits are unphysically small compared to what is expected from the photometric data. In these cases, we randomly perturb each data point by a tenth (or if necessary by a fifth) of its photometric error and refit the lightcurves. The remaining 16 SNe, where convergence can not be obtained even after perturbation of the data, are excluded from further analysis (note that these SNe are generally poorly measured and would have low weight in any cosmological analysis).

For the nearby SN sample, we use only supernovae with CMB-centric redshifts $z > 0.015$, in order to reduce the impact of uncertainty due to host galaxy peculiar velocities. We checked that our results do not depend significantly on the value of the redshift cut-off (tested for a range $z = 0.01 - 0.03$).

The number of SNe passing these cuts are summarized in Table 2. Each individual supernova is listed in Table 11, and the last column indicates any cuts that the supernova failed.

The list contains 17 supernovae from Hamuy et al. (1996), 11 from Riess et al. (1999), 16 from Jha et al. (2006), and 6 from Krisciunas et al. (2004a,b, 2001). Our lightcurve data for SN 1999aa are merged with that of Jha et al. (2006). To this list of nearby supernovae from the literature we add the new nearby supernovae presented here. For SN 1999aw, we use only the lightcurve data presented in this paper. Hence the sample contains 58 nearby supernovae.

The sample of high redshift supernovae is comparably heterogeneous. We use all of the 11 SNe from Knop et al. (2003) that have lightcurves obtained with HST. Of the 42 supernovae from Perlmutter et al. (1999), 30 satisfy the selection cuts described above (as can be seen in the photometry data of Table D1). Of the 16 SNe used by the High-Z Team (HZT) (Riess et al. 1998; Garnavich et al. 1998; Schmidt et al. 1998), two are already included in the Perlmutter et al. (1999) sample and of the remaining 14, 12 pass our cuts.

Included also are 22 SNe from Barris et al. (2004), and the 8 SNe from Tonry et al. (2003) that are typed to be secure or likely SNe Ia. We do not use SN 1999fv and SN 1999fh, as the number of available data points does not exceed the number of lightcurve fit parameters.

We add the 73 SNe Ia from the first year of SNLS (Astier et al. 2006), of which one does not pass the first phase cut (03D3cc). Note that, in Astier et al. (2006), 2 of the 73 supernovae were excluded from their cosmological parameter fits because they were significant outliers (see discussion in section 4.3). Riess et al. (2004, 2007) have published 37 supernovae which were discovered and followed using HST. Of these, 29 passed our lightcurve quality cuts. This sample contains the highest redshift supernovae in our compilation. Finally, we use the 84 SNe from the ESSENCE survey (Miknaitis et al. 2007; Wood-Vasey et al. 2007), of which 75 pass our cuts.

Requirement	$N_{\rm SN}$
all	414
$z > 0.015$	382
Fit successful	366
Color available	351
First phase < 6 d	320
≥ 5 data points	315
Outlier rejection	307

TABLE 2
Number of SNe after consecutive application of cuts. See 4.3 for a discussion of the outlier rejection cut.

3.3. *Lightcurve fitting*

The spectral-template-based fit method of Guy et al. (2005) (also known as SALT) is used to fit consistently both new and literature lightcurve data. This method is based on a spectral template (Nugent et al. 2002) which

has been adapted in an iterative procedure to reproduce a training set of nearby SNe $UBVR$ lightcurve data. The training set consists of mostly $z < 0.015$ SNe and hence does not overlap with the sample we use for determination of cosmological parameters. To obtain an expected magnitude for a supernova at a certain phase, the model spectrum is first redshifted to the corresponding redshift followed by an integration of the product of spectrum and band pass transmission. The spectral-template based fit method has the advantage that it consistently allows the simultaneous fit of multi-band light curves with arbitrary (but known) band pass transmission functions. In view of the large number of filters and instruments used for the new nearby SN samples as well as the very diverse lightcurve data found in the literature, this is particularly important here. In addition, frequent practical problems associated with K-corrections—such as the propagation of photometric errors—are handled naturally.

The spectral template based fit method of Guy et al. (2005) fits for the time of maximum, the flux normalization as well as rest-frame color at maximum defined as $c{=}B - V|_{t=B_{\max}} + 0.057$ and time-scale stretch s. It is worth noting that by construction, the stretch in SALT has a related meaning to the conventional time-axis stretch (Perlmutter et al. 1997; Goldhaber et al. 2001). However, as a parameter of the lightcurve model it also absorbs other, less pronounced, stretch dependent lightcurve dependencies. The same is true for the color c.

Recently, direct comparisons between alternative fitters, such as SALT, its update (Guy et al. 2007) as well as MLCS2k2 (Jha et al. 2007) show good consistency between the fit results, e.g. the amount of reddening (Conley et al. 2007). Our own tests have shown that for well observed supernovae, the method produces very consistent results (peak magnitude, stretch) when compared to the more traditional method of using light-curve templates (Perlmutter et al. 1997). However, we noticed that fits of poorly observed lightcurves in some cases do not converge properly. Part of the explanation is that in the case of the spectral template based fit method, the data before $t < -15$ days is not used as an additional constraint. More typically, the SALT fitter can fall into an apparent false minimum and we then found it necessary to restart it repeatedly to obtain convergence. Note that the small differences between the lightcurve fit parameters of Table 11 and the values shown in Table 10 of Wood-Vasey et al. (2007) are primarily cases where the Wood-Vasey et al. (2007) SALT fit did not converge (some of which are noted in Wood-Vasey et al. (2007)) and a few cases where we found it necessary to remove an extreme outlier photometry point from the lightcurve.

The lightcurves from Barris et al. (2003) and the I-band lightcurves of 4 supernovae of P99 (SNe 1997O, 1997Q, 1997R, and 1997am, see also Knop et al 2003) need a different analysis procedure, since in these cases the light of the host galaxy was not fully subtracted during the image reduction. We hence allow for a constant contribution of light from the host galaxy in the lightcurve fits. The supernovae were fit with additional parameters: the zero-level of the I-band lightcurve in case of the four SNe from the P99 set and the zero-level of all the bands in case of the Tonry et al. (2003) data. The additional uncertainties due to these unknown zero-levels have been propagated into the resulting lightcurve fit parameters.

The fitted lightcurve parameters of all SNe can be found in Table 11 which is also available in electronic form[42].

4. HUBBLE DIAGRAM CONSTRUCTION AND COSMOLOGICAL PARAMETER FITTING

The full set of lightcurves as described in section 3.2 have been fitted, yielding B-band maximum magnitude $m_B^{\max}$, stretch s, and color $c{=}B - V|_{t=B_{\max}} + 0.057$. In this section, these are input to the determination of the distance modulus. The analysis method is chosen to minimize bias in the estimated parameters (see section 4.2). An outlier rejection based on truncation is performed which is further described in section 4.3, before constraints on the cosmological parameters are computed.

4.1. *Blind analysis*

Following Conley et al. (2006), we adopt a blind analysis strategy. The basic aim of pursuing a blind analysis is to remove potential bias introduced by the analyst. In particular, there is a documented tendency (see for example Yao et al. (2006)) for an analysis to be checked for errors in the procedure (even as trivial as bugs in the code) up until the expected results are found but not much beyond. The idea of a blind analysis is to hide the experimental outcome until the analysis strategy is finalized and debugged. However, one does not want to blind oneself entirely to the data, as the analysis strategy will be partially determined by the properties of the data. The following blindness strategy is used, which is similar to the one invented in Conley et al. (2006). The data is fit assuming a ΛCDM cosmology, with the resulting fit for $\Omega_{\rm M}$ stored without being reported. The flux of each supernova data point is then rescaled according to the ratio of luminosity distances obtained from the fitted parameters and arbitrarily chosen dummy parameters (in this case $\Omega_{\rm M} = 0.25, \Omega_\Lambda = 0.75$). This procedure preserves the stretch and color distribution, and as long as the fitted parameters are not too different from the target parameters approximately preserves the residuals from the Hubble diagram. In developing the analysis, one is only exposed to data blinded by the procedure described above. Only after the analysis is finalized and the procedure frozen, is the blinding turned off.

Note that this prescription allows — in a consistent way — the inclusion of future data samples. A new data sample would be first investigated in a blind manner following the tests outlined in section 4.4, and if no anomalies are observed, one would combine it with the other data sets.

4.2. *Unbiased parameter estimation*

Type Ia supernova obey a redder-dimmer relation and a wider-brighter relation (Phillips 1993). The redder-dimmer relation in principle can be explained by dust extinction; however, the total to selective extinction ratios generally obtained empirically are smaller than expected from Milky-Way-like dust (Tripp 1998; Tripp & Branch 1999; Parodi et al. 2000; Guy et al. 2005; Wang et al. 2006). At the same time, the exact slope of the

[42] http://supernova.lbl.gov/Union

stretch-magnitude relation is not (yet) predicted by theory. The absence of a strong theoretical prediction motivates an empirical treatment of stretch and color corrections. Here we adopt the corrections of Tripp (1998) (see also Tripp & Branch (1999); Wang et al. (2006); Guy et al. (2005) and Astier et al. (2006)):

$$\mu_B = m_B^{\max} - M + \alpha(s-1) - \beta c, \tag{2}$$

Since the β-color correction term must account for both dust and any intrinsic color-magnitude relation, it is clearly an empirical approximation. The validity of β-color correction relies on only one assumption, that is, nearby supernovae and distant supernovae have an identical magnitude-color relation. If either the intrinsic SNe properties or the dust extinction properties of the supernovae are evolving with redshift, these assumptions may be violated. Observational selection effects may also introduce biases which invalidate equation 2. These potential sources of systematic error will be evaluated in section 5.1.

The χ^2 corresponding to that of Eq. 2 is given as:

$$\chi^2 = \sum_{\rm SNe} \frac{(\mu_B - \mu(z, \Omega_{\rm M}, \Omega_\Lambda, w))^2}{\sigma_{\rm tot}^2 + \sigma_{\rm sys}^2 + \sum_{ij} c_i c_j C_{ij}}. \tag{3}$$

The sum in the dominator represents the statistical uncertainty as obtained from the light-curve fit with C_{ij} representing the covariance matrix of fit parameters: peak magnitudes, color and stretch (i.e. $C_{11} = \sigma^2_{m_B}$) and $c_i = \{1, \alpha, -\beta\}$ are the corresponding correction parameters. $\sigma_{\rm tot}$ represents an astrophysical dispersion obtained by adding in quadrature the dispersion due to lensing, $\sigma_{\rm lens} = 0.093z$ (see Section 5.6), the uncertainty in the Milky-Way dust extinction correction (see Section 5.8) and a term reflecting the uncertainty due to host galaxy peculiar velocities of 300 km/s. The dispersion term $\sigma_{\rm sys}$ contains an observed sample-dependent dispersion due to possible unaccounted-for systematic errors. In section 4.3 we discuss the contribution $\sigma_{\rm sys}$ further.

Note that Eq. 3 can be derived using minimization of a generalized χ^2. Defining a residual vector for a supernova $\mathbf{R} = (\mu_B - \mu_{\rm model}, s - s', c - c')$ and supposing that the light-curve fit returns covariance matrix $\mathbf{C}$, we can write

$$\chi^2 = \sum_{\rm SNe} \mathbf{R}^T \mathbf{C}^{-1} \mathbf{R}. \tag{4}$$

Here, s' and c' take the role of the true stretch and color, which have to be estimated from the measured ones. Minimizing this equation over all possible values of s' and c' gives the χ^2 in Eq. 3. The χ^2 is minimized, not marginalized, over α and β; marginalization would yield a biased result due to the asymmetry of the χ^2 about the minimum.

Frequently, Eq. 3 is minimized by updating the denominator iteratively, i.e. only between minimizations (see for example Astier et al. (2006)). As shown in Fig. 5 and discussed next, this method produces biased fit results, an artifact previously noted by Wang et al. (2006).

We use a Monte Carlo simulation to estimate any biases from the fitting procedure. Random supernova samples resembling the observed one are generated and then fitted. The true stretch and color are sampled from a normal distribution of width 0.1 and for the peak magnitude

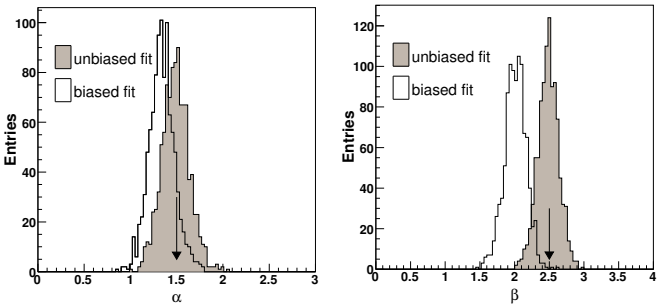

FIG. 5.— Monte Carlo simulation of the resulting α (left) and β (right) distributions as fitted with the unbiased and biased method. The true values $\alpha = 1.5$ and $\beta = 2.5$ are represented by the arrows.

an intrinsic dispersion of 0.15 magnitudes is assumed. A further dispersion corresponding to the measurement errors is added. By construction, the SN samples have the same redshift and stretch, color and peak magnitude uncertainties as the real sample. The test values for α and β were chosen as 1.5 and 2.5. This bias on α and β, as would be obtained from the iterative method's fits to the simulated data sets, is visible in Figure 5 as the unshaded histogram. The large potential bias on β ($\Delta\beta \sim -0.5$), if the χ^2 had been chosen according to Equation 3 with the iteratively updated denominator, is a result of the fact that the measurement error on c for high redshift SNe is similar to and often even exceeds the width of the color distribution itself.

We have investigated other sources of bias in the fitted parameters. A measurement bias will be introduced because overall, brighter SNe will have smaller photometric errors, and hence larger weights, than dimmer ones. If the photometric error bars are small enough that the intrinsic dispersion dominates the uncertainty, this bias will be small. Hence low-redshift, well observed SNe are biased less than high-redshift, poorly observed SNe, resulting in biased cosmological parameters. This bias was studied using the Monte Carlo simulation described above. For the sample under investigation it was found to introduce a bias $\delta M = 0.01$. In principle this bias can be corrected; however, since it is roughly a factor of three smaller than the statistical or systematic uncertainties, we choose not to carry out this step.

4.3. *Robust statistics*

Figure 6 shows the distribution of rest-frame B-band corrected magnitude residuals (left) from the best fit as obtained with the full data set. The right plot shows the pull distribution, where the pull is defined as the corrected B magnitude residual divided by its uncertainty. The distributions have outliers which, if interpreted as statistical fluctuations, are highly improbable. Hence these outliers point to non-Gaussian behavior of the underlying data, due to either systematic errors in the observations, contamination or intrinsic variations in Type Ia SNe. The fact that an outlier is present even in the high quality SNLS supernova set (see Table 3) suggests that contamination or unmodeled intrinsic variations might be present. However, other samples that typically were observed with a more heterogeneous set of telescopes and instruments show larger fractions of outliers, indicating additional potential observation-related problems.

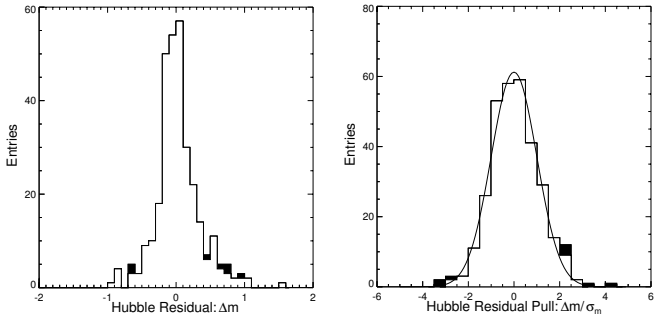

FIG. 6.— Residual of restframe, stretch and color corrected, B-band magnitude (left) and pull distribution (right) from the best fitting cosmology. The filled histogram shows the rejected outliers. The pull distribution is overlayed with a normal distribution of unit width.

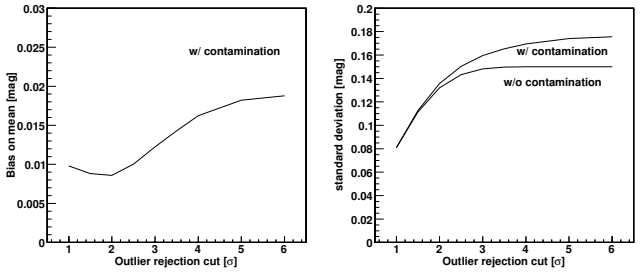

FIG. 7.— Mock simulation of bias (left panel) and standard deviation (right) of the mean magnitude as a function of the outlier rejection cut. The simulated SN set consists of one population of 270 SNe with intrinsic dispersion of 0.15 magnitudes and zero mean and a second population of 50 SNe with intrinsic dispersion of 0.26 mag and mean 0.13 mag. The effect of outlier rejection on a single population without contamination is shown as a reference curve.

In order to limit the influence of outliers, we use a robust analysis technique. First, the SN samples are fit for M, the absolute magnitude of the SNe, using median statistics (see Gott et al. (2001) for a discussion of median statistics in the context of SN cosmology). The quantity minimized is $\chi = \sum_{\rm SNe} \frac{|\mu_B - \mu_{\rm model}|}{\sigma}$, where the uncertainty σ in the denominator includes the covariance terms in the denominator of the right hand side of Equation 3. We then proceed to fit each sample by itself using the α, β, and $\Omega_{\rm M}$ from the combined fit, as χ is not a well-behaved quantity for small numbers of SNe.

For each sample, we remove SNe with a pull exceeding a certain value $\sigma_{\rm cut}$ relative to the median fit of the sample. Currently available algorithms, which correct the peak magnitude using, e.g., stretch or Δm_{15}, are capable of standardizing SNe Ia to a level of $\sim 0.10 - 0.15$ magnitudes. To reflect this we add in quadrature a systematic dispersion to the known uncertainties. The list of known uncertainties include observational errors, distance modulus uncertainties due to peculiar velocities (with Δv =300 km/s) and gravitational lensing (relevant only for the highest redshift SNe; see section 5.6 for a discussion). The additional systematic dispersion has two components: a common irreducible one, possibly associated with intrinsic variations in the SN explosion mechanism, as well as an observer-dependent component. To obtain self-consistency the systematic dispersion is recalculated during the analysis. One starts by assuming a systematic dispersion of $\sigma_{\rm sys} = 0.15$ magnitudes, then computes the best fitting cosmology for the particular sample using median statistics, removes the outlier SNe with residuals larger than a cut value $\sigma_{\rm cut}$, iterates $\sigma_{\rm sys}$ such that the total χ^2 per degree of freedom is unity, and in a final step redetermines the best fitting cosmology using regular χ^2 statistics to obtain an updated $\sigma_{\rm sys}$. From that point in the analysis, after outliers are rejected and $\sigma_{\rm sys}$ determined, only regular χ^2 statistics are applied.

When using a robust analysis, it is necessary to check that *a*) in the absence of contamination the results are not altered from the Gaussian case and *b*) in presence of a contaminating contribution, the impact of it is indeed reduced. In order to investigate this, we begin with a model for the contamination. We assume the data sample to be composed of two types of objects, one representing the desired SNe Ia and a second contribution characterizing the contamination. We then use a maximum-likelihood analysis of the observed pull distribution shown in Figure 6 (right) to determine the normalization, width and mean of the contaminating distribution. The uncontaminated pull distribution is assumed to be a Gaussian distribution of unit width and zero mean. The observed pull distribution is best fitted by an additional contaminating contribution that is 50% wider ($\sigma_m = 0.23$ mag) and which has a mean shifted by $\Delta m = 0.3\sigma_m$, normalized to 18 % of the area. A mock simulation that is based on this superposition of two normal distributions illustrates the benefits of using the robust analysis. Figure 7 (right) shows the bias of the mean relative to the center of the main component as a function of the outlier rejection cut value. Outlier rejection can reduce the bias by a factor of three with a remaining bias of less than 0.01 magnitude. Even for a wide range of contaminant parameters ($\sigma_m = 0.15 - 2; \Delta m = 0 - 2$ magnitudes) the bias obtained for the robust analysis remains below 0.015 magnitudes. Only in cases where the contamination is larger than 30% does the outlier rejection algorithm become unstable.

Besides reducing the potential bias due to contamination, robust statistics can also lead to tighter parameter constraints through reduction of the intrinsic dispersion. The right panel of Figure 7 shows for the simulated data the average standard deviation as a function of the outlier rejection cut for the 16 % contamination case described above. As a reference, the case of a single uncontaminated population of SNe is shown as well. Note that a cut at 3σ reduces the dispersion noticeably in the case of a contaminated sample, while the uncontaminated single population is affected negligibly (the standard deviation is reduced by 1.3 %, e.g. from 0.15 to 0.148 magnitudes).

For the real data, we consider two values $\sigma_{\rm cut} = 2, 3$ as well as the case in which all SNe are kept. We chose as our main cut value $\sigma_{\rm cut} = 3$ since, after application of the outlier rejection, standard χ^2 statistics is still a good approximation while at the same time a potential bias introduced by contamination is significantly reduced. Note also that the impact of individual SNe that have residuals close to $\sigma_{\rm cut}$ is small for large statistics: an additional SN will shift the mean distance modulus of $N_{\rm SNe}$ by at most $\sigma_{\rm cut}/\sqrt{N_{\rm SNe}}$ standard deviations. Hence for $N_{\rm SNe} \gtrsim 10$ and $\sigma_{\rm cut} = 3$ the algorithm can be considered stable relative to fluctuations of individual SNe.

4.4. *Sample characteristics, dispersion and pull*

Figure 8 illustrates the heterogeneous character of the samples. It shows the Hubble and residual diagrams for the various samples, as well as the histogram of the SN residuals and pulls from the best fit. The difference in photometric quality is illustrated in the right-most column of Fig. 8, by showing the error on the color measurement. As can be seen, some samples show a significant redshift dependent gradient in the errors, while others have small, nearly constant errors (most notably the sample of Knop et al. (2003)). The sample of Astier et al. (2006) shows a small color uncertainty up to $z \leq 0.8$, and degrades significantly once the color measurement relies on the poorer z-band data (c.f. SALT2 (Guy et al. 2007), which is capable of incorporating lightcurve data bluer than rest-frame U).

Our analysis is optimized for large, multi-color samples such as that of Astier et al. (2006), since these now dominate the total sample. There is often a better analysis approach for any given specific sample that would emphasise the strengths of that sample's measurements and yield a tighter dispersion and more statistical weight. However, for this combined analysis of many samples it was more important to use a single uniform analysis for every sample, at the cost of degrading the results for some of the smaller samples. This particularly affects some of the very earliest samples, such as Riess et al. (1998), Perlmutter et al. (1999), and Barris et al. (2004), where the color measurements had originally been used with different priors concerning the dust distribution. Treating these samples with the current analysis thus gives significantly larger dispersions (and hence less weight) to these samples than their original analyses. As a check, we have verified that by repeating the analysis according to Perlmutter et al. (1999) we reproduce the original dispersions.

Figure 9 shows diagnostic variables used to test for consistency between the various samples. The leftmost plot shows the systematic dispersion and RMS around the best fit model. One expects that there is an intrinsic dispersion associated with all SNe, which provides a lower limit to the sample dependent systematic dispersion. To estimate the intrinsic dispersion one can look at various quantities, as for example the smallest $\sigma_{\rm sys}$ or, perhaps more appropriate, by the median of $\sigma_{\rm sys}$. The median of $\sigma_{\rm sys}$, which is about 0.15 mag (shown as the leftmost dashed vertical line), is a robust measure of the intrinsic dispersion, as long as the majority of samples are not dominated by observer dependent, unaccounted-for uncertainties.

As a test for tension between the data sets, we compare for each sample the average residual from the best fit cosmology. This is shown in the middle panel of Fig. 9. As can be seen, most samples fall within 1σ and none deviate by more then 2σ. The larger samples show no indication of inconsistency. This changes if one considers, instead of the mean, the slope, $d\mu_{\rm residual}/dz$, of the residuals as a function of the redshift. The right panel of Fig. 9 shows a large fraction of significant outliers in the slope. The largest slope outlier is found for the Miknaitis et al. (2007) sample (see also the middle panel of Fig. 8). The sign of the slope is consistent with the presence of a Malmquist bias (see Wood-Vasey et al. (2007) for a discussion). The uncertainties associated with such a Malmquist bias are discussed in Section 5.5. While in general there is no clear trend in the sign of the slope deviations, it is clear that any results that depend on the detailed slope, such as a changing equation of state, should be treated with caution.

5. SYSTEMATIC ERRORS

Detailed studies of the systematic effects have been published as part of the analysis of individual data sets. The list includes photometric zero points, Vega spectrum, lightcurve fitting, contamination, evolution, Malmquist bias, K-corrections and gravitational lensing, which have also been discussed in earlier work by authors of this paper (Perlmutter et al. 1997, 1999; Knop et al. 2003; Astier et al. 2006; Ruiz-Lapuente 2007; Wood-Vasey et al. 2007).

Some sources of systematic errors are common to all surveys and will be specifically addressed for the full sample. Other sources of systematic errors are controlled by the individual observers. The degree with which this has been done for the various data samples entering the analysis is very different. The SNLS—which is using a single telescope and instrument for the search and followup, and which has detailed multi-band photometry for nearly all its SNe—has a strong handle on a subset of the observation-dependent systematics uncertainties. With the exception of the ESSENCE SN data sample, other high redshift samples are smaller and will contribute less to the final results.

We handle the two types of systematic errors separately: systematic errors that can be associated with a sample (e.g. due to observational effects), and those that are common to all the samples (e.g. due to astrophysical or fundamental calibration effects). To first order, the measurement of cosmological parameters depends on the relative brightness of nearby SNe ($z \sim 0.05$) compared to their high redshift counterparts ($z \sim 0.5$). If low and high redshift SNe are different, this can be absorbed in different absolute magnitudes M. We hence cast the common systematic uncertainties into an uncertainty in the difference $\Delta M = M_{\rm low-z} - M_{\rm high-z}$. 'We have chosen $z_{\rm div} = 0.2$ as the dividing redshift as it conveniently splits the samples according nearby and distant SN searches. Note, however, that our resulting systematic errors change by less than 25% of its value for $z_{\rm div}$ in the range $0.1 - 0.5$. In addition we allow for a set of extra parameters, ΔM_i, one for each sample i.

Systematic uncertainties are then propagated by adding these nuisance parameters to μ_B:

$$\mu'_B = \begin{cases} \mu_B + \Delta M_i & \text{for } z_{\rm div} < 0.2 \\ \mu_B + \Delta M_i + \Delta M & \text{for } z_{\rm div} \geq 0.2 \end{cases} \quad (5)$$

with the term $\Delta M^2/\sigma^2_{\Delta M} + \sum_{i=1}^{N_{\rm samples}} \Delta M_i^2/\sigma^2_{\Delta M_i}$ being added to the χ^2 as defined through Eq. 3. We have checked that this treatment of systematic errors is consistent (in our case to better than 5 % of its value) with the more common procedure, applicable to one-dimensional constraints, in which part of the input data is offset by $\pm\sigma_{\Delta M}$ to obtain the systematic variations in the resulting parameter (e.g. w or $\Omega_{\rm M}$).

In the following we discuss the different contributions to $\sigma_{\Delta M}$, and summarize them in section 5.9. The result-

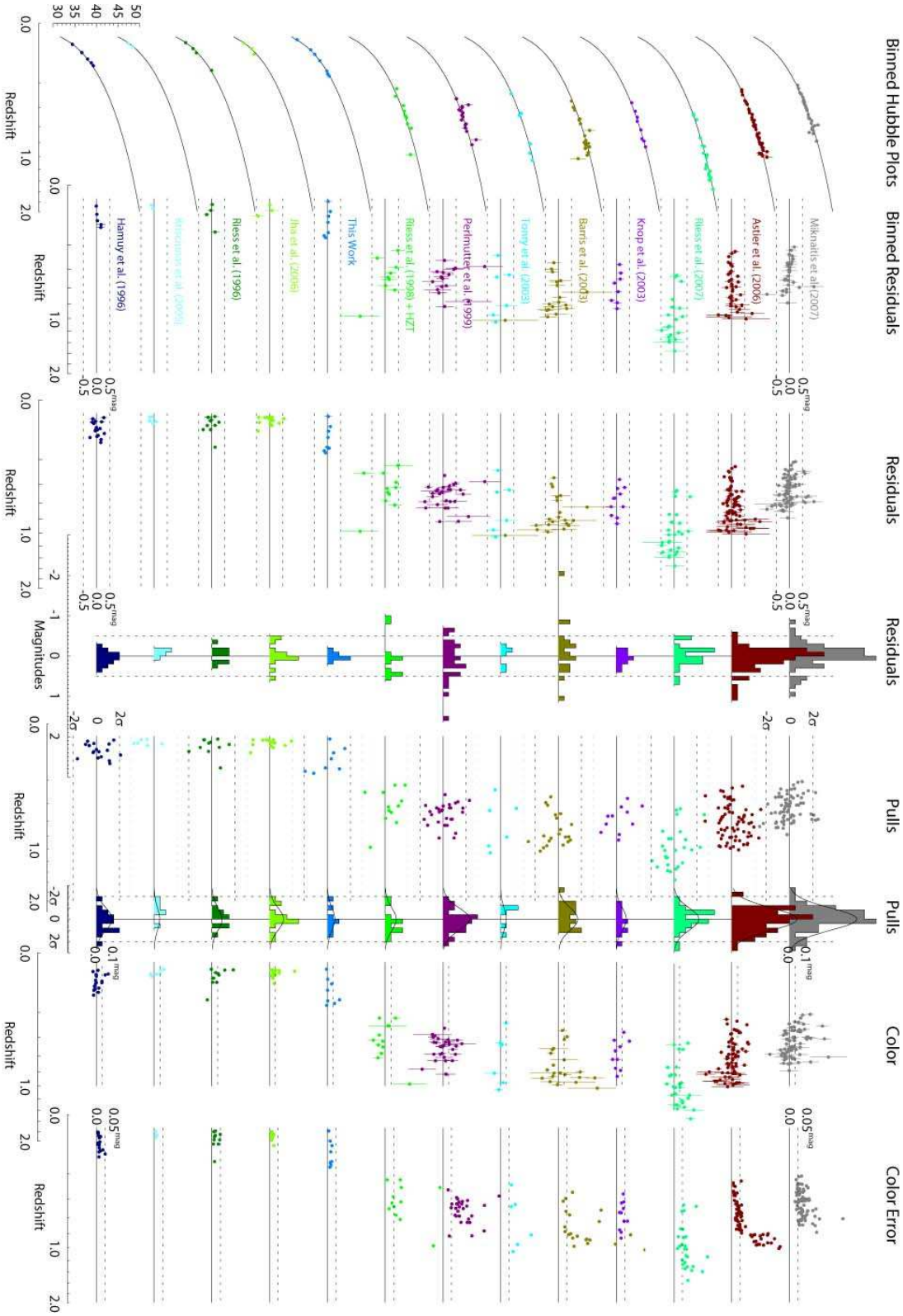

FIG. 8.— From left to right: a) Hubble diagrams for the various samples; b) binned magnitude residuals from the best fit (bin-width: $\Delta z = 0.01$); c) unbinned magnitude residuals from the best fit; d) histogram of the residuals from the best fit; e) pull of individual SNe as a function of redshift; f) histogram of pulls; g) SN color as a function of redshift; h) uncertainty of the color measurement as an illustration of the photometric quality of the data.

TABLE 3
SHOWN IS THE NUMBER OF SNE PASSING THE DIFFERENT OUTLIER REJECTION CUTS, AS WELL AS THE SAMPLE DEPENDENT SYSTEMATIC DISPERSION ($\sigma_{\rm sys}$) AND THE RMS AROUND THE BEST FIT MODEL. THE COMPILATION OBTAINED WITH THE $\sigma_{\rm cut} = 3$ CUT WILL BE REFERRED TO AS THE UNION ROBUST SET.

	No Outlier Cut			$\boldsymbol{\sigma_{\rm cut} = 3}$			$\sigma_{\rm cut} = 2$		
Set	SNe	$\sigma_{\rm sys}(68\%)$	RMS (68%)	SNe	$\sigma_{\rm sys}(68\%)$	RMS **(68%)**	SNe	$\sigma_{\rm sys}(68\%)$	RMS (68%)
Hamuy et al. (1996)	17	$0.14^{+0.04}_{-0.03}$	$0.16^{+0.03}_{-0.03}$	**17**	$\mathbf{0.14^{+0.04}_{-0.03}}$	$\mathbf{0.16^{+0.03}_{-0.03}}$	16	$0.12^{+0.05}_{-0.03}$	$0.15^{+0.02}_{-0.03}$
Krisciunas et al. (2005)	6	$0.06^{+0.11}_{-0.05}$	$0.10^{+0.03}_{-0.04}$	**6**	$\mathbf{0.05^{+0.11}_{-0.05}}$	$\mathbf{0.10^{+0.03}_{-0.04}}$	6	$0.08^{+0.12}_{-0.07}$	$0.12^{+0.03}_{-0.04}$
Riess et al. (1996)	11	$0.16^{+0.07}_{-0.04}$	$0.18^{+0.03}_{-0.04}$	**11**	$\mathbf{0.16^{+0.07}_{-0.03}}$	$\mathbf{0.17^{+0.03}_{-0.04}}$	11	$0.18^{+0.08}_{-0.04}$	$0.20^{+0.04}_{-0.05}$
Jha et al. (2006)	16	$0.30^{+0.09}_{-0.05}$	$0.31^{+0.05}_{-0.06}$	**15**	$\mathbf{0.26^{+0.08}_{-0.05}}$	$\mathbf{0.27^{+0.05}_{-0.06}}$	1 1	$0.10^{+0.08}_{-0.06}$	$0.15^{+0.03}_{-0.04}$
This Work	8	$0.01^{+0.06}_{-0.01}$	$0.09^{+0.02}_{-0.03}$	**8**	$\mathbf{0.00^{+0.05}_{-0.00}}$	$\mathbf{0.07^{+0.02}_{-0.02}}$	8	$0.07^{+0.06}_{-0.03}$	$0.12^{+0.03}_{-0.04}$
Riess et al. (1998) + HZT	12	$0.29^{+0.20}_{-0.11}$	$0.50^{+0.09}_{-0.12}$	**12**	$\mathbf{0.28^{+0.19}_{-0.10}}$	$\mathbf{0.48^{+0.09}_{-0.11}}$	10	$0.16^{+0.19}_{-0.10}$	$0.49^{+0.10}_{-0.13}$
Perlmutter et al. (1999)	30	$0.43^{+0.13}_{-0.09}$	$0.65^{+0.08}_{-0.09}$	**29**	$\mathbf{0.33^{+0.10}_{-0.07}}$	$\mathbf{0.50^{+0.06}_{-0.07}}$	24	$0.19^{+0.11}_{-0.09}$	$0.43^{+0.06}_{-0.07}$
Tonry et al. (2003)	6	$0.00^{+0.33}_{-0.00}$	$0.24^{+0.06}_{-0.09}$	**6**	$\mathbf{0.06^{+0.28}_{-0.06}}$	$\mathbf{0.24^{+0.06}_{-0.09}}$	6	$0.00^{+0.32}_{-0.00}$	$0.26^{+0.07}_{-0.09}$
Barris et al. (2003)	22	$0.31^{+0.12}_{-0.07}$	$0.64^{+0.09}_{-0.11}$	**21**	$\mathbf{0.23^{+0.12}_{-0.08}}$	$\mathbf{0.62^{+0.09}_{-0.10}}$	19	$0.11^{+0.16}_{-0.11}$	$0.71^{+0.11}_{-0.13}$
Knop et al. (2003)	11	$0.10^{+0.08}_{-0.04}$	$0.17^{+0.03}_{-0.04}$	**11**	$\mathbf{0.10^{+0.07}_{-0.04}}$	$\mathbf{0.17^{+0.03}_{-0.04}}$	11	$0.11^{+0.08}_{-0.05}$	$0.18^{+0.04}_{-0.04}$
Riess et al. (2006)	29	$0.22^{+0.05}_{-0.04}$	$0.31^{+0.04}_{-0.04}$	**27**	$\mathbf{0.16^{+0.05}_{-0.04}}$	$\mathbf{0.26^{+0.03}_{-0.04}}$	24	$0.08^{+0.05}_{-0.06}$	$0.22^{+0.03}_{-0.03}$
Astier et al. (2006)	72	$0.14^{+0.03}_{-0.02}$	$0.31^{+0.03}_{-0.03}$	**71**	$\mathbf{0.12^{+0.03}_{-0.02}}$	$\mathbf{0.29^{+0.02}_{-0.03}}$	70	$0.12^{+0.03}_{-0.02}$	$0.30^{+0.02}_{-0.03}$
Miknaitis et al. (2007)	75	$0.21^{+0.04}_{-0.03}$	$0.32^{+0.02}_{-0.03}$	**73**	$\mathbf{0.18^{+0.04}_{-0.03}}$	$\mathbf{0.30^{+0.02}_{-0.03}}$	66	$0.00^{+0.05}_{-0.00}$	$0.23^{+0.02}_{-0.02}$
Union	315			**307**			282		

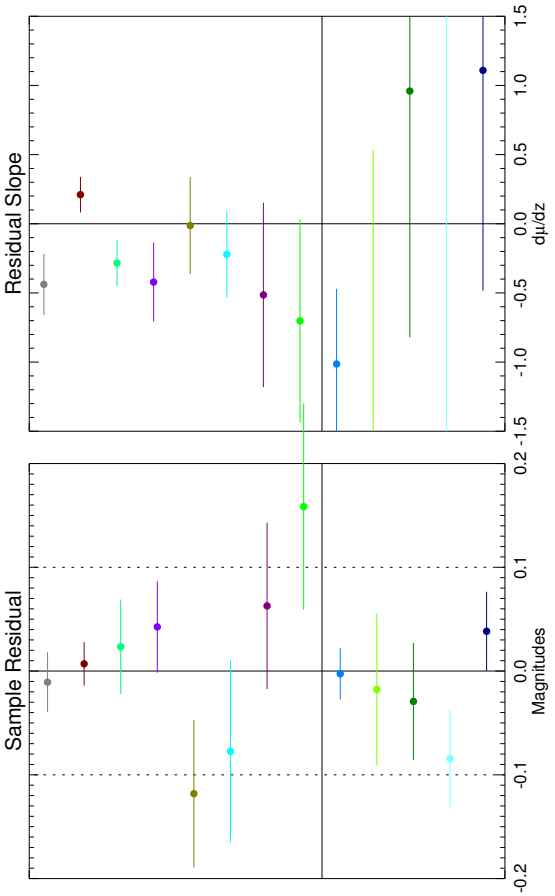

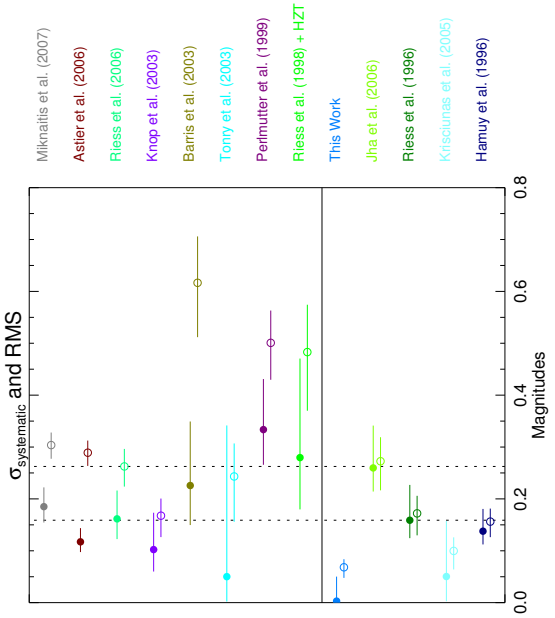

FIG. 9.— From left to right: Systematic dispersion (filled circles) and RMS around the best fit model (empty circles); The mean, sample averaged, deviation from the best fit model; The slope of the Hubble-residual (in magnitudes) versus redshift, $d\mu_{\rm residual}/dz$. The parameters characterizing the different samples are used to uncover potential systematic problems.

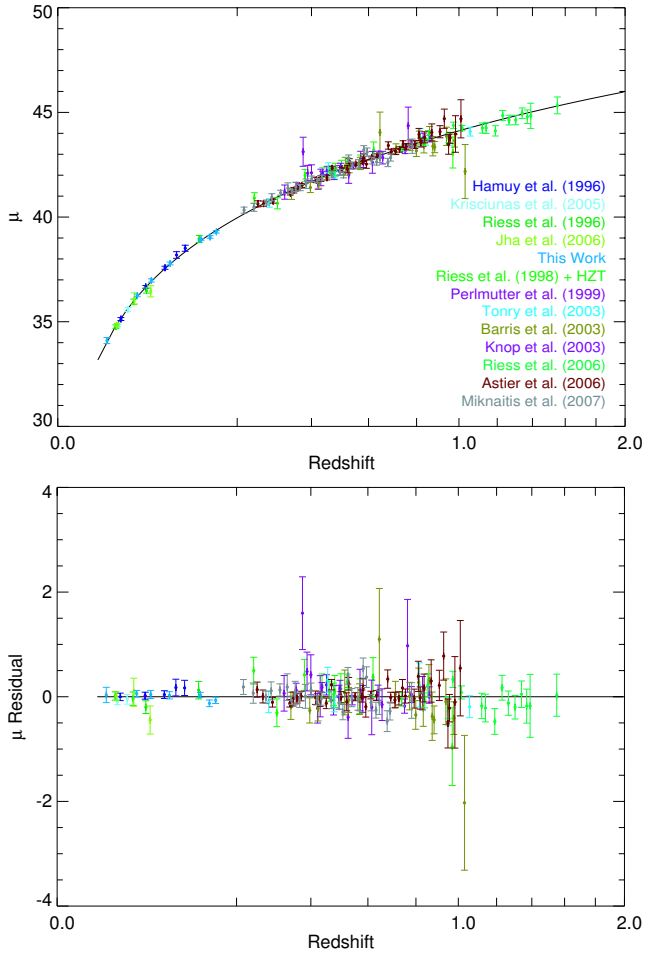

FIG. 10.— Top: Binned Hubble diagram (bin-size $\Delta z = 0.01$). Bottom: Binned residuals from the best fitting cosmology.

ing systematic errors on the cosmological parameters are discussed in section 6.

5.1. *Stretch & evolution*

With the large statistics at hand one can test the errors associated with the empirical stretch and color corrections. These corrections would become sources of systematic error if *a*) different SN populations were to require different corrections and *b*) if the SN populations were to show differences between nearby and distant objects (either due to selection effects or due to evolution of the SN environment).

A potential redshift dependence of the correction parameters can be tested by separately fitting low redshift and high redshift objects. For this test, a ΛCDM cosmology was assumed with $\Omega_{\rm M} = 0.28$ and $\Omega_{\rm M} = 0.72$ (the values we obtain from the fit of the full sample); however, the results are rather insensitive to the assumed cosmological parameters. The obtained fit parameters α and β are presented in table 4.

The values of β at high and low redshift agree very well, providing strong constraints on evolution of the color-correction. Such evolution effects could arise, for example, due to a different mix of dust reddening and intrinsic color at different redshifts. The fact that β agrees so well

subset	$N_{\rm SN}$	α	β	$\Omega_{\rm M}^a$	w^b
all	307	1.24(0.10)	2.28(0.11)	0.29(0.03)	-0.97(0.06)
$z > 0.2$	250	1.46(0.16)	2.26(0.14)	-	-
$z \leq 0.2$	57	1.07(0.12)	2.23(0.21)	-	-
$s < 0.96$	155	1.56(0.27)	2.18(0.18)	0.27(0.05)	-0.98(0.09)
$s \geq 0.96$	152	1.51(0.37)	2.34(0.17)	0.30(0.04)	-0.93(0.07)

TABLE 4
Fit parameters as obtained for different SN subsamples. (^{a})A flat Universe was assumed in the constraints on $\Omega_{\rm M}$. (^{b})Constraints on w were obtained from combining SNe with CMB and BAO measurements. A flat Universe was also assumed. (see section 6 for more details).

supports the choice of the empirical color correction[43].

The α at low-redshift and high-redshift are only marginally consistent with each other. We will take the difference at face value and estimate the impact it would have on the final result. The average stretch is $\langle s \rangle \approx 0.96$ and hence the difference in the average stretch correction is $\langle 1 - s \rangle \, \Delta\alpha \approx 0.015$. If α indeed is redshift dependent and this was not accounted for, one would obtain a bias of $\Delta M = 0.015$ mags.

Effects of potentially different SN populations should be considered as well. It has recently been argued by Scannapieco & Bildsten (2005) and Mannucci et al. (2006) that one needs to allow for two types of SN-progenitor timescales to explain the observed rates in different galaxy types. One class of objects traces the star formation rate directly, while the second class has a delay time trailing the star formation rate by a few billion years. If indeed two populations are present, they might evolve differently with redshift. It is therefore important to check that the empirical corrections suit both populations. To test the effect of different SN populations one can subdivide the sample according to SN subtypes or host environments (Sullivan et al. 2003; Howell et al. 2007). Sullivan et al. (2006) have found using well observed SNe and hosts from SNLS that the stretch of a light curve is correlated with its host environment as well as with the two classes of SN-progenitor systems postulated by Scannapieco & Bildsten (2005); Mannucci et al. (2006). Therefore, we divide the SN sample into two approximate equally large samples with $s < 0.96$ and $s \geq 0.96$. The two independent samples are then fitted, with the results shown in Table 4. The resulting parameters $\Omega_{\rm M}$ (for a flat Universe) and w (for a flat Universe together with BAO+CMB) for the two samples are less than 1σ apart and hence there is no evidence for an underlying systematic effect. Nevertheless, this will be a very important number to watch, once future high quality SN data sets will be added. (Note that, while the resulting values of αs for the two samples are consistent with each other, they appear inconsistent with the value obtained for the complete sample. This apparent inconsistency arises in part due to a bias introduced by dividing the stretch distribution in the middle. Larger stretch SNe, misclassified due to measurement errors as belonging to the low stretch SNe sample, as well as lower stretch SNe, misclassified as belonging to the large stretch SNe sample, will for both samples result in a α biased to larger values.)

We have also investigated whether the sample can be sub-divided according to the color of the SNe. We found that the results of such a test can be very misleading. While in principle one would expect to find that the best fitted cosmological parameters do not depend on color selection criteria (e.g. $c < c_{\rm cut}$ and $c > c_{\rm cut}$), we find by means of Monte Carlo simulation described in Section 4.2 that a significant bias is introduced into the measurements. This bias is also observed in the data. For example, by choosing $c_{\rm cut} = 0.02$ we find that for our sample of SNe $\Omega_{\rm M}$ changes by ± 0.1. The bias arises from truncating an asymmetric distribution. In the case of color, the asymmetry in the distribution is introduced by the fact that extinction by dust leads only to reddening. Hence the number of objects which would belong to $c_{\rm true} < c_{\rm cut}$ but, due to a large measurement error, are fitted with $c_{\rm observed} > c_{\rm cut}$, are not compensated by objects misclassified in the opposite way. The number of misclassified objects is a function of the measurement errors, and hence is larger towards higher redshift. The simulated data sets result in a significant bias both in $\Omega_{\rm M}$ as well as β. The size of the bias, however, depends on assumptions made for the underlying color distribution. Hence, for the current data sample, splitting the data set in two color bins introduces a bias so large and difficult to control, that the results of the test become meaningless. Note that if one had very small error bars on the color measurement over the full redshift range (as obtained from a dedicated space based survey (Aldering 2005)), the bias can be kept small. This would allow for additional tests of systematic uncertainties due to reddening corrections.

5.2. *Sample contamination*

As discussed in Section 4.3, the method of robust statistics was applied to limit the effect of outliers, which could be present if the data is contaminated by non Type Ia SNe, or by other events which do not have the standard candle properties of regular SN Ia. It was shown in Section 4.3 that the bias due to contamination can be limited for this analysis to $\Delta M = 0.015$ mag, which we hence use as the uncertainty due to contamination.

In previous compilations, such as that of Riess et al. (2004, 2007), no formal outlier criteria were applied. Instead, with some exceptions, the original classifications made by the authors of the data sample were used. Spurious candidates are sometimes removed from the data samples by hand (see for example Astier et al. (2006)), making it extremely difficult to estimate the effect of the remaining contamination. Our method of outlier rejection provides a simple and objective alternative.

5.3. *Lightcurve model & K-corrections*

The lightcurve model (Guy et al. 2005) is a parametric description with two free parameters. As such it has limitations in capturing the full diversity of Type Ia SNe. By visual inspection we find, for example, that the fitted maximum magnitude can differ from the data by a few hundredths of a magnitude. A particular problem could arise if the observation strategies for nearby and distant SNe differ. In fact, the high-redshift data sets have on average earlier observations of the lightcurve, which is a result of the rolling-search techniques frequently used to

[43] Note that if β were not obtained by fitting but instead was fixed, e.g. $\beta = R_{\rm B} = 4.1$, a bias can be expected (and might have already been observed, see Conley et al. (2007)) if the average reddening changes as a function of redshift.

find and follow-up SNe. Hence, when comparing low-z to high-z SNe, the fitted lightcurve parameters are obtained from slightly different parts of the lightcurve. The mismatch between template and the data lightcurve might thus be more pronounced in one sample than the other. To quantify the effect, we have performed an extensive Monte Carlo simulation. A set of BVR lightcurve templates are obtained from a quartic spline fit to data including the well observed SNe 1990N, 1994D, 1998aq, 2001el, 2002bo, 2003du, 2004eo, and 2005cf (Strovink 2007). The templates are then used to sample random realizations of the lightcurves with cadence, signal-to-noise and date of the first detection of the nearby and distant SN sample. These simulated lightcurves are then fitted. The difference in the stretch and color corrected peak magnitude between the nearby and distant sample can be used to estimate the systematic uncertainty. For the nine templates we obtain the average difference between nearby and distant SNe of -0.02 magnitudes with an RMS scatter of 0.015. We adopt an associated systematic uncertainty of $\Delta M = 0.02$ magnitudes due to this.

There is another source of uncertainty arising from the diversity of SNe Ia lightcurves. If a certain class of SNe is misrepresented (for example if they are brighter than average for their typically fitted stretch value) and if the fraction of such SNe changes as a function of redshift, it will lead to a systematic bias in the cosmological parameters. Section 5.1 has addressed this issue by subdividing the sample according to stretch and redshift. If a significant lightcurve misrepresentation were present, one would expect to see differences in the fitted lightcurve-correction parameters. No statistically significant differences have been observed and we assign no additional contribution to the uncertainties from such an effect.

The lightcurve model is based on a spectral template series. It thereby eliminates the need for a separate K-correction (see Section 3.3). The model has been trained with nearby SNe data and hence will be affected by systematic errors associated with that training data. These are largest for the U-band, which suffers from low training statistics and difficult flux calibration. However, the validity of the model in the U-band has been verified with the SNLS data set to better than 0.02 magnitudes (Astier et al. 2006). Here we adopt their assessment of the resulting systematic error of $\Delta M = 0.02$.

5.4. *Photometric zero points*

With present methods, ground based photometric zero point calibration is generally limited to an accuracy of $\gtrsim 1\%$ (Stubbs & Tonry 2006). The largest contribution to the photometric error of the peak magnitude arises from the color correction $\Delta M \sim \beta \Delta c$. The color measurement is based on the measurement of the relative flux in two (or more bands), and as a result some of the uncertainties cancel. Nevertheless, since the color of SNe at different redshifs are obtained from different spectral regions, the uncertainty in the reference Vega spectrum limits the achievable accuracy to $\Delta c \approx 0.01 - 0.015$ mag (Stritzinger et al. 2005; Bohlin & Gilliland 2004).

Here we assume an uncertainty of $\Delta M = 0.03$ for the photometric peak magnitude due to zero point calibration. Part of this uncertainty is common to all samples (as the same set of calibration stars is being used), while the other part is sample dependent (e.g. tied to the calibration procedure) and we divide the error equally among the two categories.

5.5. *Malmquist bias*

Malmquist bias arises in flux limited surveys, when SNe are detected because they are overly bright. What matters for cosmology is whether the bias is different for the low-z and high-z samples. Perlmutter et al. (1999), Knop et al. (2003) and Astier et al. (2006) have evaluated the effects of Malmquist bias for the SCP and SNLS SN samples as well as the nearby SN sample and found that they nearly cancel. Since an individual estimate of Malmquist bias for all the different samples is beyond the scope of this work, we attribute a conservative systematic uncertainty of $\Delta M = 0.02$ (Astier et al. 2006) for all samples, which is consistent with previous estimates.

In addition, we investigated whether the significant redshift dependence of the Hubble residuals observed for the Miknaitis et al. (2007) sample (see section 4.4), if interpreted as due to Malmquist bias, exceeds our claimed uncertainty. A simulation was performed in which we introduced a magnitude cut-off such that the resulting slope, $d\mu/dz$, matches the observed slope of -0.6. The associated Malmquist bias with that sample is then ~ 0.05 mags. If this is compared to the average Malmquist bias obtained for magnitude limited searches, the extra bias is only 0.03 mags larger– not much larger than the systematic uncertainty we have adopted. While we do not treat the ESSENCE data sample differently from the others, we note that Wood-Vasey et al. (2007) made their extinction prior redshift-dependent to account for the fact that at higher redshifts an increasingly larger fraction of the reddened SNe was not detected. The linear color correction employed in our analysis is independent of a prior and therefore unaffected by a redshift dependent reddening distribution.

5.6. *Gravitational lensing*

Gravitational lensing decreases the mode of the brightness distribution and causes increased dispersion in the Hubble diagram at high redshift. The effect has been discussed in detail in the literature (Sasaki 1987; Linder 1988; Bergström et al. 2000; Holz & Linder 2005). We treat lensing as a statistical phenomenon only, although with the detailed optical and NIR data available for the GOODS field, the mass-distribution in the line-of-sight and hence the lensing (de)magnification may be estimated for individual SNe (Jönsson et al. 2006). Important for this work is that they find no evidence for selection effects (i.e. Malmquist bias) due to lensing of the high redshift SNe.

Considering both strong and weak lensing, Holz & Linder (2005) found that lensing will add a dispersion of $0.093 \times z$ mag, which if the statistics of SNe is large enough, can be approximated as an additional Gaussian error. Here, we added the additional dispersion from gravitational lensing in quadrature to the "constant" systematic dispersion and observational error. This effectively deweights the high redshift SNe. However, only for the highest redshift SNe is the additional uncertainty comparable to that of the intrinsic dispersion.

Flux magnification and demagnification effects due to over- or under-densities of matter near the line of sight

cancel. But one obtains a bias if magnitudes instead of fluxes are used. However, the bias is $0.004 \times z$ mag and therefore still much smaller than the statistical error on the luminosity distance obtained from the ensemble of high redshift SNe. While not yet relevant for this analysis, future high-statistics samples will have to take this effect into account.

Another potential bias is introduced by the 3σ outlier rejection, since the lensing PDF is asymmetric. Using the PDFs of Holz & Linder (2005) we have checked that the bias is never larger than $0.006 \times z$ mag. We take the worst case value of 0.009 magnitude (i.e. for a SNe at $z \approx 1.5$) as a conservative systematic uncertainty for gravitational lensing, since this is still an almost negligible value.

5.7. *Gray intergalactic dust*

The possibility that SNe are dimmed due to hypothetical gray intergalactic dust, as suggested by Aguirre (1999), was constrained by Östman & Mörtsell (2005); Mörtsell & Goobar (2003) by studying the colors of high-redshift quasars. Applying their constraints on intergalactic dust, we find that the cosmological parameters are shifted by about one statistical standard deviation, i.e. for a flat Universe $\Delta\Omega_{\rm M} = -0.03$. This should not be considered a systematic uncertainty, but rather an upper limit on the effect of hypothetical large grains of cosmic dust in the line of sight.

5.8. *Galactic Extinction*

All lightcurve data were corrected for Galactic extinction using the extinction law of Cardelli et al. (1989) using an R_V of 3.1. The $E(B-V)$ values were derived from the sky map of Schlegel et al. (1998) and have a typical statistical error of 10%. For nearby SNe we hence obtain an additional uncertainty of

$$\Delta\mu_B \approx (R_B - \beta) \cdot \sigma\left(E(B-V)\right) \approx 0.2 \cdot E(B-V), \quad (6)$$

where β is the color correction coefficient from Eq. 2. We add this statistical error in quadrature to each nearby SNe. High redshift SNe are measured in redder bands and, since $R_R \approx \beta$, are less affected by Galactic extinction.

There is also a common systematic error of 10% in the overall reddening normalization. The average Galactic $E(B-V)$ for the low redshift sample is 0.063 and we add $0.063 \cdot 0.2 = 0.013$ mag systematic uncertainty to ΔM.

5.9. *Summary of systematic errors*

In our treatment of the above systematic errors we distinguish between systematic errors common between datasets, which are largely of astrophysical nature, and the more observer dependent ones associated with individual samples. Table 5 summarizes what are considered the relevant contributions to the systematic uncertainties in this analysis. They are propagated into the final result through Eq. 5.

Source	common (mag)	sample-dependent (mag)
$\alpha\&\beta$ correction	0.015	-
Contamination	-	0.015
Lightcurve model	0.028	-
Zero point	0.021	0.021
Malmquist bias	-	0.020
Gravitational lensing	-	0.009*
Galactic extinction	0.013	-
Total in mag	$\Delta M = 0.040$	$\Delta M_i = 0.033$

TABLE 5
Most relevant common and sample dependent systematic errors of this analysis (in magnitudes).

6. COSMOLOGICAL FIT RESULTS

Our analysis of cosmological model fits includes both statistical and systematic errors. The individual contributions to the systematic error identified in Table 5 are of very different nature and hence are assumed uncorrelated. We hence obtain the combined systematic error by adding in quadrature the individual contributions. The resulting error was propagated according to the prescription described in Section 5. Our constraints on the matter density $\Omega_{\rm M}$, assuming a flat Universe, are summarized in Table 6. Both statistical (68 % CL) and systematic errors are quoted.

Figure 11 plots our results for the joint fit to the matter density and cosmological constant energy density, $\Omega_{\rm M}$ and Ω_Λ, and the effect of varying the outlier cut, while Fig. 12 illustrates the effects of systematics. For comparison with previous work, Figure 13 shows our joint constraints on $\Omega_{\rm M}$ and Ω_Λ (statistical error only) and the Riess et al. (2007) constraints obtained from the Gold compilation of data primarily from the HZT, SCP and SNLS (Riess et al. 2007) and a recent compilation of Davis et al. (2007), which is based on lightcurve fits from Riess et al. (2007) and Wood-Vasey et al. (2007). The results obtained in this work are consistent with those of previous studies; however, compared to the recent SN fit results of Astier et al. (2006); Riess et al. (2007); Wood-Vasey et al. (2007); Davis et al. (2007), we obtain a 15-30 % reduction in the statistical error.

About half the improvement can be attributed to the new SCP Nearby 1999 SNe. Their impact is evident in the rightmost column of Fig. 13 (as well as in Fig. 14). The impact of these SNe is somewhat larger because the sample has a best-fit systematic uncertainty of zero. If instead one would introduce the requirement that $\sigma_{\rm sys} \geq 0.1$, there would be an increase of about 10% in the uncertainties of the cosmological parameters.

Figure 13 shows the constraints on the equation of state parameter w (assumed constant) and $\Omega_{\rm M}$. A flat Universe was assumed. Again, the constraints are consistent with, but stronger than, those from Riess et al. (2007) and Davis et al. (2007). The current SN data do not provide strong constraints on the equation of state parameter w by itself, since it is to a large extent degenerate with $\Omega_{\rm M}$. However, the degeneracy can be broken by combining with other measurements involving $\Omega_{\rm M}$. Figure 14 shows the constraints obtained from the detection of baryon acoustic oscillations (BAO) (Eisenstein et al. 2005) and from the five year data release of the Wilkinson Microwave Anisotropy Probe (CMB) (Dunkley et al. 2008). The constraints from the CMB data follow from the reduced distance to the surface of last scattering at $z = 1089$ (or shift parameter). It is important to realize that for parameter values far from the concordance model, the shift in the sound horizon must also be taken

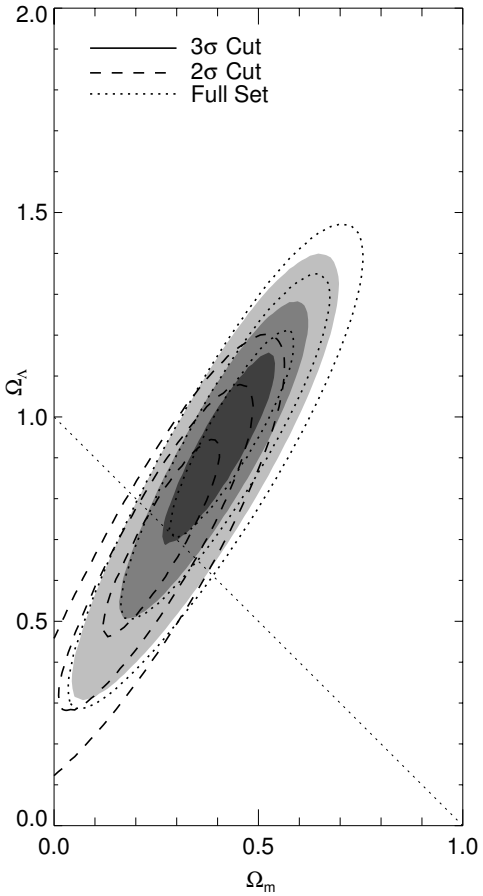

FIG. 11.— 68.3 %, 95.4 % and 99.7% confidence level contours on Ω_Λ and Ω_M plane from the Union SNe set. The result from the robustified set, obtained with a $\sigma_{cut} = 3$ outlier cut, is shown as filled contours. The empty contours are obtained with the full data set (dotted line) and $\sigma_{cut} = 2$ outlier rejected data set (dashed line). As can be seen, outlier rejection shifts the contours along the degenerate axis by as much as 0.5σ towards a flat Universe. In the remaining figures, we refer to the $\sigma_{cut} = 3$ outlier rejected set as the Union set.

into account. The reduced distance R is often written as

$$R_{\rm conc} = (\Omega_{\rm M} H_0^2)^{1/2} \int_0^{1089} dz/H(z), \qquad (7)$$

where the Hubble parameter is $H(z) = H_0 \left[\Omega_{\rm M}(1+z)^3 + (1-\Omega_{\rm M})(1+z)^{3(1+w)}\right]^{1/2}$. The WMAP-5 year CMB data alone yields $R_0 = 1.715 \pm 0.021$ for a fit assuming a constant w (?Lambda-website 2008). Defining the corresponding χ^2 as $\chi^2 = [(R_{\rm conc} - R_0)/\sigma_{R_0}]^2$ one can then deduce constraints on $\Omega_{\rm M}$ and w. However, this assumes a standard matter (and radiation) dominated epoch for calculating the sound horizon. The more proper expression for the shift parameter accounts for deviation in the sound horizon:

$$R = (\Omega_m H_0^2)^{1/2} \int_0^{1089} dz/H(z) \qquad (8)$$
$$\times \left[\int_{1089}^{\infty} dz/\sqrt{\Omega_m (1+z)^3} \Big/ \int_{1089}^{\infty} dz/(H(z)/H_0) \right].$$

Since dark energy is generally negligible at high redshift, the factor in square brackets is usually unity (for example, it deviates from unity by less than 1% even for

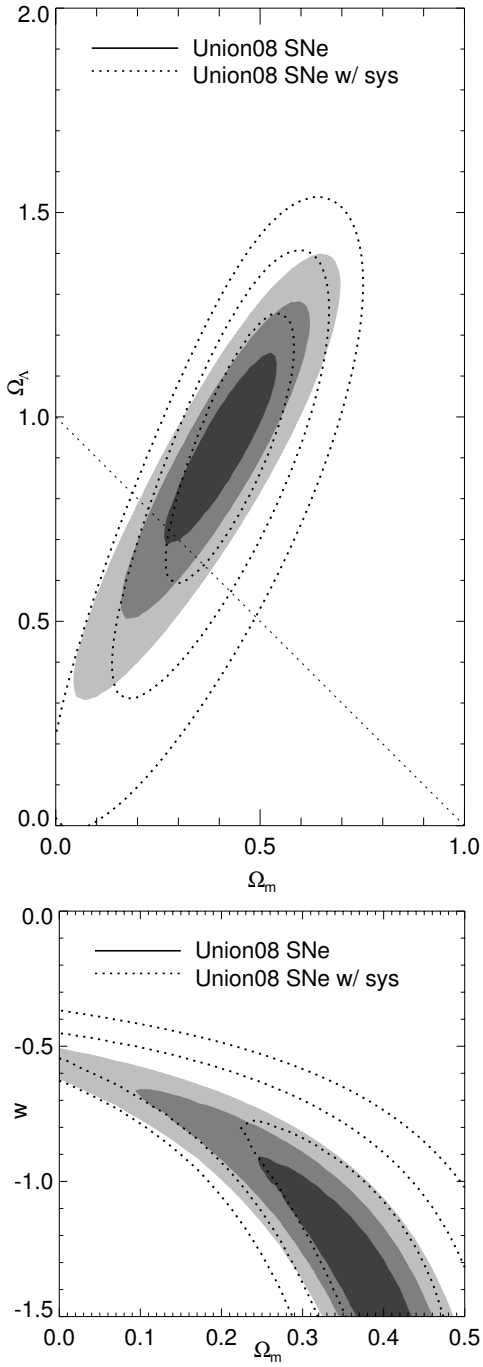

FIG. 12.— Left plot: 68.3 %, 95.4 % and 99.7% confidence level contours on Ω_Λ and $\Omega_{\rm M}$ obtained with the Union set, without (filled contours) and with inclusion of systematic errors (empty contours). The right plot shows the corresponding confidence level contours on the equation of state parameter w and $\Omega_{\rm M}$, assuming a constant w.

$w_0 = -1$, $w_a = 0.9$, i.e. $w(z = 1089) = -0.1$). However, for extreme models that upset the matter dominated behavior at high redshifts, the correction will be important in calculating whether the geometric shift parameter accords with CMB observations (apart from any issue of fitting other observations). Violation of early matter domination causes the "wall" in likelihood apparent in Fig. 16. Also see, for example, Linder & Miquel (2004); Wright (2007).

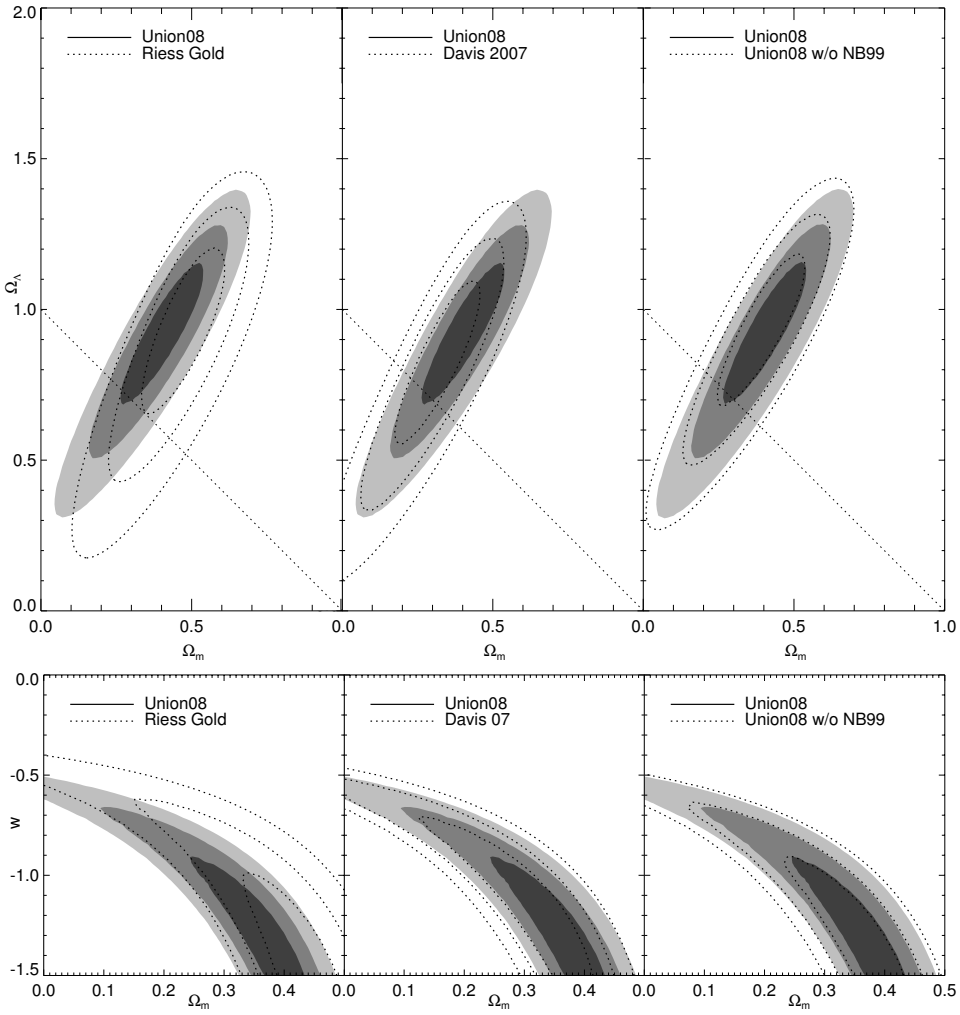

FIG. 13.— 68.3 %, 95.4 % and 99.7% confidence level contours on Ω_Λ and $\Omega_{\rm M}$ (top row) and $\Omega_{\rm M}$ and w (bottom row). The results from the Union set are shown as filled contours. The empty contours in the left column represent the Gold sample (Riess et al. 2004, 2007) and the middle column the constraints from Davis et al. (2007). While our results are statistically consistent with the previous work, the improvements in the constraints on the cosmological parameters are evident. The right column shows the impact of the SCP Nearby 1999 data.

BAO measurements from the SDSS data (Eisenstein et al. 2005) provide a distance constraint at a redshift $z = 0.35$. Percival et al. (2007) have derived BAO distances for $z = 0.2$, in addition to the $z = 035$ SDSS-data point, using the combined data from SDSS and 2dFGRS. However, some points of tension were noted between the data sets (Percival et al 2007, see also Sánchez & Cole (2008)), especially evident for ΛCDM models. We confirm this observation and found that the $z = 0.2$ data point, if combined with SN and CMB data according to the prescription in Appendix A of Percival (2007) leads to an 2.5 sigma inconsistency. Neither the $z = 0.35$ BAO data point from Percival et al. (2007) nor the slightly weaker constraint from Eisenstein et al. (2005) shows such kind of tension. Given the differences between the two data sets, we use the $z = 0.35$ SDSS data point of Eisenstein et al. (2005), but with the caveat that BAO constraints need further clarification. Eisenstein et al. (2005) provides a constraint on the distance parameter A:

$$A(z) = (\Omega_{\rm M} H_0^2)^{1/2} H(z)^{-1/3} z^{-2/3} \left[\int_0^z dz'/H(z')\right]^{2/3} \times \left[\int_{1089}^{\infty} dz/\sqrt{\Omega_m (1+z)^3} \Big/ \int_{1089}^{\infty} dz/(H(z)/H_0)\right], \quad (9)$$

to be $A(z = 0.35) = 0.469 \pm 0.17$. Note that BAO also depend on accurate accounting of the sound horizon and receive the same correction factor shown in brackets in Eq. 9. This results in a similar wall to the acceptable confidence contour reflecting violation of early matter domination. To see that such violation has severe implications, note that most models above the wall have a total linear growth factor a factor ten below the concordance cosmology.

The joint constraints from SN data, BAO, and CMB are shown in Fig. 14 and the corresponding numbers are given in Table 6. As can be seen, the constraints obtained from combining either BAO or CMB with SNe data give consistent results and comparable error bars, while the combination of all three measurements improves only the statistical error. The impact of including systematic er-

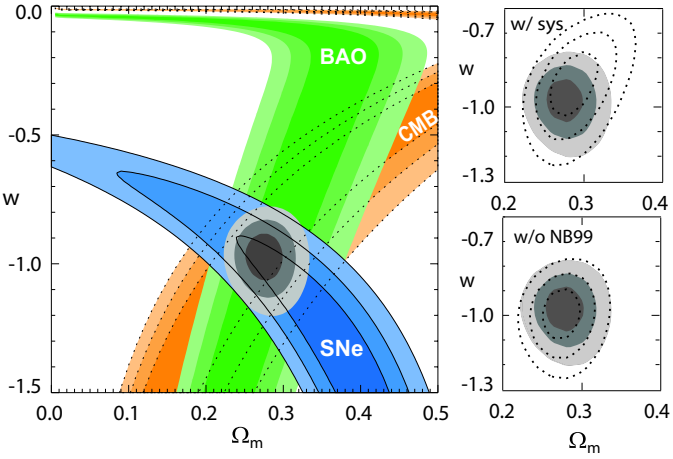

FIG. 14.— 68.3 %, 95.4 % and 99.7% confidence level contours on w and Ω_M, for a flat Universe. The top plot shows the individual constraints from CMB, BAO and the Union SN set, as well as the combined constraints (filled gray contours, statistical errors only). The upper right plot shows the effect of including systematic errors. The lower right plot illustrates the impact of the SCP Nearby 1999 data.

rors (only from SNe, from Eq. 5) is shown in the upper right panel of Fig. 14.

The results quoted so far were derived assuming a flat Universe. Allowing for spatial curvature Ω_k, our constraints from combining SNe, CMB and BAO are consistent with a flat ΛCDM Universe (as seen in Table 6). Fig. 15 shows the corresponding constraints in the $\Omega_M - \Omega_\Lambda$ plane.

Finally, one can attempt to investigate constraints on a redshift dependent equation of state (EOS) parameter $w(z)$. Initially we consider this in terms of

$$w(z) = w_0 + w_a \frac{z}{1+z}, \qquad (10)$$

shown by Linder (2003) to provide excellent approximation to a wide variety of scalar field and other dark energy models. Later, we examine other aspects of time variation of the dark energy EOS. Assuming a flat Universe and combining the Union set with constraints from CMB, we obtain constraints on w_0, the present value of the EOS, and w_a, giving a measure of its time variation, as shown in Fig. 16. (A cosmological constant has $w_0 = -1$, $w_a = 0$.) Due to degeneracies within the EOS and between the EOS and the matter density Ω_M, the SN dataset alone does not give appreciable leverage on the dark energy properties. By adding other measurements, the degeneracies can be broken and currently modest cosmology constraints obtained.

Fig. 16 (left) shows the combination of the SN data with either the CMB constraints or the BAO constraints. The results are similar; note that including either one results in a sharp cut-off at $w_0+w_a = 0$, from the physics as mentioned in regards to Eq. 9. Since $w(z \gg 1) = w_0+w_a$ in this parameterization, any model with more positive high-redshift w will not yield a matter-dominated early Universe, altering the sound horizon in conflict with observations.

Note that BAO do not provide a purely "low" redshift constraint, because implicit within the BAO data analysis, and hence the constraint, is that the high redshift Universe was matter dominated (so the sound horizon

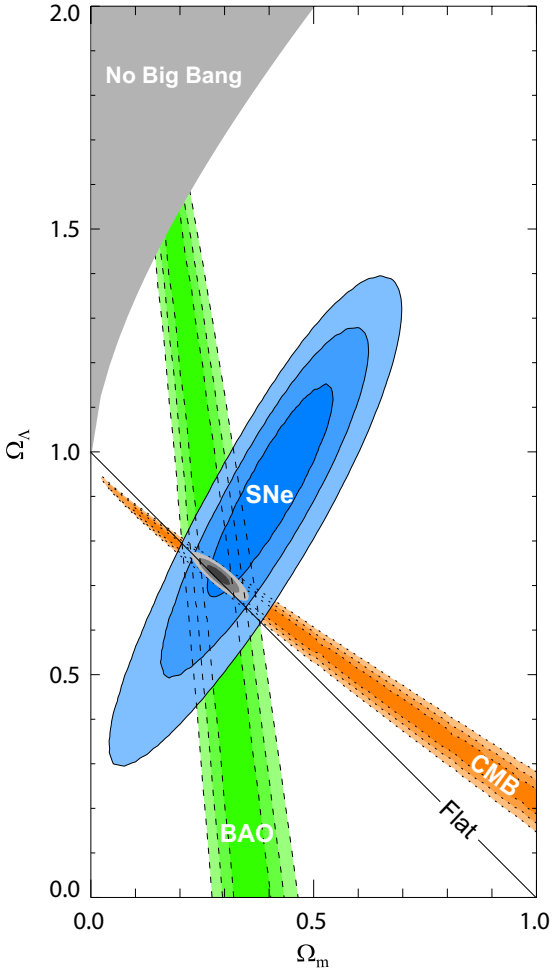

FIG. 15.— 68.3 %, 95.4 % and 99.7% confidence level contours on Ω_Λ and Ω_M obtained from CMB, BAO and the Union SN set, as well as their combination (assuming $w = -1$).

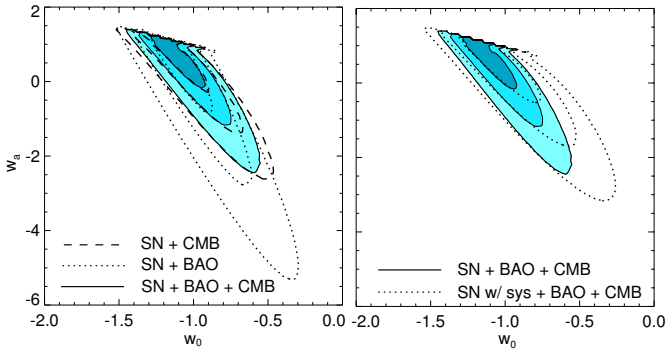

FIG. 16.— 68.3 %, 95.4 % and 99.7% confidence level contours on w_a and w_0 for a flat Universe. Left: The Union SN set was combined with CMB or BAO constraints. Right: Combination of SNe, CMB and BAO data, with and and without systematic uncertainties included. The diagonal line represents $w_0 + w_a = 0$; note how the likelihoods based on observational data remain below it, favoring matter domination at $z \gg 1$.

at decoupling is properly calculated). Thus, one cannot avoid the issue of modeling how the dark energy EOS behaves at high redshifts by using this constraint rather than the CMB. (We differ here from Riess et al. 2007, who treat BAO as a low-redshift constraint.) SN data are especially useful in constraining $w(z)$ because there

Fit	$\Omega_{\rm M}$	Ω_k	w
SNe	$0.287^{+0.029+0.039}_{-0.027-0.036}$	0 (fixed)	-1 (fixed)
SNe+BAO	$0.285^{+0.020+0.011}_{-0.020-0.009}$	0 (fixed)	$-1.011^{+0.076+0.083}_{-0.082-0.087}$
SNe+CMB	$0.265^{+0.022+0.018}_{-0.021-0.016}$	0 (fixed)	$-0.955^{+0.060+0.059}_{-0.066-0.060}$
SNe+BAO+CMB	$0.274^{+0.016+0.013}_{-0.016-0.012}$	0 (fixed)	$-0.969^{+0.059+0.063}_{-0.063-0.066}$
SNe+BAO+CMB	$0.285^{+0.020+0.011}_{-0.019-0.011}$	$-0.009^{+0.009+0.002}_{-0.010-0.003}$	-1 (fixed)
SNe+BAO+CMB	$0.285^{+0.020+0.010}_{-0.020-0.010}$	$-0.010^{+0.010+0.006}_{-0.011-0.004}$	$-1.001^{+0.069+0.080}_{-0.073-0.082}$

TABLE 6

FIT RESULTS ON COSMOLOGICAL PARAMETERS $\Omega_{\rm M}$, Ω_k AND w. THE PARAMETER VALUES ARE FOLLOWED BY THEIR STATISTICAL ($\sigma_{\rm stat}$) AND SYSTEMATIC ($\sigma_{\rm sys}$) UNCERTAINTIES. THE PARAMETER VALUES AND THEIR STATISTICAL ERRORS WERE OBTAINED FROM MINIMIZING THE χ^2 OF EQ. 3. THE FIT TO THE SNE DATA ALONE RESULTS IN A χ^2 OF 310.8 FOR 303 DEGREES OF FREEDOM WITH A $\Delta\chi^2$ OF LESS THAN ONE FOR THE OTHER FITS. THE SYSTEMATIC ERRORS WERE OBTAINED FROM FITTING WITH EXTRA NUISANCE PARAMETERS ACCORDING EQ. 5 AND SUBTRACTING FROM THE RESULTING ERROR, $\sigma_{\rm w/sys}$, THE STATISTICAL ERROR: $\sigma_{\rm sys} = (\sigma^2_{\rm w/sys} - \sigma^2_{\rm stat})^{1/2}$.

is no dependence at all on the high redshift behavior, unlike CMB and BAO data.

As one might expect, because of the different orientations of the confidence contours and the different physics that enters, combining both the CMB and BAO constraints with the SN data clears up the degeneracies somewhat, as seen in Fig. 16, with and without systematics. Inclusion of curvature does not substantially increase the contours.

We emphasize that the wall in w_0-w_a space is not imposed a priori and does not represent a breakdown of the parameterization, but a real physical effect from violating early matter domination. Nevertheless, we can ask what limits could be put on the early dark energy behavior – either its presence or its equation of state – if we do not use the w_0-w_a parameterization. A simple, but general model for $w(z)$ creates a series of redshift bins and assumes w is constant over each bin. The constraints from this are shown in Fig. 17. Note that the data points are correlated.

Riess et al. (2007) made a somewhat similar investigation with the emphasis on the impact of the highest redshift SNe. A difference to the work of Riess et al. (2007) is that we do not decorrelate the constraints in the different redshift bins. While this implies that the bin-wise constraints shown in Fig. 17 are correlated, it ensures that the w-constraints shown for a given bin are confined to the exact redshift range of the bin. If instead one applies a decorrelation procedure, some of the tight constraints from lower redshifts feed through to higher redshifts (i.e. $z > 1$). See de Putter & Linder (2007) for general discussion of this issue. Unlike Riess et al. (2007), we additionally place a w bin at higher redshift than the SN data ($z > 2$), to account for the expansion history of the early Universe, and do not fix w in this bin. The Riess "strong" prior has a fourth bin for $z > 1.8$, but fixes $w = -1$. The "strongest" prior does not have a fourth bin. Forcing either of these behaviors on the $z > 2$ Universe results in unfairly tight constraints and the danger of bias (Linder 2007; de Putter & Linder 2007); in failing to separate the SN bins from those of the CMB and BAO essentially the entire constraint in the redshift $z \gtrsim 1$ bin is from the CMB (see also Wright 2007).

Consider the top row of Fig. 17. These results are for bins with $z < 0.5, 0.5 < z < 1.0, 1.0 < z < 2.0$ and $z > 2.0$. The only constraint that can be concluded from the highest redshift bin is that $w_{[2,\infty]} \lesssim 0$, but this constraint comes entirely from CMB and BAO, which

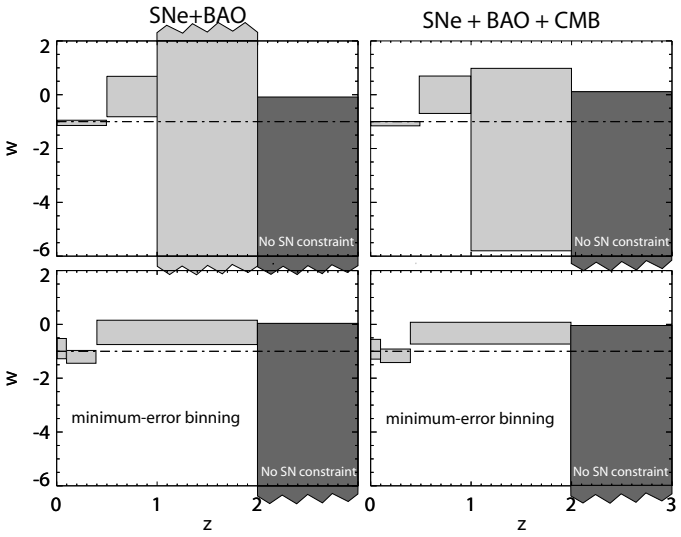

FIG. 17.— 68 % constraints on $w(z)$, where $w(z)$ is assumed to be constant over each redshift bin. The left column combines the Union SN set with BAO constraints only, while the right column includes also constraints from the CMB. The top row illustrates the fact that only extremely weak constraints on the equation of state exist at $z > 1$. The bottom row shows a different binning that minimizes the mean bin error. Note that for $z > 2$ (dark gray-"No SN constraint") only upper limits exist, basically enforcing matter domination, coming from either CMB data or, in the case without CMB data, from requiring substantial structure formation (a linear growth factor within a factor of 10 of that observed).

requires that the early Universe is matter-dominated (see the above discussion of the wall in the $w_a - w_0$ plane). We then look at the $z = 1 - 2$ bin for constraints on w which would be due to the $z > 1$ SNe and we find essentially no constraint.

The lowest redshift bin is constrained to $w_{[0,0.5]} \approx -1 \pm 0.1$. The next bin is compatible with -1, but the central value is high. This deviation from -1 seems to be due to the unexpected brightness (by about 0.1 magnitudes) of the Hubble data at $z > 1$ (see Fig. 10). (Recall that w at some z influences distances at larger redshifts.) We clearly see that to be sensitive to appreciable deviations from $w = -1$ such as 0.1 mags at $z \sim 1$, which is key to constraining theories of dark energy, one requires better statistics for the very high-redshift supernovae (and comparably good systematics).

Given that the strongest constraints on w are contained in the first bin, one might attempt to search for a redshift dependence of w at lower redshifts by changing the bor-

ders of the bins. The smallest errors are obtained roughly with the binning $z < 0.1, 0.1 < z < 0.4, 0.4 < z < 2.0$, and $2.0 < z$. These constraints are shown in the bottom row of Fig. 17. The results are similar to the results from the other binning, with the lowest two bins centered around $w = -1$ and the next bin centered around a more positive value. No significant redshift dependence is observed. Note the tight limit on the $0.4 < z < 2$ bin is *not* saying $w(z > 1) \approx -1$, even approximately, since the leverage on $w(z)$ is coming from the $0.4 < z < 1$ part of the bin (this illustrates the importance of considering multiple binnings).

To sum up, even in combination with current BAO and CMB data, current SN data sets cannot tell us whether an energy density component other than matter existed at $z > 1$, and cannot tell us whether such a component if it existed had an equation of state with negative pressure. In the future, however, SN data that achieves Hubble diagram accuracy of 0.02 mag out to $z = 1.7$ will be able to address these questions and provide independent checks of the $z > 1$ Universe.

Note that while constraints on a possible redshift dependency of w have been shown in Figures 16 and 17, we do not present values for the projected, one-dimensional constraints for several reasons. First, the bounds are still very weak and as a result the error bars show highly non-gaussian errors (as visible in Fig. 16). In addition, our treatment of systematic errors has not been optimized for a redshift dependent w and a potential systematic redshift dependence of the distance modulus is only partially taken into account. As a consequence, the resulting (already large) systematic errors on $w(z)$ would be underestimated.

In this analysis so far we have not excluded any SNe based on extreme values of stretch or color, therefore including also the peculiar class of under-luminous 1991bg-like SNe that are typically associated with small stretch values. After unblinding, in an effort to study the robustness of our results, we have introduced a stretch cut, $s > 0.6$, to eliminate SN1991bg-like SNe from the sample. The most significant consequence of this cut came with the removal of SN 1995ap, a supernova in the Riess et al. (1998) sample. By itself the removal of this one supernova can change the cosmological fit parameters in the $\Omega_{\rm M} - \Omega_\Lambda$ and $\Omega_{\rm M} - w$ planes by nearly 1σ along the more degenerate contour axis (and away from a flat Universe). However, without SN 1995ap, the test for tension between data sets that we applied in Section 4.4 would show the Riess et al. (1998) dataset to be a 3.5σ outlier and one would be forced, unless the tension can be resolved otherwise, to remove the data set from the compilation. The net result of the $s > 0.6$ cut would then be a 0.25σ change in w, Ω_M and Ω_Λ in the direction of the more degenerate contour axis. The results presented in this paper are based on the sample without the stretch cut; however, since the parameters along the direction of the degeneracy are well constrained once CMB or BAO data are added, the combined constraints essentially do not depend on whether or not the stretch cut is applied.

7. CONCLUSION

The cosmological parameter constraints from the Union SN Ia compilation shown in Figures 12, 14, 16 and 17 reflect the current best knowledge of the world's Type Ia supernova datasets. Specifically, in addition to the older data, they include the new datasets of nearby Hubble-flow SNe Ia we presented in this paper, the recent large, homogeneous, high-signal-to-noise SNLS and ESSENCE datasets published by Astier et al. (2006) and Miknaitis et al. (2007) as well as the high redshift supernovae in Riess et al. (2004, 2007). Equally important is that a number of outstanding analysis issues have been addressed that improve the reliability and reduce the biases of the current Union SN Ia compilation, and should stand us in good stead for future compilations. We are making the ingredients and results of the Union compilation available at the associated web site[44] and we intend to provide occasional updates to this as new information becomes available.

Several conclusions can be drawn from the new larger SCP Union SN Ia compilation that could not be approached with smaller datasets. In particular the large statistics can be used to address systematic uncertainties in novel ways.

We test for evolution by subdividing the sample into low-stretch and high-stretch SNe. According to recent evidence (Sullivan et al. 2006) these two samples might be dominated by different progenitor systems (Scannapieco & Bildsten 2005; Mannucci et al. 2006), which are likely to show different evolution. Hence performing consistent but independent cosmology fits for the two subsamples provides a powerful test for potential evolutionary effects. The resulting cosmological fit parameters are found to be consistent. This comparison is particularly meaningful, as the statistical uncertainties from the subsamples are comparable to the total ($stat + sys$) uncertainties obtained from the full sample.

With the larger Union dataset, it is possible to begin to examine the rate of true outliers from the Hubble-plot fit. It appears that the current selection criteria for SNe Ia can find very homogeneous sets of supernovae, but not perfectly homogeneous sets. With these criteria, there are apparently true outliers, at the percent level for the SNLS sample and up to 10% for other samples. The analysis performed here was made robust to outliers, reducing the associated error on cosmological parameters to a level comparable to other sources of systematic error.

Compilations offer the chance to test for observer dependent systematic effects, i.e. tension between the datasets. The blind analysis performed here is an important element in rigorous estimation of systematics. While in general we find a high degree of consistency between samples, we see modest tension when comparing the slope of the Hubble-residuals as a function of redshift, $d\mu/dz$. For the present compilation, our cosmology results are expected to hold within the quoted systematic uncertainties. However, once the homogeneous datasets get larger—and the systematic errors dominate over the statistical ones for the different sets—such tests will become even more important, as they allow one to perform cross-checks with different datasets calibrated in different ways. Future data samples can be added to the Union set, by first blinding the data and then performing a diagnostic analysis similar to the one performed here. Only after any inconsistencies can be resolved, would the new data be unblinded.

[44] http://supernova.lbl.gov/Union

We proposed a scheme to incorporate both sample dependent and common systematic errors. We showed in Section 5 that systematic errors can be approached by treating the systematics as a normal distribution of a parameterized systematic term. We find that the combination of SNe constraints with CMB constraints, due to their larger complementarity with SNe data, results in smaller systematic errors than the combination with BAO constraints. Adding BAO, CMB and SNe constraints leads to yet smaller statistical error bars, while the error bars including systematics do not improve.

The robustness of the detection of the accelerating expansion of the Universe is continually increasing as improved systematics analysis is reinforced by larger SN data sets. The current knowledge of the nature of dark energy is still modest, however, with the uncertainty on the assumed-constant equation of state only under 10% *if* multiple probes are combined. The current "world" estimate presented here employing the full set of current SN data, plus other measurements, gives a best constraint of $w = -0.969^{+0.059}_{-0.063}(\mathrm{stat})^{+0.063}_{-0.066}(\mathrm{sys})$ on a constant EOS parameter w at 68.3% confidence level. However, allowing for time variation in the dark energy equation of state further opens the possibilities for the physics driving the acceleration, consistent with all current observations. In particular, present SN data sets do not have the sensitivity to answer the questions of whether dark energy persists to $z > 1$, or whether it had negative pressure then.

On the positive side, with the more sophisticated analyses and tests carried out here, we still have encountered no limits to the potential use of future, high accuracy SN data as cosmological probes. New data sets for nearby, moderate, and high redshift well-characterized SNe Ia are forthcoming and we expect realistic, robust constraints to catch up with our optimistic hopes on understanding the accelerating Universe.

This work is based on observations made with: the Lick and Keck Observatories; the Cerro Tololo Inter-American Observatory 4-m Blanco Telescope; the Yale/AURA/Lisbon/OSU (YALO) 1-m Telescope at Cerro Tololo Inter-American Observatory; the Apache Point Observatory 3.5-meter telescope, which is owned and operated by the Astrophysical Research Consortium; the WIYN Observatory, owned and operated by the WIYN Consortium, which consists of the University of Wisconsin, Indiana University, Yale University, and the National Optical Astronomy Observatory (NOAO); the Isaac Newton Telescope, which is operated on the island of La Palma by the Isaac Newton Group in the Spanish Observatorio del Roque de los Muchachos of the Instituto de Astrofsica de Canarias; the Nordic Optical Telescope, operated on the island of La Palma jointly by Denmark, Finland, Iceland, Norway, and Sweden, in the Spanish Observatorio del Roque de los Muchachos of the Instituto de Astrofisica de Canarias; and the MDM Observatory 2.4-m Hiltner Telescope. The authors wish to thank the telescope allocation committees and the observatory staffs for their support for the extensive supernova search campaign and followup observations that contributed to the results reported here. In particular, we wish to thank C. Bailyn and S. Tourtellotte for assistance with YALO observations, D. Harner for obtaining WIYN data, and D. Folha and S. Smartt for the INT 2.5-m service observing. For their efforts in the coordinated supernova search, we wish to acknowledge the NEAT search team (E. Helin, S. Pravdo, D. Rabinowitz,and K. Lawrence) at JPL and the Spacewatch program at the University of Arizona (which includes R. S. McMillan, T. Gehrels, J.A. Larsen, J. L. Montani, J. V. Scotti, N. Danzl, and A. Gleason). We also wish to thank B. Schmidt, A. Filippenko, M. Schwartz, A. Gal-Yam, D. Maoz for providing us with early announcements of supernova candidates.

This work was supported in part by the Director, Office of Science, Office of High Energy and Nuclear Physics, U.S. Department of Energy, through contract DE-AC02-05CH11231. This research used resources of the National Energy Research Scientific Computing Center, which is supported by the Office of Science of the U.S. Department of Energy under Contract No. DE-AC02-05CH11231. The use of Portuguese time for the YALO telescope was supported by Fundação para a Ciência e Tecnologia, Portugal and by Project PESO/ESO/P/PRO/1257/98.

M.K. acknowledges support from the Deutsche Forschungsgemeinschaft (DFG). P.E.N. acknowledges support from the US Department of Energy Scientific Discovery through Advanced Computing program under contract DE-FG02-06ER06-04. A.M.M. acknowledges financial support from Fundação para a Ciência e Tecnologia (FCT), Portugal, through project PESO/P/PRO/15139/99.

REFERENCES

Aguirre, A. 1999, ApJ, 525, 583

Aldering, G. 2000, in American Institute of Physics Conference Series, Vol. 522, American Institute of Physics Conference Series, ed. S. S. Holt & W. W. Zhang, 75–84

Aldering, G. 2005, New Astronomy Review, 49, 346

Aldering, G., Nugent, P., Helin, E., Pravdo, S., Rabinowitz, D., Lawrence, K., Kunkel, W., & Phillips, M. 1999, IAU Circ., 7122, 1

Altavilla, G., Fiorentino, G., Marconi, M., Musella, I., Cappellaro, E., Barbon, R., Benetti, S., Pastorello, A., Riello, M., Turatto, M., & Zampieri, L. 2004, MNRAS, 349, 1344

Armstrong, M., & Schwartz, M. 1999, IAU Circ., 7108, 1

Astier, P., Guy, J., Regnault, N., Pain, R., Aubourg, E., Balam, D., Basa, S., Carlberg, R. G., Fabbro, S., Fouchez, D., Hook, I. M., Howell, D. A., Lafoux, H., Neill, J. D., Palanque-Delabrouille, N., Perrett, K., Pritchet, C. J., Rich, J., Sullivan, M., Taillet, R., Aldering, G., Antilogus, P., Arsenijevic, V., Balland, C., Baumont, S., Bronder, J., Courtois, H., Ellis, R. S., Filiol, M., Gonçalves, A. C., Goobar, A., Guide, D., Hardin, D., Lusset, V., Lidman, C., McMahon, R., Mouchet, M., Mourao, A., Perlmutter, S., Ripoche, P., Tao, C., & Walton, N. 2006, A&A, 447, 31

Barris, B. J., Tonry, J. L., Blondin, S., Challis, P., Chornock, R., Clocchiatti, A., Filippenko, A. V., Garnavich, P., Holland, S. T., Jha, S., Kirshner, R. P., Krisciunas, K., Leibundgut, B., Li, W., Matheson, T., Miknaitis, G., Riess, A. G., Schmidt, B. P., Smith, R. C., Sollerman, J., Spyromilio, J., Stubbs, C. W., Suntzeff, N. B., Aussel, H., Chambers, K. C., Connelley, M. S., Donovan, D., Henry, J. P., Kaiser, N., Liu, M. C., Martín, E. L., & Wainscoat, R. J. 2004, ApJ, 602, 571

Bergström, L., Goliath, M., Goobar, A., & Mörtsell, E. 2000, A&A, 358, 13

Bessell, M. S. 1990, PASP, 102, 1181

Blanc, G., Afonso, C., Alard, C., Albert, J. N., Aldering, G., Amadon, A., Andersen, J., Ansari, R., Aubourg, É., Balland, C., Bareyre, P., Beaulieu, J. P., Charlot, X., Conley, A., Coutures, C., Dahlén, T., Derue, F., Fan, X., Ferlet, R., Folatelli, G., Fouqué, P., Garavini, G., Glicenstein, J. F., Goldman, B., Goobar, A., Gould, A., Graff, D., Gros, M., Haissinski, J., Hamadache, C., Hardin, D., Hook, I. M., de Kat, J., Kent, S., Kim, A., Lasserre, T., Le Guillou, L., Lesquoy, É., Loup, C., Magneville, C., Marquette, J. B., Maurice, É., Maury, A., Milsztajn, A., Moniez, M., Mouchet, M., Newberg, H., Nobili, S., Palanque-Delabrouille, N., Perdereau, O., Prévot, L., Rahal, Y. R., Regnault, N., Rich, J., Ruiz-Lapuente, P., Spiro, M., Tisserand, P., Vidal-Madjar, A., Vigroux, L., Walton, N. A., & Zylberajch, S. 2004, A&A, 423, 881

Bohlin, R. C., & Gilliland, R. L. 2004, AJ, 127, 3508

Cardelli, J. A., Clayton, G. C., & Mathis, J. S. 1989, ApJ, 345, 245

Conley, A., Carlberg, R. G., Guy, J., Howell, D. A., Jha, S., Riess, A. G., & Sullivan, M. 2007, ApJ, 664, L13

Conley, A., Goldhaber, G., Wang, L., Aldering, G., Amanullah, R., Commins, E. D., Fadeyev, V., Folatelli, G., Garavini, G., Gibbons, R., Goobar, A., Groom, D. E., Hook, I., Howell, D. A., Kim, A. G., Knop, R. A., Kowalski, M., Kuznetsova, N., Lidman, C., Nobili, S., Nugent, P. E., Pain, R., Perlmutter, S., Smith, E., Spadafora, A. L., Stanishev, V., Strovink, M., Thomas, R. C., & Wood-Vasey, W. M. 2006, ApJ, 644, 1

Davis, T. M., Mörtsell, E., Sollerman, J., Becker, A. C., Blondin, S., Challis, P., Clocchiatti, A., Filippenko, A. V., Foley, R. J., Garnavich, P. M., Jha, S., Krisciunas, K., Kirshner, R. P., Leibundgut, B., Li, W., Matheson, T., Miknaitis, G., Pignata, G., Rest, A., Riess, A. G., Schmidt, B. P., Smith, R. C., Spyromilio, J., Stubbs, C. W., Suntzeff, N. B., Tonry, J. L., Wood-Vasey, W. M., & Zenteno, A. 2007, ApJ, 666, 716

de Putter, R., & Linder, E. V. 2007, arXiv:astro-ph/0710.0373

Dunkley, J., et al. 2008

Eisenstein, D. J., Zehavi, I., Hogg, D. W., Scoccimarro, R., Blanton, M. R., Nichol, R. C., Scranton, R., Seo, H.-J., Tegmark, M., Zheng, Z., Anderson, S. F., Annis, J., Bahcall, N., Brinkmann, J., Burles, S., Castander, F. J., Connolly, A., Csabai, I., Doi, M., Fukugita, M., Frieman, J. A., Glazebrook, K., Gunn, J. E., Hendry, J. S., Hennessy, G., Ivezić, Z., Kent, S., Knapp, G. R., Lin, H., Loh, Y.-S., Lupton, R. H., Margon, B., McKay, T. A., Meiksin, A., Munn, J. A., Pope, A., Richmond, M. W., Schlegel, D., Schneider, D. P., Shimasaku, K., Stoughton, C., Strauss, M. A., SubbaRao, M., Szalay, A. S., Szapudi, I., Tucker, D. L., Yanny, B., & York, D. G. 2005, ApJ, 633, 560

Filippenko, A. V., Li, W. D., Treffers, R. R., & Modjaz, M. 2001, in Astronomical Society of the Pacific Conference Series, Vol. 246, IAU Colloq. 183: Small Telescope Astronomy on Global Scales, ed. B. Paczynski, W.-P. Chen, & C. Lemme, 121–+

Folatelli, G. . 2004, PhD thesis, Stockholm University

Gal-Yam, A., & Maoz, D. 2000, in American Institute of Physics Conference Series, Vol. 522, American Institute of Physics Conference Series, ed. S. S. Holt & W. W. Zhang, 107–110

Gal-Yam, A., Maoz, D., Strolger, L. G., Smith, R. C., Goobar, A., Dahlen, T., Hook, I., Nugent, P. E., Phillips, M., & Lidman, C. 1999, IAU Circ., 7130, 1

Garavini, G., Aldering, G., Amadon, A., Amanullah, R., Astier, P., Balland, C., Blanc, G., Conley, A., Dahlén, T., Deustua, S. E., Ellis, R., Fabbro, S., Fadeyev, V., Fan, X., Folatelli, G., Frye, B., Gates, E. L., Gibbons, R., Goldhaber, G., Goldman, B., Goobar, A., Groom, D. E., Haissinski, J., Hardin, D., Hook, I., Howell, D. A., Kent, S., Kim, A. G., Knop, R. A., Kowalski, M., Kuznetsova, N., Lee, B. C., Lidman, C., Mendez, J., Miller, G. J., Moniez, M., Mouchet, M., Mourão, A., Newberg, H., Nobili, S., Nugent, P. E., Pain, R., Perdereau, O., Perlmutter, S., Quimby, R., Regnault, N., Rich, J., Richards, G. T., Ruiz-Lapuente, P., Schaefer, B. E., Schahmaneche, K., Smith, E., Spadafora, A. L., Stanishev, V., Thomas, R. C., Walton, N. A., Wang, L., & Wood-Vasey, W. M. 2005, AJ, 130, 2278

Garavini, G., Folatelli, G., Goobar, A., Nobili, S., Aldering, G., Amadon, A., Amanullah, R., Astier, P., Balland, C., Blanc, G., Burns, M. S., Conley, A., Dahlén, T., Deustua, S. E., Ellis, R., Fabbro, S., Fan, X., Frye, B., Gates, E. L., Gibbons, R., Goldhaber, G., Goldman, B., Groom, D. E., Haissinski, J., Hardin, D., Hook, I. M., Howell, D. A., Kasen, D., Kent, S., Kim, A. G., Knop, R. A., Lee, B. C., Lidman, C., Mendez, J., Miller, G. J., Moniez, M., Mourão, A., Newberg, H., Nugent, P. E., Pain, R., Perdereau, O., Perlmutter, S., Prasad, V., Quimby, R., Raux, J., Regnault, N., Rich, J., Richards, G. T., Ruiz-Lapuente, P., Sainton, G., Schaefer, B. E., Schahmaneche, K., Smith, E., Spadafora, A. L., Stanishev, V., Walton, N. A., Wang, L., & Wood-Vasey, W. M. 2004, AJ, 128, 387

Garavini, G., Folatelli, G., Nobili, S., Aldering, G., Amanullah, R., Antilogus, P., Astier, P., Blanc, G., Bronder, T., Burns, M. S., Conley, A., Deustua, S. E., Doi, M., Fabbro, S., Fadeyev, V., Gibbons, R., Goldhaber, G., Goobar, A., Groom, D. E., Hook, I., Howell, D. A., Kashikawa, N., Kim, A. G., Kowalski, M., Kuznetsova, N., Lee, B. C., Lidman, C., Mendez, J., Morokuma, T., Motohara, K., Nugent, P. E., Pain, R., Perlmutter, S., Quimby, R., Raux, J., Regnault, N., Ruiz-Lapuente, P., Sainton, G., Schahmaneche, K., Smith, E., Spadafora, A. L., Stanishev, V., Thomas, R. C., Walton, N. A., Wang, L., Wood-Vasey, W. M., & Yasuda, N. 2007, A&A, 470, 411

Garnavich, P. M., Jha, S., Challis, P., Clocchiatti, A., Diercks, A., Filippenko, A. V., Gilliland, R. L., Hogan, C. J., Kirshner, R. P., Leibundgut, B., Phillips, M. M., Reiss, D., Riess, A. G., Schmidt, B. P., Schommer, R. A., Smith, R. C., Spyromilio, J., Stubbs, C., Suntzeff, N. B., Tonry, J., & Carroll, S. M. 1998, ApJ, 509, 74

Germany, L. M., Reiss, D. J., Schmidt, B. P., Stubbs, C. W., & Suntzeff, N. B. 2004, A&A, 415, 863

Goldhaber, G., Groom, D. E., Kim, A., Aldering, G., Astier, P., Conley, A., Deustua, S. E., Ellis, R., Fabbro, S., Fruchter, A. S., Goobar, A., Hook, I., Irwin, M., Kim, M., Knop, R. A., Lidman, C., McMahon, R., Nugent, P. E., Pain, R., Panagia, N., Pennypacker, C. R., Perlmutter, S., Ruiz-Lapuente, P., Schaefer, B., Walton, N. A., & York, T. 2001, ApJ, 558, 359

Gott, J. R. I., Vogeley, M. S., Podariu, S., & Ratra, B. 2001, ApJ, 549, 1

Gunn, J. E., & Stryker, L. L. 1983, ApJS, 52, 121

Guy, J., Astier, P., Baumont, S., Hardin, D., Pain, R., Regnault, N., Basa, S., Carlberg, R. G., Conley, A., Fabbro, S., Fouchez, D., Hook, I. M., Howell, D. A., Perrett, K., Pritchet, C. J., Rich, J., Sullivan, M., Antilogus, P., Aubourg, E., Bazin, G., Bronder, J., Filiol, M., Palanque-Delabrouille, N., Ripoche, P., & Ruhlmann-Kleider, V. 2007, A&A, 466, 11

Guy, J., Astier, P., Nobili, S., Regnault, N., & Pain, R. 2005, A&A, 443, 781

Hamuy, M., Phillips, M. M., Suntzeff, N. B., Schommer, R. A., Maza, J., Antezan, A. R., Wischnjewsky, M., Valladares, G., Muena, C., Gonzales, L. E., Aviles, R., Wells, L. A., Smith, R. C., Navarrete, M., Covarrubias, R., Williger, G. M., Walker, A. R., Layden, A. C., Elias, J. H., Baldwin, J. A., Hernandez, M., Tirado, H., Ugarte, P., Elston, R., Saavedra, N., Barrientos, F., Costa, E., Lira, P., Ruiz, M. T., Anguita, C., Gomez, X., Ortiz, P., della Valle, M., Danziger, J., Storm, J., Kim, Y.-C., Bailyn, C., Rubenstein, E. P., Tucker, D., Cersosimo, S., Mendez, R. A., Siciliano, L., Sherry, W., Chaboyer, B., Koopmann, R. A., Geisler, D., Sarajedini, A., Dey, A., Tyson, N., Rich, R. M., Gal, R., Lamontagne, R., Caldwell, N., Guhathakurta, P., Phillips, A. C., Szkody, P., Prosser, C., Ho, L. C., McMahan, R., Baggley, G., Cheng, K.-P., Havlen, R., Wakamatsu, K., Janes, K., Malkan, M., Baganoff, F., Seitzer, P., Shara, M., Sturch, C., Hesser, J., Hartig, A. N. P., Hughes, J., Welch, D., Williams, T. B., Ferguson, H., Francis, P. J., French, L., Bolte, M., Roth, J., Odewahn, S., Howell, S., & Krzeminski, W. 1996, AJ, 112, 2408

Holz, D. E., & Linder, E. V. 2005, ApJ, 631, 678

Howell, D. A., Sullivan, M., Conley, A., & Carlberg, R. 2007, ApJ, 667, L37

Jha, S., Kirshner, R. P., Challis, P., Garnavich, P. M., Matheson, T., Soderberg, A. M., Graves, G. J. M., Hicken, M., Alves, J. F., Arce, H. G., Balog, Z., Barmby, P., Barton, E. J., Berlind, P., Bragg, A. E., Briceño, C., Brown, W. R., Buckley, J. H., Caldwell, N., Calkins, M. L., Carter, B. J., Concannon, K. D., Donnelly, R. H., Eriksen, K. A., Fabricant, D. G., Falco, E. E., Fiore, F., Garcia, M. R., Gómez, M., Grogin, N. A., Groner, T., Groot, P. J., Haisch, Jr., K. E., Hartmann, L., Hergenrother, C. W., Holman, M. J., Huchra, J. P., Jayawardhana, R., Jerius, D., Kannappan, S. J., Kim, D.-W., Kleyna, J. T., Kochanek, C. S., Koranyi, D. M., Krockenberger, M., Lada, C. J., Luhman, K. L., Luu, J. X., Macri, L. M., Mader, J. A., Mahdavi, A., Marengo, M., Marsden, B. G., McLeod, B. A., McNamara, B. R., Megeath, S. T., Moraru, D., Mossman, A. E., Muench, A. A., Muñoz, J. A., Muzerolle, J., Naranjo, O., Nelson-Patel, K., Pahre, M. A., Patten, B. M., Peters, J., Peters, W., Raymond, J. C., Rines, K., Schild, R. E., Sobczak, G. J., Spahr, T. B., Stauffer, J. R., Stefanik, R. P., Szentgyorgyi, A. H., Tollestrup, E. V., Väisänen, P., Vikhlinin, A., Wang, Z., Willner, S. P., Wolk, S. J., Zajac, J. M., Zhao, P., & Stanek, K. Z. 2006, AJ, 131, 527

Jha, S., Riess, A. G., & Kirshner, R. P. 2007, ApJ, 659, 122

Jönsson, J., Dahlén, T., Goobar, A., Gunnarsson, C., Mörtsell, E., & Lee, K. 2006, ApJ, 639, 991

Kim, A., Regnault, N., Nugent, P., Aldering, G., Dahlen, T., Goobar, A., & Hook, I. 1999a, IAU Circ., 7136, 1

Kim, A., Regnault, N., Nugent, P., Fan, X., Newberg, H., Aldering, G., Deustua, S., Goobar, A., & Hook, I. 1999b, IAU Circ., 7117, 1

Knop, R. A., Aldering, G., Amanullah, R., Astier, P., Blanc, G., Burns, M. S., Conley, A., Deustua, S. E., Doi, M., Ellis, R., Fabbro, S., Folatelli, G., Fruchter, A. S., Garavini, G., Garmond, S., Garton, K., Gibbons, R., Goldhaber, G., Goobar, A., Groom, D. E., Hardin, D., Hook, I., Howell, D. A., Kim, A. G., Lee, B. C., Lidman, C., Mendez, J., Nobili, S., Nugent, P. E., Pain, R., Panagia, N., Pennypacker, C. R., Perlmutter, S., Quimby, R., Raux, J., Regnault, N., Ruiz-Lapuente, P., Sainton, G., Schaefer, B., Schahmaneche, K., Smith, E., Spadafora, A. L., Stanishev, V., Sullivan, M., Walton, N. A., Wang, L., Wood-Vasey, W. M., & Yasuda, N. 2003, ApJ, 598, 102

Krisciunas, K., Hastings, N. C., Loomis, K., McMillan, R., Rest, A., Riess, A. G., & Stubbs, C. 2000, ApJ, 539, 658

Krisciunas, K., Phillips, M. M., Stubbs, C., Rest, A., Miknaitis, G., Riess, A. G., Suntzeff, N. B., Roth, M., Persson, S. E., & Freedman, W. L. 2001, AJ, 122, 1616

Krisciunas, K., Phillips, M. M., Suntzeff, N. B., Persson, S. E., Hamuy, M., Antezana, R., Candia, P., Clocchiatti, A., DePoy, D. L., Germany, L. M., Gonzalez, L., Gonzalez, S., Krzeminski, W., Maza, J., Nugent, P. E., Qiu, Y., Rest, A., Roth, M., Stritzinger, M., Strolger, L.-G., Thompson, I., Williams, T. B., & Wischnjewsky, M. 2004a, AJ, 127, 1664

Krisciunas, K., Suntzeff, N. B., Phillips, M. M., Candia, P., Prieto, J. L., Antezana, R., Chassagne, R., Chen, H.-W., Dickinson, M., Eisenhardt, P. R., Espinoza, J., Garnavich, P. M., González, D., Harrison, T. E., Hamuy, M., Ivanov, V. D., Krzemiński, W., Kulesa, C., McCarthy, P., Moro-Martín, A., Muena, C., Noriega-Crespo, A., Persson, S. E., Pinto, P. A., Roth, M., Rubenstein, E. P., Stanford, S. A., Stringfellow, G. S., Zapata, A., Porter, A., & Wischnjewsky, M. 2004b, AJ, 128, 3034

Lambda-website. 2008, http://lambda.gsfc.nasa.gov/product/map/dr3/paramete

Landolt, A. U. 1992, AJ, 104, 340

Linder, E. V. 1988, A&A, 206, 190

—. 2003, Physical Review Letters, 90, 091301

—. 2006, Phys. Rev. D, 74, 103518

—. 2007, arXiv:astro-ph/0708.0024

Linder, E. V., & Miquel, R. 2004, Phys. Rev. D, 70, 123516

Mannucci, F., Della Valle, M., & Panagia, N. 2006, MNRAS, 370, 773

Miknaitis, G., Pignata, G., Rest, A., Wood-Vasey, W. M., Blondin, S., Challis, P., Smith, R. C., Stubbs, C. W., Suntzeff, N. B., Foley, R. J., Matheson, T., Tonry, J. L., Aguilera, C., Blackman, J. W., Becker, A. C., Clocchiatti, A., Covarrubias, R., Davis, T. M., Filippenko, A. V., Garg, A., Garnavich, P. M., Hicken, M., Jha, S., Krisciunas, K., Kirshner, R. P., Leibundgut, B., Li, W., Miceli, A., Narayan, G., Prieto, J. L., Riess, A. G., Salvo, M. E., Schmidt, B. P., Sollerman, J., Spyromilio, J., & Zenteno, A. 2007, ApJ, 666, 674

Mörtsell, E., & Goobar, A. 2003, Journal of Cosmology and Astro-Particle Physics, 9, 9

Nugent, P., Aldering, G., & Phillips, M. M. 1999a, IAU Circ., 7133, 1

Nugent, P., Kim, A., & Perlmutter, S. 2002, PASP, 114, 803

Nugent, P., McMillan, R. S., Gehrels, T., Larsen, J. A., Montani, J. L., Scotti, J. V., Danzl, N., Gleason, A., & Aldering, G. 1999b, IAU Circ., 7134, 1

—. 1999c, IAU Circ., 7134, 1

Östman, L., & Mörtsell, E. 2005, Journal of Cosmology and Astro-Particle Physics, 2, 5

Parodi, B. R., Saha, A., Sandage, A., & Tammann, G. A. 2000, ApJ, 540, 634

Percival, W. J., Cole, S., Eisenstein, D. J., Nichol, R. C., Peacock, J. A., Pope, A. C., & Szalay, A. S. 2007, MNRAS, 381, 1053

Perlmutter, S., Aldering, G., della Valle, M., Deustua, S., Ellis, R. S., Fabbro, S., Fruchter, A., Goldhaber, G., Groom, D. E., Hook, I. M., Kim, A. G., Kim, M. Y., Knop, R. A., Lidman, C., McMahon, R. G., Nugent, P., Pain, R., Panagia, N., Pennypacker, C. R., Ruiz-Lapuente, P., Schaefer, B., & Walton, N. 1998, Nature, 391, 51

Perlmutter, S., Aldering, G., Goldhaber, G., Knop, R. A., Nugent, P., Castro, P. G., Deustua, S., Fabbro, S., Goobar, A., Groom, D. E., Hook, I. M., Kim, A. G., Kim, M. Y., Lee, J. C., Nunes, N. J., Pain, R., Pennypacker, C. R., Quimby, R., Lidman, C., Ellis, R. S., Irwin, M., McMahon, R. G., Ruiz-Lapuente, P., Walton, N., Schaefer, B., Boyle, B. J., Filippenko, A. V., Matheson, T., Fruchter, A. S., Panagia, N., Newberg, H. J. M., Couch, W. J., & The Supernova Cosmology Project. 1999, ApJ, 517, 565

Perlmutter, S., Gabi, S., Goldhaber, G., Goobar, A., Groom, D. E., Hook, I. M., Kim, A. G., Kim, M. Y., Lee, J. C., Pain, R., Pennypacker, C. R., Small, I. A., Ellis, R. S., McMahon, R. G., Boyle, B. J., Bunclark, P. S., Carter, D., Irwin, M. J., Glazebrook, K., Newberg, H. J. M., Filippenko, A. V., Matheson, T., Dopita, M., Couch, W. J., & The Supernova Cosmology Project. 1997, ApJ, 483, 565

Perlmutter, S., & Schmidt, B. P. 2003, in Lecture Notes in Physics, Berlin Springer Verlag, Vol. 598, Supernovae and Gamma-Ray Bursters, ed. K. Weiler, 195–217

Phillips, M. M. 1993, ApJ, 413, L105

Pravdo, S. H., Rabinowitz, D. L., Helin, E. F., Lawrence, K. J., Bambery, R. J., Clark, C. C., Groom, S. L., Levin, S., Lorre, J., Shaklan, S. B., Kervin, P., Africano, J. A., Sydney, P., & Soohoo, V. 1999, AJ, 117, 1616

Qiao, Q. Y., Wei, J. Y., Qiu, Y. L., & Hu, J. Y. 1999, IAU Circ., 7109, 3

Reiss, D., Sabine, S., Germany, L., & Schmidt, B. 1999, IAU Circ., 7124, 2

Rengstorf, A. W., Mufson, S. L., Abad, C., Adams, B., Andrews, P., Bailyn, C., Baltay, C., Bongiovanni, A., Briceño, C., Bruzual, G., Coppi, P., Della Prugna, F., Emmet, W., Ferrín, I., Fuenmayor, F., Gebhard, M., Hernández, J., Honeycutt, R. K., Magris, G., Musser, J., Naranjo, O., Oemler, A., Rosenzweig, P., Sabbey, C. N., Sánchez, G., Sánchez, G., Schaefer, B., Schenner, H., Sinnott, J., Snyder, J. A., Sofia, S., Stock, J., van Altena, W., & Vivas, A. K. 2004, ApJ, 606, 741

Riess, A. G., Filippenko, A. V., Challis, P., Clocchiatti, A., Diercks, A., Garnavich, P. M., Gilliland, R. L., Hogan, C. J., Jha, S., Kirshner, R. P., Leibundgut, B., Phillips, M. M., Reiss, D., Schmidt, B. P., Schommer, R. A., Smith, R. C., Spyromilio, J., Stubbs, C., Suntzeff, N. B., & Tonry, J. 1998, AJ, 116, 1009

Riess, A. G., Kirshner, R. P., Schmidt, B. P., Jha, S., Challis, P., Garnavich, P. M., Esin, A. A., Carpenter, C., Grashius, R., Schild, R. E., Berlind, P. L., Huchra, J. P., Prosser, C. F., Falco, E. E., Benson, P. J., Briceño, C., Brown, W. R., Caldwell, N., dell'Antonio, I. P., Filippenko, A. V., Goodman, A. A., Grogin, N. A., Groner, T., Hughes, J. P., Green, P. J., Jansen, R. A., Kleyna, J. T., Luu, J. X., Macri, L. M., McLeod, B. A., McLeod, K. K., McNamara, B. R., McLean, B., Milone, A. A. E., Mohr, J. J., Moraru, D., Peng, C., Peters, J., Prestwich, A. H., Stanek, K. Z., Szentgyorgyi, A., & Zhao, P. 1999, AJ, 117, 707

Riess, A. G., Strolger, L.-G., Casertano, S., Ferguson, H. C., Mobasher, B., Gold, B., Challis, P. J., Filippenko, A. V., Jha, S., Li, W., Tonry, J., Foley, R., Kirshner, R. P., Dickinson, M., MacDonald, E., Eisenstein, D., Livio, M., Younger, J., Xu, C., Dahlén, T., & Stern, D. 2007, ApJ, 659, 98

Riess, A. G., Strolger, L.-G., Tonry, J., Casertano, S., Ferguson, H. C., Mobasher, B., Challis, P., Filippenko, A. V., Jha, S., Li, W., Chornock, R., Kirshner, R. P., Leibundgut, B., Dickinson, M., Livio, M., Giavalisco, M., Steidel, C. C., Benítez, T., & Tsvetanov, Z. 2004, ApJ, 607, 665

Ruiz-Lapuente, P. 2007, Class. Quant. Grav., 24, 91

Sánchez, A. G., & Cole, S. 2008, MNRAS, 243

Sasaki, M. 1987, MNRAS, 228, 653

Scannapieco, E., & Bildsten, L. 2005, ApJ, 629, L85

Schlegel, D. J., Finkbeiner, D. P., & Davis, M. 1998, ApJ, 500, 525

Schmidt, B. P., Suntzeff, N. B., Phillips, M. M., Schommer, R. A., Clocchiatti, A., Kirshner, R. P., Garnavich, P., Challis, P., Leibundgut, B., Spyromilio, J., Riess, A. G., Filippenko, A. V., Hamuy, M., Smith, R. C., Hogan, C., Stubbs, C., Diercks, A., Reiss, D., Gilliland, R., Tonry, J., Maza, J., Dressler, A., Walsh, J., & Ciardullo, R. 1998, ApJ, 507, 46

Stritzinger, M., Hamuy, M., Suntzeff, N. B., Smith, R. C., Phillips, M. M., Maza, J., Strolger, L.-G., Antezana, R., González, L., Wischnjewsky, M., Candia, P., Espinoza, J., González, D., Stubbs, C., Becker, A. C., Rubenstein, E. P., & Galaz, G. 2002, AJ, 124, 2100

Stritzinger, M., Suntzeff, N. B., Hamuy, M., Challis, P., Demarco, R., Germany, L., & Soderberg, A. M. 2005, PASP, 117, 810

Strolger, L.-G. 2003, PhD thesis, AA(UNIVERSITY OF MICHIGAN)

Strolger, L. G., Ho, L. C., Covarrubias, R., Hamuy, M., Smith, R. C., Aldering, G., Knop, R., York, T., Kim, M., Filippenko, A. V., Li, W. D., & Schmidt, B. 1999a, IAU Circ., 7125, 1

Strolger, L. G., Smith, R. C., Nugent, P., & Phillips, M. 1999b, IAU Circ., 7131, 1

Strolger, L.-G., Smith, R. C., Suntzeff, N. B., Phillips, M. M., Aldering, G., Nugent, P., Knop, R., Perlmutter, S., Schommer, R. A., Ho, L. C., Hamuy, M., Krisciunas, K., Germany, L. M., Covarrubias, R., Candia, P., Athey, A., Blanc, G., Bonacic, A., Bowers, T., Conley, A., Dahlén, T., Freedman, W., Galaz, G., Gates, E., Goldhaber, G., Goobar, A., Groom, D., Hook, I. M., Marzke, R., Mateo, M., McCarthy, P., Méndez, J., Muena, C., Persson, S. E., Quimby, R., Roth, M., Ruiz-Lapuente, P., Seguel, J., Szentgyorgyi, A., von Braun, K., Wood-Vasey, W. M., & York, T. 2002, AJ, 124, 2905

Strovink, M. 2007, arXiv:astro-ph/0705.0726

Stubbs, C. W., & Tonry, J. L. 2006, ApJ, 646, 1436

Sullivan, M., Ellis, R. S., Aldering, G., Amanullah, R., Astier, P., Blanc, G., Burns, M. S., Conley, A., Deustua, S. E., Doi, M., Fabbro, S., Folatelli, G., Fruchter, A. S., Garavini, G., Gibbons, R., Goldhaber, G., Goobar, A., Groom, D. E., Hardin, D., Hook, I., Howell, D. A., Irwin, M., Kim, A. G., Knop, R. A., Lidman, C., McMahon, R., Mendez, J., Nobili, S., Nugent, P. E., Pain, R., Panagia, N., Pennypacker, C. R., Perlmutter, S., Quimby, R., Raux, J., Regnault, N., Ruiz-Lapuente, P., Schaefer, B., Schahmaneche, K., Spadafora, A. L., Walton, N. A., Wang, L., Wood-Vasey, W. M., & Yasuda, N. 2003, MNRAS, 340, 1057

Sullivan, M., Le Borgne, D., Pritchet, C. J., Hodsman, A., Neill, J. D., Howell, D. A., Carlberg, R. G., Astier, P., Aubourg, E., Balam, D., Basa, S., Conley, A., Fabbro, S., Fouchez, D., Guy, J., Hook, I., Pain, R., Palanque-Delabrouille, N., Perrett, K., Regnault, N., Rich, J., Taillet, R., Baumont, S., Bronder, J., Ellis, R. S., Filiol, M., Lusset, V., Perlmutter, S., Ripoche, P., & Tao, C. 2006, ApJ, 648, 868

Suntzeff, N. B. 2000, in American Institute of Physics Conference Series, Vol. 522, American Institute of Physics Conference Series, ed. S. S. Holt & W. W. Zhang, 65–74

Tonry, J. L., Schmidt, B. P., Barris, B., Candia, P., Challis, P., Clocchiatti, A., Coil, A. L., Filippenko, A. V., Garnavich, P., Hogan, C., Holland, S. T., Jha, S., Kirshner, R. P., Krisciunas, K., Leibundgut, B., Li, W., Matheson, T., Phillips, M. M., Riess, A. G., Schommer, R., Smith, R. C., Sollerman, J., Spyromilio, J., Stubbs, C. W., & Suntzeff, N. B. 2003, ApJ, 594, 1

Tripp, R. 1998, A&A, 331, 815

Tripp, R., & Branch, D. 1999, ApJ, 525, 209

Wang, L., Strovink, M., Conley, A., Goldhaber, G., Kowalski, M., Perlmutter, S., & Siegrist, J. 2006, ApJ, 641, 50

Wood-Vasey, W. M., Miknaitis, G., Stubbs, C. W., Jha, S., Riess, A. G., Garnavich, P. M., Kirshner, R. P., Aguilera, C., Becker, A. C., Blackman, J. W., Blondin, S., Challis, P., Clocchiatti, A., Conley, A., Covarrubias, R., Davis, T. M., Filippenko, A. V., Foley, R. J., Garg, A., Hicken, M., Krisciunas, K., Leibundgut, B., Li, W., Matheson, T., Miceli, A., Narayan, G., Pignata, G., Prieto, J. L., Rest, A., Salvo, M. E., Schmidt, B. P., Smith, R. C., Sollerman, J., Spyromilio, J., Tonry, J. L., Suntzeff, N. B., & Zenteno, A. 2007, ApJ, 666, 694

Wright, E. L. 2007, ApJ, 664, 633

Yao, W. M., et al. 2006, J. Phys., G33, 1

APPENDIX

INSTRUMENTS AND COLOR TERMS

Telescope & Instrument	c_b^{bv}	c_v^{bv}	c_r^{vr}	c_i^{vi}
CTIO 1.5m SITE2K6	-0.095 (0.003)	0.029 (0.001)	0.028 (0.002)	0.018 (0.001)
CTIO 1.5m TK1	-0.017 (0.002)	0.037 (0.001)	0.026 (0.002)	0.015 (0.001)
CTIO 0.9m TK2	-0.097 (0.005)	0.016 (0.002)	0.006 (0.004)	0.022 (0.002)
DANISH DFOSC	0.133 (0.002)	0.033 (0.001)	0.067 (0.001)	-0.000 (0.3001)
JKT Tek1	0.055 (0.006)	0.020 (0.004)	0.030 (0.008)	0.053 (0.007)
LICK 1m DEWAR2	0.094 (0.007)	-0.026 (0.007)	-0.052 (0.007)	0.018 (0.004)
LICK 1m DEWAR5	0.226 (0.033)	-0.073 (0.016)	-0.106 (0.007)	0.034 (0.002)
YALO ANDICAM	0.094 (0.002)	-0.035 (0.001)	0.373 (0.002)	-0.041 (0.001)
ESO 3.6m EFOSC	0.048 (0.005)	0.048 (0.002)	0.048 (0.002)	-0.010 (0.001)
KPNO 2.1m T1KA	0.103 (0.006)	-0.021 (0.002)	0.029 (0.007)	0.023 (0.002)
CFHT STIS2	0.105 (0.009)	0.002 (0.009)	-0.079 (0.005)	0.043 (0.002)
WIYN S2KB	0.059 (0.019)	-0.002 (0.019)	-0.018 (0.035)	0.016 (0.015)
MARLY	-	-	-0.296 (0.003)	-0.017 (0.002)

TABLE A1
Color term for instruments and bands.

Instrument	$\Delta\lambda_B$(Å)	$\Delta\lambda_V$(Å)	$\Delta\lambda_R$(Å)	$\Delta\lambda_I$(Å)
CTIO 1.5m SITE2K6	-20	0	-30	80
CTIO 1.5m SITE2K6 (small)	-20	0	-30	90
CTIO 1.5m TK1	10	-10	-40	90
CTIO 0.9m TK2	-10	-10	-10	-10
DANISH DFOSC	100	30	30	50
JKT Tek1	0	-20	-50	60
LICK 1 m DEWAR5 (small)	90	-10	-30	-40
LICK 1m DEWAR2	90	10	-10	0
LICK 1m DEWAR5	100	-30	-40	0
YALO ANDICAM	10	-20	-340	-50
ESO 3.6m EFOSC	20	-20	0	50
KPNO 2.1m T1KA	-30	-30	-40	-60
CFHT STIS2	-70	-10	-100	-50

TABLE A2
The applied shifts in Angstroms of the pass-bands, which are needed to reproduce the colors of the observed standard and field stars.

TERTIARY STANDARD STAR CATALOG

TABLE B1
Coordinates and magnitudes of tertiary calibration stars.

#	Ra	Dec	V	B-V	V-R	V-I
			SN 1999aa			
1	08:27:37.43	21:31:18.8	14.495(0.003)	0.5145(0.006)	0.3005(0.005)	0.6109(0.006)
2	08:27:41.27	21:25:01.9	14.978(0.006)	0.6927(0.013)	0.4188(0.004)	0.2622(0.008)
3	08:28:02.64	21:33:56.1	14.817(0.005)	0.9347(0.014)	0.4969(0.004)	0.1772(0.012)
4	08:27:38.16	21:29:54.5	15.115(0.004)	0.6558(0.008)	0.4143(0.004)	0.7879(0.006)
5	08:27:47.99	21:33:01.1	15.550(0.007)	0.5243(0.010)	0.3240(0.005)	0.6872(0.007)
6	08:27:44.64	21:31:11.6	15.382(0.004)	0.7130(0.010)	0.4010(0.004)	0.7809(0.007)
7	08:27:48.47	21:33:20.1	15.575(0.008)	0.5614(0.016)	0.3434(0.006)	0.7287(0.008)
8	08:27:21.11	21:29:17.8	15.438(0.007)	0.7989(0.015)	0.4610(0.005)	0.8839(0.007)
9	08:27:55.51	21:24:46.4	15.693(0.008)	0.6203(0.018)	0.3835(0.006)	0.8045(0.008)
10	08:27:29.04	21:27:07.9	15.514(0.006)	0.8045(0.013)	0.4345(0.005)	0.6378(0.008)
11	08:27:37.92	21:26:48.1	15.576(0.005)	0.7630(0.012)	0.4337(0.005)	0.7750(0.009)
12	08:27:40.80	21:27:20.8	15.833(0.006)	0.8071(0.013)	0.4834(0.005)	0.9523(0.007)
13	08:27:19.19	21:27:01.8	16.134(0.010)	0.5442(0.021)	0.3412(0.007)	0.6888(0.011)
14	08:27:21.59	21:26:25.4	16.285(0.010)	0.5031(0.018)	0.3226(0.008)	0.6664(0.012)
15	08:27:32.64	21:23:15.3	16.206(0.010)	0.6747(0.023)	0.4123(0.007)	0.8274(0.011)
			SN 1999ao			
1	06:27:36.74	−03:53:38.3	15.107(0.002)	0.6067(0.004)	0.3511(0.003)	0.6784(0.003)
2	06:27:41.40	−03:53:22.1	15.502(0.002)	0.6906(0.005)	0.4015(0.003)	0.7726(0.003)
3	06:27:22.63	−03:53:38.7	15.508(0.002)	0.7517(0.005)	0.4147(0.003)	0.7974(0.003)

TABLE B1
Coordinates and magnitudes of tertiary calibration stars.

4	06:27:25.20	−03:48:25.9	16.079(0.003)	0.6060(0.006)	0.3418(0.003)	0.6923(0.004)
5	06:27:37.10	−03:53:12.8	16.208(0.003)	0.6375(0.007)	0.3601(0.003)	0.7146(0.005)
6	06:27:28.36	−03:49:49.4	16.157(0.003)	0.7476(0.007)	0.4128(0.003)	0.8109(0.004)
7	06:27:40.34	−03:50:28.6	16.267(0.003)	0.7019(0.008)	0.3920(0.004)	0.7670(0.005)
8	06:27:37.72	−03:50:36.5	16.389(0.003)	0.5809(0.008)	0.3479(0.004)	0.7040(0.005)
9	06:27:35.75	−03:50:50.9	15.908(0.003)	1.2193(0.008)	0.7316(0.003)	1.3661(0.003)
10	06:27:43.29	−03:48:58.3	16.436(0.003)	0.7252(0.009)	0.3919(0.004)	0.7779(0.005)
11	06:27:29.13	−03:50:47.7	16.541(0.003)	0.9069(0.009)	0.5084(0.004)	0.9881(0.005)
12	06:27:24.96	−03:53:06.0	17.008(0.004)	0.5529(0.010)	0.3218(0.005)	0.6624(0.006)
13	06:27:14.32	−03:51:15.4	17.007(0.004)	0.6639(0.010)	0.3674(0.005)	0.7494(0.006)
14	06:27:24.38	−03:52:16.6	17.115(0.004)	0.5890(0.010)	0.3449(0.005)	0.7006(0.007)
15	06:27:42.83	−03:50:36.5	16.486(0.004)	1.3436(0.012)	0.7711(0.004)	1.4946(0.004)
			SN 1999ar			
1	09:20:08.21	00:30:33.4	16.171(0.001)	0.8004(0.006)	0.4723(0.005)	0.9351(0.008)
2	09:20:17.99	00:35:12.8	16.686(0.001)	0.9286(0.007)	0.5630(0.003)	1.0558(0.007)
3	09:20:20.64	00:35:36.9	17.091(0.001)	1.1732(0.009)	0.7022(0.004)	1.2897(0.008)
4	09:20:10.56	00:31:24.5	18.259(0.002)	0.4198(0.011)	0.2998(0.007)	0.6285(0.019)
5	09:20:03.12	00:35:33.3	17.243(0.002)	1.5085(0.013)	0.9605(0.004)	1.9942(0.007)
6	09:20:19.20	00:35:00.2	18.145(0.002)	0.6676(0.012)	0.4272(0.007)	0.8714(0.016)
7	09:20:05.28	00:33:09.0	18.433(0.003)	0.4290(0.013)	0.2966(0.008)	0.6377(0.021)
8	09:20:22.79	00:31:52.6	17.664(0.002)	1.4364(0.014)	0.8927(0.004)	1.7588(0.008)
9	09:20:05.76	00:31:13.7	18.120(0.002)	1.0351(0.014)	0.6051(0.006)	1.1305(0.014)
10	09:20:12.00	00:33:15.8	18.505(0.002)	0.7828(0.015)	0.4759(0.008)	0.9108(0.019)
11	09:20:16.32	00:30:27.7	18.981(0.004)	0.5168(0.018)	0.3627(0.011)	0.7139(0.027)
12	09:20:12.95	00:32:35.5	18.296(0.002)	1.4334(0.018)	0.9206(0.006)	1.8531(0.011)
13	09:20:26.16	00:31:35.7	19.072(0.003)	0.7714(0.019)	0.4754(0.011)	0.9423(0.024)
14	09:20:29.04	00:31:21.7	19.606(0.006)	0.2868(0.022)	0.4442(0.016)	0.8304(0.041)
15	09:20:23.04	00:36:08.3	19.123(0.004)	0.8993(0.021)	0.5386(0.011)	1.0421(0.023)
			SN 1999aw			
1	11:1:27.12	−06:05:58.5	15.056(0.002)	0.5450(0.004)	0.3425(0.004)	0.6843(0.005)
2	11:1:25.79	−06:06:15.4	15.655(0.003)	0.9432(0.006)	0.5452(0.004)	1.0382(0.006)
3	11:1:47.03	−06:07:33.2	16.245(0.003)	0.8172(0.007)	0.4892(0.004)	0.9397(0.007)
4	11:1:39.60	−06:07:01.6	16.648(0.004)	0.5704(0.007)	0.3487(0.006)	0.6935(0.009)
5	11:1:28.79	−06:06:05.4	17.380(0.006)	0.5567(0.011)	0.3747(0.008)	0.7612(0.014)
6	11:1:28.55	−06:07:33.9	17.492(0.006)	0.9241(0.014)	0.5201(0.008)	0.9968(0.013)
7	11:1:37.68	−06:05:28.6	17.593(0.006)	0.8457(0.013)	0.4903(0.008)	0.9323(0.013)
8	11:1:40.32	−06:04:47.6	17.831(0.007)	0.7261(0.014)	0.4306(0.009)	0.8378(0.015)
9	11:1:26.40	−06:07:54.8	18.212(0.009)	0.5630(0.016)	0.3575(0.013)	0.7299(0.021)
10	11:1:26.03	−06:04:48.0	18.204(0.009)	0.6604(0.017)	0.4117(0.013)	0.8060(0.021)
11	11:1:37.68	−06:05:58.9	18.479(0.009)	0.6983(0.019)	0.4017(0.013)	0.8037(0.021)
12	11:1:34.80	−06:08:40.9	18.547(0.009)	0.7571(0.019)	0.4580(0.013)	0.9350(0.020)
13	11:1:46.79	−06:05:35.1	18.930(0.012)	0.5160(0.021)	0.3654(0.016)	0.7138(0.028)
14	11:1:42.00	−06:04:25.3	20.010(0.020)	0.4755(0.034)	0.3571(0.027)	0.6634(0.046)
15	11:1:24.48	−06:07:03.7	19.726(0.019)	1.0304(0.046)	0.5975(0.024)	1.1836(0.035)
			SN 1999bi			
1	11:1:23.04	−01:45:07.9	16.239(0.002)	0.6816(0.012)	0.4285(0.006)	0.8460(0.003)
2	11:1:08.64	−01:47:23.6	16.602(0.003)	0.6566(0.015)	0.4065(0.005)	0.7533(0.003)
3	11:1:14.40	−01:42:15.8	16.571(0.003)	0.7183(0.014)	0.4343(0.005)	0.8341(0.006)
4	11:1:29.51	−01:48:40.6	17.097(0.004)	0.7244(0.025)	0.4351(0.007)	0.7601(0.008)
5	11:1:14.64	−01:43:52.6	17.590(0.004)	0.6290(0.022)	0.4239(0.007)	0.7588(0.005)
6	11:1:16.55	−01:44:42.3	17.780(0.005)	0.6009(0.024)	0.4070(0.008)	0.7334(0.005)
7	11:1:14.15	−01:42:33.8	17.068(0.003)	1.3451(0.025)	0.8558(0.006)	1.6694(0.006)
8	11:1:24.48	−01:46:45.4	18.490(0.007)	0.5265(0.033)	0.3976(0.012)	0.7205(0.016)
9	11:1:11.28	−01:47:57.4	18.024(0.005)	1.0996(0.036)	0.6973(0.008)	1.2341(0.005)
10	11:1:13.91	−01:46:48.7	18.535(0.007)	0.8339(0.035)	0.4927(0.011)	0.9033(0.007)
11	11:1:07.68	−01:43:53.7	19.090(0.009)	0.4049(0.041)	0.3179(0.015)	0.5723(0.012)
12	11:1:30.24	−01:45:28.0	18.284(0.006)	1.2594(0.042)	0.8142(0.009)	1.4305(0.011)
13	11:1:27.83	−01:42:56.1	18.174(0.006)	1.4716(0.045)	0.9573(0.009)	1.8042(0.008)
14	11:1:13.67	−01:47:40.9	18.556(0.007)	1.2586(0.048)	0.8304(0.009)	1.5248(0.006)
15	11:1:19.20	−01:47:38.0	18.743(0.008)	1.2488(0.053)	0.8467(0.010)	1.5656(0.006)
			SN 1999bm			
1	12:44:52.15	−06:27:07.2	16.654(0.004)	0.8226(0.010)	0.4947(0.007)	1.1478(0.017)
2	12:45:06.24	−06:28:48.7	18.794(0.010)	0.7981(0.025)	0.5201(0.017)	1.0221(0.028)
3	12:44:59.28	−06:27:45.0	19.392(0.013)	0.4104(0.028)	0.3032(0.022)	0.6162(0.046)
4	12:44:57.84	−06:28:35.0	19.368(0.012)	0.8124(0.033)	0.4834(0.020)	0.8897(0.039)
5	12:44:52.80	−06:27:13.3	18.768(0.009)	1.4648(0.033)	0.8968(0.013)	1.7639(0.020)
6	12:45:00.48	−06:29:57.4	19.599(0.013)	1.5270(0.050)	0.9405(0.018)	1.8491(0.028)
7	12:44:55.67	−06:25:11.9	19.883(0.016)	1.2895(0.051)	0.8278(0.022)	1.5446(0.037)
8	12:44:57.36	−06:29:48.8	20.111(0.017)	1.4846(0.063)	0.8758(0.025)	1.7727(0.038)
9	12:44:59.75	−06:28:51.9	20.401(0.020)	1.4484(0.070)	0.9520(0.026)	1.8677(0.042)
			SN 1999bn			
1	11:59:27.60	−01:45:06.1	16.774(0.009)	0.6156(0.015)	0.3900(0.017)	0.8245(0.023)
2	11:59:43.92	−01:48:01.4	17.149(0.008)	0.7446(0.017)	0.4522(0.015)	0.9144(0.026)
3	11:59:43.67	−01:47:14.6	17.510(0.011)	0.9933(0.022)	0.5647(0.021)	1.0699(0.029)
4	11:59:29.95	−01:40:10.9	17.091(0.008)	1.4450(0.022)	0.9077(0.015)	1.7471(0.017)
5	11:59:38.39	−01:45:02.9	18.271(0.015)	0.8989(0.030)	0.5085(0.027)	1.0054(0.043)
6	11:59:37.91	−01:46:42.9	18.713(0.018)	0.5126(0.032)	0.3288(0.033)	0.6705(0.061)

TABLE B1
Coordinates and magnitudes of tertiary calibration stars.

7	11:59:35.76	−01:46:56.2	17.667(0.012)	1.6142(0.030)	1.0129(0.019)	2.3098(0.018)
8	11:59:32.63	−01:41:06.4	18.752(0.018)	1.2817(0.044)	0.7398(0.032)	1.4050(0.044)
9	11:59:33.36	−01:42:37.7	19.979(0.030)	0.4443(0.057)	0.3535(0.055)	0.5282(0.117)
10	11:59:36.95	−01:44:00.6	20.207(0.032)	0.5354(0.064)	0.3052(0.061)	0.6123(0.125)
11	11:59:38.15	−01:43:23.5	20.224(0.032)	0.5850(0.066)	0.2988(0.064)	0.6199(0.126)
12	11:59:43.44	−01:45:02.5	20.255(0.033)	0.7108(0.071)	0.3943(0.061)	0.8314(0.116)
13	11:59:33.83	−01:47:16.8	19.454(0.023)	1.5694(0.070)	0.9617(0.036)	1.9965(0.046)
14	11:59:32.88	−01:42:55.8	20.681(0.040)	0.6182(0.087)	0.4557(0.070)	0.9940(0.131)
15	11:59:24.96	−01:47:15.3	19.814(0.026)	1.5891(0.094)	1.0562(0.041)	2.3242(0.047)
			SN 1999bp			
1	11:39:43.92	−08:50:32.9	16.293(0.003)	0.5914(0.008)	0.2163(0.007)	0.7302(0.007)
2	11:39:55.08	−08:49:09.1	16.647(0.004)	0.6786(0.010)	0.4143(0.006)	0.8160(0.008)
3	11:39:44.40	−08:53:16.0	16.592(0.004)	0.8936(0.010)	0.4562(0.007)	1.0276(0.007)
4	11:39:47.64	−08:54:30.9	16.847(0.004)	0.7113(0.011)	0.4483(0.005)	0.8592(0.008)
5	11:39:43.44	−08:51:12.2	17.039(0.005)	0.5330(0.010)	0.3636(0.006)	0.7057(0.010)
6	11:39:42.47	−08:53:38.0	17.594(0.006)	0.5763(0.013)	0.3706(0.008)	0.7320(0.012)
7	11:39:45.59	−08:46:13.4	16.984(0.005)	1.3441(0.022)	0.8656(0.005)	1.6703(0.007)
8	11:39:48.96	−08:54:31.3	16.988(0.004)	1.3632(0.016)	0.8748(0.005)	1.7601(0.006)
9	11:39:40.80	−08:51:57.9	18.432(0.009)	0.6316(0.020)	0.4030(0.011)	0.7769(0.017)
10	11:39:41.40	−08:49:45.8	17.945(0.007)	1.2899(0.023)	0.7811(0.008)	1.4110(0.011)
11	11:39:42.00	−08:48:39.2	18.851(0.011)	0.5547(0.026)	0.3637(0.014)	0.7236(0.021)
12	11:39:37.92	−08:48:40.3	18.809(0.010)	0.7168(0.028)	0.4423(0.013)	0.8404(0.019)
13	11:39:43.92	−08:51:27.7	19.012(0.011)	0.7382(0.028)	0.4262(0.015)	0.8385(0.021)
14	11:39:44.63	−08:55:19.9	18.497(0.010)	1.5862(0.040)	1.1371(0.009)	2.4759(0.009)
15	11:39:45.59	−08:46:41.1	19.654(0.017)	0.5811(0.048)	0.3944(0.021)	0.7329(0.034)

LIGHTCURVES FROM THE NEARBY SUPERNOVA CAMPAIGN

TABLE C1
B,V,R,I magnitudes, uncertainties are given in brackets.

JD	Telescope	B	V	R	I
		SN 1999aa			
221.81	LICK 1m DEWAR2	15.828 (0.032)	-	-	-
222.67	YALO	15.642 (0.018)	15.680 (0.028)	15.689 (0.040)	15.717 (0.105)
223.67	YALO	15.462 (0.020)	-	15.486 (0.036)	15.514 (0.083)
225.65	YALO	15.211 (0.017)	15.260 (0.028)	15.276 (0.030)	15.312 (0.025)
227.73	LICK 1m DEWAR2	15.006 (0.016)	15.060 (0.024)	15.080 (0.018)	-
229.62	YALO	14.924 (0.017)	14.965 (0.026)	15.092 (0.030)	-
232.61	YALO	14.908 (0.017)	14.913 (0.028)	15.062 (0.030)	15.253 (0.025)
235.60	YALO	14.919 (0.021)	14.898 (0.032)	15.037 (0.031)	15.307 (0.029)
241.60	YALO	15.183 (0.013)	15.062 (0.027)	15.266 (0.030)	15.575 (0.024)
243.88	LICK 1m DEWAR5	-	-	15.236 (0.051)	15.724 (0.039)
244.64	YALO	15.406 (0.018)	15.222 (0.027)	15.481 (0.031)	15.792 (0.025)
247.58	YALO	15.667 (0.016)	15.379 (0.026)	15.619 (0.030)	15.932 (0.024)
247.75	LICK 1m DEWAR5	15.713 (0.023)	15.426 (0.042)	15.492 (0.032)	15.888 (0.028)
252.59	YALO	16.222 (0.016)	15.670 (0.026)	15.715 (0.030)	15.929 (0.024)
255.54	YALO	16.534 (0.017)	15.811 (0.026)	15.706 (0.030)	15.851 (0.024)
258.57	CTIO 1.5m T2K	16.964 (0.017)	15.940 (0.026)	15.718 (0.030)	15.762 (0.017)
259.60	YALO	16.902 (0.017)	15.990 (0.026)	15.724 (0.030)	15.784 (0.024)
265.52	YALO	17.362 (0.019)	16.278 (0.027)	15.823 (0.030)	15.728 (0.024)
274.57	CTIO 1.5m T2K	17.910 (0.018)	16.739 (0.026)	-	-
281.68	LICK 1m DEWAR2	17.976 (0.036)	17.025 (0.041)	16.746 (0.034)	-
284.70	LICK 1m DEWAR2	17.986 (0.032)	17.140 (0.039)	16.932 (0.044)	-
288.40	JKT 1m	-	-	-	16.804 (0.032)
289.67	LICK 1m DEWAR2	18.082 (0.069)	17.262 (0.047)	17.049 (0.040)	-
293.71	LICK 1m DEWAR2	18.182 (0.042)	17.319 (0.069)	17.091 (0.041)	17.157 (0.039)
294.70	LICK 1m DEWAR2	18.301 (0.084)	17.380 (0.105)	-	-
303.69	LICK 1m DEWAR5	18.341 (0.032)	-	17.440 (0.036)	17.520 (0.032)
304.71	LICK 1m DEWAR5	18.263 (0.025)	17.680 (0.041)	17.463 (0.035)	17.529 (0.031)
308.70	LICK 1m DEWAR5	18.298 (0.046)	-	-	-
		SN 1999ao			
246.59	CTIO 1.5m T2K	18.244 (0.020)	18.062 (0.022)	17.921 (0.036)	18.411 (0.054)
248.52	YALO	18.197 (0.021)	18.123 (0.028)	17.999 (0.048)	18.321 (0.063)
251.57	YALO	18.385 (0.016)	18.143 (0.019)	18.046 (0.036)	18.433 (0.056)
255.63	YALO	18.748 (0.016)	18.412 (0.029)	18.396 (0.055)	18.639 (0.084)
258.53	CTIO 1.5m T2K	19.301 (0.029)	18.604 (0.029)	18.528 (0.045)	19.144 (0.096)
259.54	YALO	19.211 (0.030)	18.656 (0.036)	18.617 (0.082)	-
263.53	YALO	19.739 (0.038)	-	18.635 (0.061)	18.986 (0.113)
265.50	DANISH 1m	20.038 (0.063)	-	18.581 (0.048)	18.743 (0.072)
266.50	DANISH 1m	-	18.940 (0.036)	-	-
274.52	CTIO 1.5m T2K	20.816 (0.045)	19.333 (0.030)	18.794 (0.038)	18.508 (0.066)
284.55	ESO 3.6m	21.267 (0.055)	19.889 (0.039)	19.598 (0.060)	19.415 (0.127)

TABLE C1
B,V,R,I MAGNITUDES, UNCERTAINTIES ARE GIVEN IN BRACKETS.

290.55	ESO 3.6m	21.322 (0.057)	20.139 (0.050)	19.806 (0.061)	19.708 (0.104)
295.40	CTIO 1.5m T2K	-	-	-	19.781 (0.117)
297.53	DANISH 1m	-	20.579 (0.132)	-	-
298.54	YALO	21.341 (0.181)	-	-	-
301.54	DANISH 1m	22.351 (0.659)	20.700 (0.227)	20.064 (0.125)	20.030 (0.202)
314.47	YALO	-	21.095 (0.121)	-	-
315.48	YALO	21.779 (0.080)	-	20.707 (0.241)	-
			SN 1999ar		
246.62	CTIO 1.5m T2K	-	-	19.924 (0.042)	-
247.67	LICK 1m DEWAR5	-	20.015 (0.086)	19.787 (0.052)	-
248.64	YALO	20.061 (0.023)	19.864 (0.044)	19.784 (0.049)	19.677 (0.068)
252.67	YALO	20.168 (0.017)	19.965 (0.045)	19.904 (0.051)	19.670 (0.072)
256.62	YALO	20.342 (0.019)	20.046 (0.048)	19.915 (0.053)	19.783 (0.068)
257.69	CTIO 0.9m	20.739 (0.035)	20.153 (0.051)	-	-
258.62	CTIO 1.5m T2K	20.791 (0.032)	20.167 (0.054)	20.025 (0.049)	20.278 (0.112)
259.73	LICK 1m DEWAR2	-	20.319 (0.171)	20.275 (0.134)	-
261.51	YALO	20.716 (0.030)	20.243 (0.056)	20.193 (0.058)	19.961 (0.074)
266.61	CTIO 0.9m	21.866 (0.296)	20.530 (0.160)	-	-
267.67	CTIO 0.9m	21.925 (0.320)	20.583 (0.205)	-	-
274.61	CTIO 1.5m T2K	22.214 (0.185)	21.263 (0.092)	-	-
274.67	CTIO 0.9m	-	-	20.514 (0.115)	20.451 (0.185)
275.65	CTIO 0.9m	22.328 (0.478)	21.330 (0.331)	20.550 (0.112)	-
276.64	CTIO 1.5m T2K	22.919 (0.187)	21.659 (0.126)	20.883 (0.058)	20.659 (0.130)
277.67	CTIO 1.5m T2K	22.482 (0.124)	21.343 (0.115)	-	-
284.67	KPNO 2.1m	23.078 (0.092)	22.273 (0.169)	21.066 (0.106)	-
288.73	KPNO 2.1m	22.134 (0.465)	22.327 (0.185)	-	-
296.52	CTIO 1.5m T2K	23.772 (0.777)	21.896 (0.300)	-	-
305.56	CTIO 1.5m T2K	23.637 (0.242)	22.447 (0.256)	21.584 (0.141)	21.317 (0.230)
308.50	DANISH 1m	22.765 (0.090)	22.496 (0.119)	21.680 (0.074)	20.886 (0.087)
			SN 1999aw		
249.75	YALO	16.946 (0.019)	17.026 (0.019)	17.074 (0.021)	17.116 (0.031)
254.65	YALO	16.861 (0.016)	16.855 (0.016)	16.937 (0.020)	-
257.80	CTIO 0.9m	16.982 (0.021)	16.868 (0.020)	-	-
258.66	YALO	16.994 (0.012)	16.889 (0.012)	16.883 (0.014)	-
258.67	CTIO 1.5m T2K	-	-	-	17.294 (0.018)
261.63	YALO	17.049 (0.018)	16.964 (0.017)	17.049 (0.020)	17.369 (0.024)
265.54	YALO	17.301 (0.018)	17.150 (0.018)	-	-
265.55	DANISH 1m	-	-	17.159 (0.015)	17.589 (0.019)
266.69	CTIO 0.9m	17.477 (0.033)	17.222 (0.042)	-	-
274.72	CTIO 0.9m	-	-	-	17.754 (0.027)
275.69	CTIO 0.9m	18.293 (0.021)	17.650 (0.020)	17.636 (0.017)	18.010 (0.027)
275.82	LICK 1m DEWAR2	-	17.515 (0.060)	17.717 (0.032)	-
276.72	CTIO 1.5m T2K	18.359 (0.014)	17.694 (0.013)	17.655 (0.014)	17.991 (0.018)
277.69	CTIO 1.5m T2K	18.450 (0.013)	17.719 (0.013)	17.644 (0.014)	17.948 (0.017)
280.84	LICK 1m DEWAR2	-	17.809 (0.065)	-	-
284.72	LICK 1m DEWAR2	-	17.925 (0.056)	17.722 (0.037)	-
285.46	JKT 1m	-	18.029 (0.018)	-	-
291.70	CTIO 1.5m T2K	19.404 (0.020)	18.253 (0.032)	17.827 (0.020)	-
293.73	LICK 1m DEWAR2	-	18.512 (0.085)	18.025 (0.038)	-
296.56	CTIO 1.5m T2K	19.603 (0.033)	18.582 (0.023)	18.150 (0.022)	17.854 (0.026)
301.65	DANISH 1m	-	-	18.385 (0.023)	-
303.67	CTIO 1.5m T2K	19.896 (0.037)	18.898 (0.145)	-	-
303.77	LICK 1m DEWAR5	-	19.152 (0.049)	-	-
304.63	CTIO 1.5m T2K	19.860 (0.023)	18.950 (0.023)	18.526 (0.021)	18.273 (0.024)
313.52	YALO	19.823 (0.014)	19.283 (0.013)	18.915 (0.012)	18.762 (0.019)
337.79	CFHT	-	19.984 (0.036)	19.579 (0.025)	19.093 (0.036)
338.82	CFHT	20.383 (0.036)	-	-	-
			SN 1999bi		
192.84	MARLY	-	-	-	22.523 (0.923)
227.72	MARLY	-	-	-	22.004 (0.806)
248.66	MARLY	-	-	19.533 (0.081)	19.688 (0.170)
252.75	MARLY	-	-	19.408 (0.074)	19.674 (0.158)
253.65	YALO	20.023 (0.031)	19.618 (0.041)	19.486 (0.072)	19.493 (0.063)
258.57	YALO	20.216 (0.027)	19.703 (0.045)	19.619 (0.091)	19.868 (0.071)
258.69	CTIO 1.5m T2K	20.366 (0.031)	19.660 (0.043)	19.579 (0.064)	-
263.61	YALO	20.581 (0.059)	19.950 (0.067)	19.823 (0.110)	19.852 (0.098)
274.67	CTIO 1.5m T2K	21.639 (0.143)	20.665 (0.086)	20.192 (0.116)	-
275.68	CTIO 1.5m T2K	-	-	-	20.106 (0.103)
284.79	KPNO 2.1m	22.564 (0.230)	21.067 (0.212)	20.124 (0.082)	19.859 (0.068)
308.64	DANISH 1m	-	22.561 (0.178)	21.495 (0.151)	22.398 (0.377)
337.78	CFHT	-	-	21.879 (0.283)	21.530 (0.241)
			SN 1999bm		
255.72	MARLY	-	-	20.239 (0.095)	-
256.75	MARLY	-	-	20.122 (0.074)	-
258.81	CTIO 1.5m T2K	20.843 (0.030)	20.288 (0.035)	-	-
261.73	YALO	20.868 (0.020)	20.253 (0.039)	20.167 (0.047)	20.101 (0.062)
265.71	YALO	21.348 (0.079)	20.674 (0.093)	20.328 (0.059)	-

TABLE C1
B,V,R,I magnitudes, uncertainties are given in brackets.

274.80	CTIO 1.5m T2K	-	21.525 (0.167)	-	-
284.89	KPNO 2.1m	-	22.416 (0.321)	21.523 (0.135)	-
316.63	DANISH 1m	25.004 (0.683)	-	-	-
		SN 1999bn			
257.58	YALO	19.811 (0.029)	19.647 (0.042)	19.618 (0.053)	19.567 (0.078)
261.71	DANISH 1m	19.898 (0.028)	19.637 (0.034)	19.477 (0.040)	-
262.74	YALO	19.876 (0.030)	19.701 (0.041)	19.640 (0.046)	19.590 (0.060)
265.67	YALO	20.058 (0.041)	19.779 (0.053)	-	-
301.68	DANISH 1m	21.896 (0.454)	22.163 (0.448)	20.912 (0.118)	20.541 (0.160)
305.66	DANISH 1m	23.175 (0.390)	22.321 (0.292)	21.254 (0.083)	20.696 (0.138)
312.62	DANISH 1m	22.697 (0.081)	22.325 (0.107)	-	-
337.85	CFHT	-	-	22.217 (0.159)	21.915 (0.294)
		SN 1999bp			
202.81	MARLY	-	-	22.564 (0.350)	-
229.74	MARLY	-	-	22.564 (0.455)	-
257.70	MARLY	-	-	18.608 (0.035)	-
259.68	MARLY	-	-	18.449 (0.032)	-
260.68	YALO	18.541 (0.015)	18.574 (0.022)	18.430 (0.031)	18.577 (0.035)
263.71	YALO	18.478 (0.016)	18.505 (0.025)	18.385 (0.032)	18.633 (0.051)
266.62	YALO	18.533 (0.020)	18.546 (0.028)	18.340 (0.031)	18.623 (0.041)
275.62	CTIO 1.5m T2K	19.132 (0.018)	18.748 (0.024)	18.599 (0.031)	19.127 (0.048)
281.78	LICK 1m DEWAR2	20.128 (0.150)	-	19.091 (0.080)	-
286.43	JKT 1m	20.242 (0.040)	19.438 (0.038)	-	-
288.83	KPNO 2.1m	20.377 (0.030)	-	-	-
289.74	LICK 1m DEWAR2	-	20.086 (0.427)	19.536 (0.205)	-
293.75	LICK 1m DEWAR2	-	-	-	19.573 (0.109)
302.72	CTIO 1.5m T2K	-	20.306 (0.269)	-	-
306.57	YALO	21.723 (0.039)	20.603 (0.042)	19.646 (0.046)	-
337.81	CFHT	-	-	20.612 (0.060)	20.904 (0.144)
338.83	CFHT	22.208 (0.107)	-	-	-

TABLE C2
SNe of the Union compilation

Name	z	$m_B^{\max}$	s	c	μ	ref.	cut
1993ag	0.0500	17.79(0.05)	0.91(0.02)	0.09(0.02)	36.77(0.15)	1	
1993o	0.0529	17.61(0.05)	0.90(0.01)	-0.01(0.02)	36.82(0.15)	1	
1993h	0.0251	16.74(0.09)	0.68(0.01)	0.21(0.01)	35.17(0.17)	1	
1993b	0.0701	18.38(0.09)	0.99(0.03)	0.04(0.04)	37.57(0.15)	1	
1992bs	0.0627	18.18(0.05)	1.00(0.02)	-0.03(0.02)	37.55(0.15)	1	
1992br	0.0876	19.40(0.11)	0.65(0.04)	0.03(0.05)	38.19(0.16)	1	
1992bp	0.0786	18.28(0.03)	0.87(0.02)	-0.04(0.02)	37.52(0.15)	1	
1992bo	0.0172	15.75(0.13)	0.74(0.01)	0.03(0.01)	34.65(0.19)	1	
1992bl	0.0422	17.29(0.06)	0.79(0.02)	-0.01(0.02)	36.36(0.15)	1	
1992bh	0.0453	17.59(0.05)	0.98(0.01)	0.10(0.01)	36.66(0.15)	1	
1992bc	0.0196	15.07(0.11)	1.01(0.01)	-0.06(0.01)	34.52(0.18)	1	
1992aq	0.1009	19.30(0.03)	0.84(0.02)	-0.05(0.02)	38.51(0.15)	1	
1992al	0.0135	14.44(0.16)	0.93(0.01)	-0.05(0.01)	33.78(0.21)	1	z
1992ag	0.0273	16.24(0.09)	1.03(0.04)	0.15(0.02)	35.23(0.17)	1	
1992ae	0.0746	18.39(0.05)	0.94(0.02)	-0.02(0.02)	37.67(0.15)	1	
1992p	0.0265	16.03(0.08)	1.14(0.08)	-0.01(0.02)	35.52(0.18)	1	
1990af	0.0499	17.73(0.04)	0.74(0.01)	0.00(0.01)	36.70(0.15)	1	
1990o	0.0306	16.20(0.08)	1.04(0.03)	0.00(0.02)	35.54(0.16)	1	
1993ah	0.0285	16.07(0.08)	0.90(0.00)	-0.12(0.03)	35.53(0.10)	1	p
1992bk	0.0589	18.04(0.09)	0.77(0.02)	-0.03(0.04)	37.13(0.06)	1	p
1992bg	0.0365	16.53(0.10)	0.98(0.02)	-0.06(0.03)	35.95(0.08)	1	p
1992au	0.0603	17.47(0.14)	0.65(0.05)	-0.25(0.06)	36.92(0.08)	1	p
1992k	0.0111	15.09(0.20)	0.68(0.04)	0.22(0.02)	33.48(0.21)	1	p,z
1992j	0.0461	18.28(0.23)	0.80(0.07)	0.40(0.09)	36.41(0.08)	1	p
1991ag	0.0139	14.16(0.17)	1.10(0.02)	-0.05(0.02)	33.70(0.16)	1	p,z
1991u	0.0324	16.33(0.13)	1.04(0.03)	0.05(0.05)	35.58(0.08)	1	p
1991s	0.0561	17.66(0.07)	1.06(0.02)	-0.02(0.02)	37.08(0.05)	1	p
1990y	0.0387	17.50(0.14)	1.04(0.05)	0.24(0.05)	36.31(0.10)	1	p
1990t	0.0397	17.26(0.18)	1.00(0.04)	0.08(0.08)	36.37(0.08)	1	p
2001cz	0.0163	15.03(0.13)	1.01(0.02)	0.11(0.01)	34.09(0.14)	2	
2001cn	0.0154	15.22(0.14)	0.92(0.01)	0.17(0.01)	34.03(0.15)	2	
2001bt	0.0144	15.26(0.15)	0.87(0.01)	0.22(0.01)	33.90(0.16)	2	z
2001ba	0.0305	16.18(0.07)	1.00(0.01)	-0.04(0.01)	35.58(0.09)	2	
2000ca	0.0245	15.51(0.09)	1.00(0.03)	-0.06(0.01)	34.96(0.11)	2	
2000bh	0.0240	15.94(0.09)	0.94(0.04)	0.10(0.02)	34.94(0.12)	2	
1999gp	0.0260	15.99(0.09)	1.13(0.03)	0.04(0.01)	35.36(0.11)	2	
1999dk	0.0139	14.81(0.16)	1.06(0.06)	0.07(0.02)	34.03(0.18)	2	z
1999da	0.0125	16.45(0.20)	0.57(0.05)	0.41(0.06)	34.28(0.21)	2	z

TABLE C2
SNe of the Union compilation

1999cp	0.0104	13.93(0.21)	0.96(0.03)	-0.02(0.02)	33.23(0.22)	2	z
1999cl	0.0087	14.84(0.25)	0.95(0.03)	1.08(0.01)	31.62(0.26)	2	z
2000ce	0.0165	17.04(0.16)	0.98(0.04)	0.53(0.04)	35.10(0.14)	2	p
2000bk	0.0266	16.72(0.11)	0.75(0.02)	0.08(0.04)	35.52(0.09)	2	p
1993ac	0.0489	17.80(0.13)	0.78(0.06)	0.08(0.04)	36.64(0.18)	3	
1994m	0.0243	16.30(0.10)	0.78(0.02)	0.11(0.02)	35.08(0.19)	3	
1994s	0.0152	14.77(0.15)	1.09(0.05)	-0.01(0.02)	34.20(0.23)	3	
1994t	0.0357	17.05(0.11)	0.84(0.04)	0.02(0.05)	36.11(0.19)	3	
1995d	0.0065	13.23(0.33)	1.11(0.02)	-0.00(0.01)	32.67(0.37)	3	z
1995e	0.0117	16.69(0.19)	0.93(0.02)	0.78(0.02)	34.13(0.25)	3	z
1994ae	0.0043	13.10(0.51)	0.98(0.01)	0.13(0.01)	32.07(0.53)	3	z
1995al	0.0050	13.29(0.43)	1.06(0.02)	0.12(0.01)	32.38(0.46)	3	z
1995ac	0.0488	17.03(0.05)	1.04(0.01)	0.01(0.01)	36.35(0.17)	3	
1995ak	0.0220	15.87(0.14)	0.89(0.04)	0.07(0.05)	34.88(0.20)	3	
1995bd	0.0144	15.26(0.18)	1.00(0.02)	0.31(0.02)	33.85(0.24)	3	z
1996c	0.0275	16.65(0.08)	1.01(0.02)	0.12(0.02)	35.67(0.18)	3	
1996x	0.0070	12.94(0.31)	0.88(0.01)	-0.01(0.01)	32.11(0.35)	3	z
1996z	0.0086	14.19(0.26)	0.86(0.05)	0.24(0.02)	32.75(0.30)	3	z
1996ab	0.1244	19.53(0.03)	0.96(0.03)	-0.08(0.02)	38.95(0.17)	3	
1996ai	0.0030	16.89(0.72)	1.14(0.03)	1.61(0.01)	32.70(0.74)	3	z
1996bl	0.0360	16.62(0.07)	0.99(0.02)	0.03(0.01)	35.83(0.17)	3	
1996bv	0.0167	15.35(0.14)	1.01(0.04)	0.22(0.01)	34.16(0.21)	3	
1996bo	0.0163	15.82(0.13)	0.87(0.02)	0.37(0.01)	34.11(0.21)	3	
1993ae	0.0180	15.22(0.12)	0.79(0.02)	-0.07(0.01)	34.41(0.13)	3	p
1994q	0.0299	16.17(0.12)	1.13(0.04)	0.02(0.04)	35.58(0.08)	3	p
1996bk	0.0066	14.84(0.33)	0.66(0.06)	0.49(0.03)	32.61(0.34)	3	p,z
2000fa	0.0218	15.84(0.11)	0.96(0.03)	0.08(0.02)	34.90(0.28)	4	
2000dk	0.0164	15.33(0.13)	0.73(0.01)	0.05(0.01)	34.18(0.29)	4	
2000cn	0.0232	16.53(0.10)	0.73(0.01)	0.17(0.01)	35.12(0.28)	4	
2000cf	0.0365	17.09(0.07)	0.88(0.02)	0.05(0.01)	36.11(0.27)	4	
1999gd	0.0193	16.94(0.11)	0.92(0.03)	0.43(0.01)	35.16(0.29)	4	
1999ek	0.0176	15.59(0.17)	0.91(0.01)	0.17(0.01)	34.39(0.31)	4	
1999ej	0.0128	15.44(0.18)	0.65(0.04)	0.05(0.02)	34.19(0.31)	4	z
1999dq	0.0135	14.39(0.16)	1.07(0.01)	0.12(0.01)	33.50(0.31)	4	z
1999cc	0.0315	16.78(0.07)	0.82(0.02)	0.06(0.01)	35.73(0.27)	4	
1998es	0.0096	13.80(0.23)	1.06(0.01)	0.10(0.01)	32.95(0.35)	4	z
1998eg	0.0235	16.10(0.10)	0.93(0.03)	0.05(0.01)	35.19(0.28)	4	
1998ef	0.0167	14.81(0.13)	0.85(0.02)	0.02(0.01)	33.89(0.29)	4	
1998dx	0.0537	17.64(0.06)	0.75(0.04)	0.08(0.03)	36.46(0.27)	4	
1998dh	0.0077	13.83(0.28)	0.87(0.01)	0.12(0.01)	32.70(0.38)	4	z
1998de	0.0156	17.21(0.14)	0.57(0.01)	0.49(0.03)	34.87(0.30)	4	o
1998co	0.0170	15.70(0.13)	0.61(0.03)	0.11(0.01)	34.27(0.29)	4	
1998bp	0.0102	15.31(0.21)	0.64(0.01)	0.29(0.01)	33.51(0.34)	4	z
1998ab	0.0279	16.05(0.08)	0.93(0.02)	0.10(0.02)	35.03(0.27)	4	
1998v	0.0172	15.10(0.13)	0.93(0.03)	0.05(0.01)	34.19(0.29)	4	
1997dt	0.0061	15.40(0.36)	0.88(0.03)	0.56(0.03)	33.28(0.44)	4	z
1997do	0.0105	14.32(0.21)	0.94(0.02)	0.12(0.02)	33.28(0.33)	4	z
1997dg	0.0300	16.83(0.08)	0.92(0.04)	0.03(0.02)	35.96(0.27)	4	
1997bq	0.0096	14.44(0.23)	0.91(0.02)	0.16(0.02)	33.27(0.35)	4	z
1997bp	0.0094	13.95(0.23)	0.98(0.03)	0.24(0.02)	32.69(0.35)	4	z
1997y	0.0166	15.31(0.13)	0.88(0.02)	0.04(0.01)	34.38(0.29)	4	
1997e	0.0133	15.09(0.17)	0.82(0.02)	0.09(0.01)	33.97(0.31)	4	z
2000b	0.0201	15.83(0.22)	0.82(0.06)	0.18(0.09)	34.49(0.14)	4	p
1999gh	0.0088	14.20(0.25)	0.68(0.01)	0.22(0.02)	32.60(0.25)	4	p,z
1999ef	0.0380	17.05(0.14)	1.01(0.07)	0.02(0.04)	36.31(0.09)	4	p
1999cw	0.0113	14.14(0.29)	0.96(0.34)	0.12(0.08)	33.12(0.34)	4	p,d,z
1999x	0.0258	16.24(0.18)	0.93(0.05)	0.06(0.05)	35.30(0.09)	4	p
1998ec	0.0201	16.16(0.18)	1.02(0.06)	0.19(0.06)	35.05(0.12)	4	p
1998dm	0.0056	14.71(0.40)	1.01(0.05)	0.30(0.04)	33.34(0.39)	4	p,z
1998dk	0.0120	14.61(0.24)	0.95(0.10)	0.09(0.08)	33.64(0.20)	4	p,z
1997cn	0.0170	16.33(0.15)	0.59(0.03)	0.21(0.03)	34.64(0.15)	4	p
1997cw	0.0160	15.88(0.14)	1.12(0.04)	0.38(0.03)	34.46(0.14)	4	p
1999aa	0.0150	14.69(0.15)	1.05(0.01)	-0.02(0.01)	34.10(0.15)	5	
1999ac	0.0095	14.13(0.23)	0.97(0.02)	0.10(0.02)	33.17(0.23)	5	z
1999ao	0.0544	17.89(0.06)	0.96(0.04)	0.07(0.03)	36.97(0.08)	5	
1999ar	0.1561	19.97(0.03)	0.99(0.04)	-0.01(0.02)	39.29(0.06)	5	
1999aw	0.0393	16.78(0.06)	1.20(0.03)	0.01(0.02)	36.31(0.07)	5	
1999bi	0.1241	19.76(0.05)	1.18(0.06)	0.21(0.03)	38.81(0.07)	5	
1999bm	0.1441	20.43(0.04)	0.68(0.03)	0.12(0.02)	39.05(0.06)	5	
1999bn	0.1299	19.60(0.03)	1.09(0.04)	0.01(0.02)	39.00(0.06)	5	
1999bp	0.0784	18.39(0.03)	1.09(0.03)	0.00(0.02)	37.78(0.07)	5	
1996h	0.6200	23.50(0.09)	1.10(0.17)	-0.12(0.09)	43.21(0.37)	6	
1996i	0.5700	23.40(0.07)	0.82(0.05)	-0.06(0.06)	42.63(0.33)	6	
1996j	0.3000	22.03(0.10)	0.79(0.06)	0.07(0.09)	40.91(0.32)	6	
1996k	0.3800	22.64(0.05)	0.85(0.01)	-0.10(0.05)	41.98(0.29)	6	
1996u	0.4300	22.61(0.05)	0.92(0.07)	-0.21(0.09)	42.29(0.35)	6	
1995ao	0.2400	21.60(0.08)	1.35(0.39)	0.18(0.09)	40.92(0.60)	6	

TABLE C2
SNe of the Union compilation

1995ap	0.3000	21.53(0.38)	0.54(0.20)	0.05(0.32)	40.15(0.46)	6	
1996t	0.2400	20.99(0.03)	1.30(0.03)	-0.10(0.01)	40.89(0.28)	6	
1997ce	0.4400	22.80(0.06)	0.86(0.03)	-0.04(0.04)	42.02(0.29)	6	
1997cj	0.5000	23.14(0.05)	0.91(0.02)	-0.04(0.02)	42.43(0.29)	6	
1997ck	0.9700	24.72(0.15)	1.03(0.12)	0.42(0.28)	43.08(0.74)	6	
1995k	0.4790	22.72(0.06)	0.98(0.04)	-0.12(0.05)	42.26(0.31)	6	
1996e	0.4300	22.38(0.19)	0.92(0.07)	0.07(0.08)	41.42(0.11)	6	p
1996r	0.1600	-	-	-	-	6	f
1997ap	0.8300	24.34(0.09)	1.00(0.02)	0.06(0.04)	43.49(0.37)	7	
1997am	0.4160	22.46(0.07)	1.08(0.05)	-0.08(0.14)	42.04(0.44)	7	
1997aj	0.5810	23.16(0.09)	1.01(0.06)	0.22(0.10)	41.98(0.42)	7	
1997ai	0.4500	22.92(0.05)	0.74(0.07)	0.05(0.05)	41.80(0.37)	7	
1997af	0.5790	23.57(0.10)	0.90(0.05)	-0.16(0.17)	43.11(0.56)	7	
1997ac	0.3200	21.89(0.04)	1.05(0.02)	0.03(0.03)	41.19(0.34)	7	
1997r	0.6570	23.92(0.12)	0.98(0.11)	0.05(0.16)	43.08(0.55)	7	
1997q	0.4300	22.82(0.07)	0.97(0.03)	0.97(0.30)	39.87(0.73)	7	o
1997p	0.4720	23.13(0.06)	0.94(0.04)	0.11(0.14)	42.10(0.47)	7	
1997o	0.3740	23.32(0.15)	1.06(0.06)	-0.18(0.33)	43.12(0.69)	7	
1997h	0.5260	23.18(0.06)	0.93(0.02)	0.17(0.09)	42.01(0.40)	7	
1997g	0.7630	24.37(0.29)	0.90(0.12)	-0.36(0.24)	44.37(0.89)	7	
1997f	0.5800	23.41(0.07)	1.11(0.05)	-0.04(0.08)	42.94(0.40)	7	
1996cn	0.4300	23.22(0.05)	0.95(0.07)	0.25(0.09)	41.89(0.39)	7	
1996cm	0.4500	23.25(0.06)	0.98(0.04)	0.11(0.11)	42.28(0.42)	7	
1996cl	0.8280	24.55(0.17)	1.38(0.56)	0.05(0.17)	44.20(0.61)	7	
1996ck	0.6560	23.77(0.11)	0.85(0.09)	-0.13(0.14)	43.18(0.53)	7	
1996ci	0.4950	22.82(0.05)	0.92(0.09)	-0.04(0.08)	42.12(0.40)	7	
1996cg	0.4900	23.07(0.05)	0.98(0.03)	0.23(0.05)	41.82(0.36)	7	
1996cf	0.5700	23.31(0.06)	1.08(0.10)	-0.01(0.07)	42.74(0.40)	7	
1995ba	0.3880	22.55(0.07)	0.95(0.04)	-0.14(0.08)	42.10(0.37)	7	
1995az	0.4500	22.61(0.06)	0.95(0.04)	-0.16(0.08)	42.21(0.38)	7	
1995ay	0.4800	23.06(0.06)	0.84(0.05)	0.01(0.10)	42.13(0.40)	7	
1995ax	0.6150	23.22(0.10)	1.12(0.16)	0.02(0.15)	42.61(0.52)	7	
1995aw	0.4000	22.18(0.05)	1.20(0.05)	-0.17(0.09)	42.11(0.38)	7	
1995at	0.6550	23.22(0.11)	1.15(0.13)	0.16(0.11)	42.33(0.50)	7	
1995as	0.4980	23.66(0.06)	1.04(0.13)	-0.01(0.12)	43.03(0.45)	7	
1995ar	0.4650	23.37(0.11)	0.93(0.14)	0.33(0.24)	41.84(0.68)	7	
1995aq	0.4530	23.20(0.06)	0.93(0.05)	-0.12(0.09)	42.69(0.39)	7	
1994g	0.4250	22.34(0.15)	0.90(0.10)	0.09(0.11)	41.30(0.37)	7	
1997n	0.1800	20.47(0.03)	0.99(0.02)	0.00(0.00)	39.76(0.05)	7	c
1997i	0.1720	20.23(0.03)	0.93(0.02)	0.00(0.00)	39.45(0.03)	7	c
1994an	0.3780	22.63(0.11)	0.95(0.23)	0.00(0.00)	41.87(0.31)	7	c
1994am	0.3720	22.00(0.08)	0.88(0.07)	0.00(0.00)	41.16(0.15)	7	c
1994al	0.4200	22.89(0.06)	0.94(0.08)	0.00(0.00)	42.12(0.13)	7	c
1994h	0.3740	21.80(0.08)	1.00(0.15)	0.00(0.00)	41.10(0.25)	7	c
1994f	0.3540	22.51(0.16)	0.70(0.14)	0.00(0.00)	41.45(0.33)	7	c
1992bi	0.4580	22.83(0.05)	1.33(0.19)	0.00(0.00)	42.54(0.24)	7	c
1997s	0.6120	-	-	-	-	7	f
1997l	0.5500	-	-	-	-	7	f
1997k	0.5920	-	-	-	-	7	f
1997j	0.6190	-	-	-	-	7	f
1999fw	0.2780	21.72(0.06)	0.89(0.10)	0.09(0.06)	40.67(0.21)	8	
1999fn	0.4770	22.72(0.07)	1.03(0.05)	0.02(0.06)	42.01(0.15)	8	
1999fm	0.9500	24.30(0.10)	1.16(0.03)	0.04(0.10)	43.70(0.27)	8	
1999fk	1.0570	24.77(0.13)	0.95(0.13)	-0.03(0.07)	44.08(0.21)	8	
1999fj	0.8160	24.22(0.09)	1.02(0.05)	-0.11(0.18)	43.80(0.42)	8	
1999ff	0.4550	23.21(0.07)	0.86(0.08)	-0.00(0.09)	42.35(0.24)	8	
1999fv	1.1950	23.88(0.54)	0.56(0.02)	-0.85(0.42)	44.57(0.49)	8	d
1999fh	0.3690	23.45(0.06)	0.70(0.19)	0.44(0.09)	41.37(0.38)	8	d
2002ad	0.5140	23.06(0.24)	0.89(0.05)	-0.09(0.25)	42.43(0.43)	9	
2002ab	0.4230	22.60(0.05)	0.96(0.07)	0.10(0.03)	41.61(0.24)	9	
2002aa	0.9460	24.60(0.19)	0.96(0.15)	0.30(0.33)	43.16(0.81)	9	
2002x	0.8590	24.73(0.10)	0.82(0.08)	-0.10(0.08)	44.02(0.30)	9	
2002w	1.0310	24.47(0.18)	0.95(0.12)	0.67(0.51)	42.18(1.29)	9	
2001kd	0.9360	24.96(0.16)	0.64(0.17)	-0.15(0.17)	44.15(0.52)	9	
2001jp	0.5280	22.89(0.08)	0.94(0.04)	-0.10(0.04)	42.35(0.24)	9	
2001jn	0.6450	24.55(0.17)	1.33(0.48)	0.10(0.24)	44.04(0.96)	9	
2001jm	0.9780	24.50(0.10)	0.85(0.04)	-0.01(0.09)	43.65(0.31)	9	
2001jh	0.8850	24.31(0.11)	0.94(0.07)	-0.28(0.18)	44.18(0.47)	9	
2001jf	0.8150	25.19(0.20)	0.57(0.10)	-0.07(0.42)	44.14(0.92)	9	
2001jb	0.6980	24.39(0.08)	0.61(0.04)	-0.30(0.07)	43.88(0.30)	9	o
2001iy	0.5680	23.07(0.06)	0.92(0.06)	-0.13(0.07)	42.56(0.29)	9	
2001ix	0.7110	23.80(0.08)	0.96(0.03)	-0.09(0.04)	43.25(0.25)	9	
2001iw	0.3396	22.10(0.09)	0.89(0.04)	0.07(0.08)	41.10(0.26)	9	
2001iv	0.3965	22.47(0.06)	0.98(0.03)	0.15(0.04)	41.41(0.24)	9	
2001hy	0.8120	24.95(0.09)	0.71(0.05)	0.03(0.06)	43.81(0.28)	9	
2001hx	0.7990	24.78(0.08)	0.96(0.08)	0.38(0.07)	43.17(0.27)	9	
2001hu	0.8820	24.91(0.10)	1.13(0.18)	0.63(0.16)	42.93(0.32)	9	

TABLE C2
SNe of the Union compilation

2001hs	0.8330	24.26(0.09)	1.09(0.05)	0.12(0.11)	43.41(0.35)	9	
2001fs	0.8740	25.12(0.14)	0.84(0.10)	0.37(0.17)	43.39(0.46)	9	
2001fo	0.7720	23.75(0.08)	0.96(0.03)	-0.19(0.04)	43.44(0.26)	9	
2002p	0.7190	-	-	-	-	9	f
2000fr	0.5430	23.03(0.06)	1.03(0.02)	-0.01(0.03)	42.39(0.14)	10	
1998bi	0.7500	23.91(0.07)	0.95(0.02)	-0.01(0.02)	43.17(0.14)	10	
1998be	0.6400	23.80(0.08)	0.73(0.04)	0.02(0.07)	42.73(0.23)	10	
1998ba	0.4300	22.87(0.08)	0.96(0.04)	-0.03(0.04)	42.20(0.14)	10	
1998ay	0.6400	23.72(0.09)	1.02(0.05)	-0.06(0.05)	43.19(0.19)	10	
1998ax	0.4970	23.15(0.06)	1.10(0.03)	0.07(0.04)	42.41(0.16)	10	
1998aw	0.4400	23.20(0.05)	1.01(0.02)	0.23(0.03)	42.00(0.13)	10	
1998as	0.3550	22.67(0.05)	0.88(0.02)	0.13(0.04)	41.52(0.13)	10	
1997ez	0.7800	24.26(0.09)	1.09(0.04)	0.08(0.03)	43.49(0.15)	10	
1997eq	0.5400	23.16(0.05)	0.95(0.02)	-0.02(0.02)	42.43(0.12)	10	
1997ek	0.8600	24.48(0.08)	1.00(0.03)	0.02(0.03)	43.75(0.16)	10	
04Eag	1.0200	24.97(0.10)	0.99(0.05)	0.03(0.06)	44.20(0.22)	11	
04Gre	1.1400	24.73(0.12)	1.14(0.14)	-0.03(0.08)	44.28(0.28)	11	
04Man	0.8540	24.53(0.09)	0.94(0.06)	-0.07(0.06)	43.92(0.22)	11	
04Mcg	1.3700	25.73(0.18)	0.91(0.19)	0.06(0.10)	44.79(0.32)	11	
04Omb	0.9750	24.88(0.09)	1.22(0.06)	0.10(0.03)	44.23(0.20)	11	
04Pat	0.9700	25.02(0.09)	0.99(0.09)	-0.12(0.06)	44.58(0.24)	11	
04Rak	0.7400	23.84(0.12)	1.02(0.04)	-0.11(0.05)	43.42(0.20)	11	
04Sas	1.3900	25.82(0.17)	1.39(0.64)	0.34(0.17)	44.83(0.59)	11	
04Yow	0.4600	23.59(0.11)	0.86(0.07)	0.24(0.06)	42.16(0.19)	11	
05Fer	1.0200	24.83(0.20)	1.08(0.10)	0.11(0.07)	43.98(0.24)	11	
05Gab	1.1200	25.07(0.11)	0.96(0.05)	0.03(0.07)	44.25(0.24)	11	
05Lan	1.2300	26.02(0.12)	0.88(0.10)	0.14(0.06)	44.85(0.24)	11	
05Red	1.1900	25.76(0.13)	0.70(0.10)	0.25(0.05)	44.12(0.25)	11	
05Spo	0.8390	24.20(0.14)	1.00(0.05)	-0.04(0.07)	43.60(0.21)	11	
05Str	1.0100	25.03(0.10)	1.08(0.04)	-0.01(0.02)	44.45(0.20)	11	
05Zwi	0.5210	23.07(0.08)	1.21(0.06)	0.09(0.06)	42.43(0.19)	11	
2002dc	0.4750	23.09(0.15)	0.83(0.05)	0.00(0.13)	42.19(0.22)	11	
2002dd	0.9500	24.66(0.10)	1.09(0.08)	0.13(0.05)	43.77(0.21)	11	
2002fw	1.3000	25.65(0.14)	1.02(0.09)	0.01(0.11)	44.95(0.35)	11	
2002hp	1.3050	25.41(0.16)	0.86(0.04)	0.05(0.08)	44.42(0.29)	11	
2002hr	0.5260	24.04(0.12)	1.03(0.09)	0.16(0.05)	43.02(0.23)	11	
2002kc	0.2160	22.13(0.08)	1.03(0.04)	0.32(0.04)	40.75(0.17)	11	o
2002kd	0.7350	24.02(0.08)	0.92(0.01)	0.04(0.04)	43.11(0.18)	11	
2002ki	1.1400	25.35(0.16)	1.00(0.36)	0.27(0.20)	44.03(0.77)	11	
2003ak	1.5510	26.64(0.26)	1.04(0.46)	0.29(0.08)	45.33(0.40)	11	
2003az	1.2650	25.68(0.12)	0.99(0.07)	0.15(0.05)	44.63(0.23)	11	
2003dy	1.3400	25.77(0.14)	1.23(0.15)	0.18(0.07)	44.95(0.25)	11	
2003eb	0.9000	24.08(0.09)	0.98(0.03)	0.08(0.03)	43.18(0.20)	11	o
2003eq	0.8400	24.35(0.08)	0.97(0.05)	0.02(0.03)	43.56(0.20)	11	
04Kur	0.3590	23.97(0.05)	0.91(0.03)	0.00(0.00)	43.16(0.07)	11	c,d
04Tha	0.9540	24.37(0.24)	0.99(0.08)	-0.17(0.10)	44.04(0.18)	11	p
05Dic	0.6380	23.59(0.06)	1.07(0.06)	0.13(0.02)	42.69(0.13)	11	d
05Koe	1.2300	24.93(0.16)	1.07(0.07)	-0.12(0.07)	44.58(0.21)	11	p
2002fx	1.4000	26.57(1.16)	0.94(5.73)	0.00(0.00)	45.80(5.94)	11	c,d
2003aj	1.3070	26.54(0.17)	0.68(0.15)	0.08(0.10)	45.27(0.34)	11	d
2003bd	0.6700	24.21(0.10)	0.89(0.03)	0.11(0.03)	43.13(0.07)	11	p
2003be	0.6400	24.00(0.35)	0.95(0.10)	0.12(0.13)	42.97(0.13)	11	p
2003es	0.9540	24.50(0.34)	0.90(0.10)	-0.17(0.11)	44.06(0.15)	11	p
2003XX	0.9350	24.31(0.11)	1.07(0.04)	-0.00(0.06)	43.69(0.14)	11	p
04Haw	0.4900	-	-	-	-	11	f
03D4bc	0.5720	24.60(0.09)	0.77(0.05)	0.03(0.08)	43.56(0.23)	12	o
03D4au	0.4680	23.86(0.05)	1.00(0.03)	0.29(0.04)	42.49(0.16)	12	
04D4bk	0.8400	24.31(0.09)	1.05(0.06)	0.14(0.12)	43.35(0.33)	12	
04D3nr	0.9600	24.54(0.13)	0.92(0.06)	0.07(0.14)	43.59(0.43)	12	
04D3lu	0.8218	24.34(0.09)	0.95(0.03)	0.02(0.12)	43.54(0.35)	12	
04D3ki	0.9300	24.87(0.17)	0.90(0.05)	-0.26(0.23)	44.64(0.69)	12	
04D3gt	0.4510	23.23(0.04)	0.95(0.01)	0.28(0.02)	41.85(0.14)	12	
04D3do	0.6100	23.57(0.06)	0.86(0.02)	-0.08(0.03)	42.88(0.15)	12	
04D3cp	0.8300	24.24(0.10)	1.11(0.03)	-0.45(0.17)	44.69(0.46)	12	
04D2gp	0.7070	24.15(0.09)	0.80(0.05)	-0.05(0.08)	43.32(0.25)	12	
04D2fp	0.4150	22.53(0.04)	0.96(0.01)	0.01(0.02)	41.77(0.13)	12	
04D1ag	0.5570	23.00(0.06)	0.94(0.03)	-0.18(0.03)	42.65(0.15)	12	
03D4fd	0.7910	24.21(0.08)	0.94(0.05)	0.04(0.06)	43.33(0.19)	12	
03D4cz	0.6950	24.03(0.08)	0.75(0.03)	-0.06(0.05)	43.16(0.18)	12	
03D4at	0.6330	23.74(0.07)	0.98(0.06)	-0.08(0.06)	43.20(0.20)	12	
03D3bh	0.2486	21.13(0.08)	0.99(0.03)	-0.09(0.06)	40.63(0.14)	12	
03D3af	0.5320	23.49(0.06)	0.94(0.04)	0.03(0.05)	42.65(0.20)	12	
03D1fc	0.3310	21.80(0.03)	0.94(0.01)	0.04(0.01)	40.93(0.12)	12	
03D1bp	0.3460	22.45(0.04)	0.84(0.01)	0.12(0.03)	41.28(0.13)	12	
04D4dw	0.9610	24.57(0.15)	0.96(0.08)	-0.12(0.19)	44.09(0.54)	12	
04D4an	0.6130	24.02(0.06)	0.82(0.02)	0.06(0.02)	42.96(0.15)	12	
04D3nh	0.3402	22.14(0.03)	1.01(0.01)	0.08(0.01)	41.26(0.12)	12	

TABLE C2
SNe of the Union compilation

04D3lp	0.9830	24.93(0.24)	0.83(0.06)	0.02(0.28)	43.97(0.87)	12	
04D3is	0.7100	24.26(0.08)	0.98(0.04)	0.22(0.05)	43.03(0.19)	12	
04D3fq	0.7300	24.13(0.07)	0.92(0.03)	0.01(0.04)	43.31(0.17)	12	
04D3df	0.4700	23.47(0.05)	0.73(0.02)	0.06(0.03)	42.30(0.15)	12	
04D3co	0.6200	23.78(0.06)	0.89(0.02)	-0.06(0.03)	43.10(0.15)	12	
04D2gc	0.5210	23.32(0.06)	1.07(0.05)	0.18(0.04)	42.28(0.17)	12	
04D2cf	0.3690	22.34(0.04)	0.89(0.02)	-0.00(0.01)	41.51(0.13)	12	
03D4gl	0.5710	23.26(0.07)	0.98(0.06)	0.03(0.05)	42.46(0.18)	12	
03D4dy	0.6040	23.32(0.06)	1.06(0.02)	0.11(0.02)	42.44(0.14)	12	
03D4cy	0.9271	24.72(0.16)	1.05(0.06)	-0.29(0.21)	44.74(0.62)	12	
03D4ag	0.2850	21.21(0.03)	1.02(0.02)	-0.08(0.01)	40.71(0.13)	12	
03D3ba	0.2912	22.05(0.05)	1.04(0.03)	0.26(0.02)	40.79(0.13)	12	
03D1gt	0.5480	24.12(0.08)	0.86(0.05)	0.24(0.06)	42.68(0.16)	12	
03D1ew	0.8680	24.37(0.14)	1.02(0.06)	-0.11(0.25)	43.96(0.70)	12	
03D1ax	0.4960	22.96(0.05)	0.88(0.02)	-0.05(0.04)	42.22(0.16)	12	
04D4dm	0.8110	24.39(0.09)	1.00(0.05)	-0.16(0.14)	44.06(0.36)	12	
04D3oe	0.7560	24.08(0.09)	0.81(0.03)	-0.23(0.06)	43.67(0.20)	12	
04D3nc	0.8170	24.27(0.08)	1.11(0.05)	0.06(0.11)	43.57(0.31)	12	
04D3ks	0.7520	23.88(0.08)	1.01(0.04)	0.02(0.05)	43.14(0.18)	12	
04D3hn	0.5516	23.47(0.05)	0.90(0.02)	0.11(0.03)	42.41(0.15)	12	
04D3fk	0.3578	22.53(0.04)	0.92(0.00)	0.15(0.01)	41.39(0.13)	12	
04D3dd	1.0100	25.12(0.27)	1.09(0.10)	-0.07(0.28)	44.69(0.91)	12	
04D2ja	0.7410	24.10(0.07)	0.95(0.02)	-0.07(0.03)	43.48(0.16)	12	
04D2gb	0.4300	22.80(0.05)	0.78(0.02)	-0.01(0.03)	41.84(0.14)	12	
04D1ak	0.5260	23.63(0.06)	0.82(0.03)	0.02(0.04)	42.67(0.15)	12	
03D4gg	0.5920	23.40(0.07)	1.00(0.08)	0.08(0.05)	42.52(0.20)	12	
03D4di	0.9050	24.29(0.12)	1.10(0.05)	0.02(0.14)	43.69(0.42)	12	
03D4cx	0.9490	24.50(0.14)	0.90(0.06)	0.09(0.15)	43.47(0.47)	12	
03D3cd	0.4607	22.56(0.10)	1.13(0.18)	0.02(0.06)	41.97(0.26)	12	
03D3ay	0.3709	22.20(0.04)	0.97(0.02)	-0.02(0.02)	41.50(0.13)	12	
03D1fq	0.8000	24.52(0.10)	0.77(0.06)	-0.39(0.21)	44.42(0.54)	12	
03D1co	0.6790	24.10(0.07)	1.01(0.03)	0.00(0.05)	43.42(0.18)	12	
03D1aw	0.5817	23.59(0.07)	0.98(0.04)	0.01(0.06)	42.84(0.18)	12	
04D4bq	0.5500	23.36(0.06)	1.00(0.04)	0.11(0.04)	42.40(0.16)	12	
04D3ny	0.8100	24.27(0.10)	1.01(0.10)	-0.07(0.18)	43.73(0.49)	12	
04D3ml	0.9500	24.55(0.13)	1.19(0.15)	0.13(0.16)	43.78(0.42)	12	
04D3kr	0.3373	21.97(0.03)	1.06(0.01)	0.07(0.01)	41.18(0.12)	12	
04D3gx	0.9100	24.71(0.11)	0.95(0.04)	-0.20(0.13)	44.41(0.39)	12	
04D3ez	0.2630	21.68(0.03)	0.89(0.02)	0.09(0.01)	40.64(0.12)	12	
04D3cy	0.6430	23.80(0.07)	0.96(0.02)	0.02(0.04)	43.01(0.16)	12	
04D2iu	0.6910	24.26(0.07)	0.80(0.02)	0.07(0.04)	43.14(0.17)	12	
04D2fs	0.3570	22.42(0.04)	0.94(0.02)	0.13(0.02)	41.36(0.13)	12	
04D1aj	0.7210	23.90(0.08)	1.07(0.09)	0.07(0.05)	43.13(0.19)	12	
03D4gf	0.5810	23.35(0.06)	1.02(0.03)	-0.05(0.03)	42.79(0.15)	12	
03D4dh	0.6268	23.39(0.06)	1.04(0.02)	0.01(0.02)	42.71(0.15)	12	
03D4cn	0.8180	24.65(0.10)	0.75(0.08)	0.03(0.21)	43.57(0.56)	12	
03D3aw	0.4490	22.55(0.05)	0.95(0.02)	-0.05(0.03)	41.90(0.15)	12	
03D1fl	0.6880	23.63(0.07)	0.96(0.05)	-0.07(0.04)	43.04(0.18)	12	
03D1cm	0.8700	24.46(0.11)	1.19(0.06)	-0.04(0.17)	44.08(0.50)	12	
03D1au	0.5043	22.98(0.05)	1.08(0.02)	0.03(0.03)	42.30(0.14)	12	
03D3cc	0.4627	22.62(0.19)	1.05(0.06)	-0.05(0.09)	42.09(0.10)	12	p
b010	0.5910	23.40(0.08)	1.24(0.09)	-0.14(0.08)	43.31(0.27)	13	
b013	0.4260	22.68(0.05)	1.01(0.04)	0.08(0.03)	41.81(0.20)	13	
b016	0.3290	22.50(0.21)	1.14(0.11)	0.26(0.09)	41.38(0.25)	13	
d033	0.5310	23.23(0.06)	1.15(0.12)	-0.15(0.08)	43.06(0.30)	13	
d058	0.5830	23.59(0.10)	1.09(0.21)	0.18(0.15)	42.60(0.46)	13	
d083	0.3330	21.03(0.04)	1.18(0.04)	-0.02(0.03)	40.60(0.20)	13	o
d084	0.5190	23.64(0.09)	1.09(0.17)	-0.01(0.14)	43.09(0.39)	13	
d085	0.4010	22.48(0.07)	1.02(0.06)	0.08(0.08)	41.62(0.26)	13	
d087	0.3400	21.91(0.18)	0.99(0.07)	0.04(0.08)	41.10(0.22)	13	
d089	0.4360	22.50(0.05)	1.04(0.04)	0.00(0.05)	41.84(0.22)	13	
d093	0.3630	21.89(0.07)	1.04(0.03)	-0.07(0.06)	41.40(0.21)	13	
d097	0.4360	22.50(0.05)	1.26(0.06)	0.09(0.05)	41.92(0.21)	13	
d117	0.3090	22.36(0.07)	0.83(0.02)	0.07(0.06)	41.29(0.21)	13	
d149	0.3420	22.19(0.06)	1.01(0.03)	0.07(0.04)	41.33(0.20)	13	
e029	0.3320	22.52(0.06)	0.84(0.06)	0.17(0.06)	41.24(0.22)	13	
e108	0.4690	22.55(0.05)	1.10(0.05)	-0.05(0.05)	42.09(0.22)	13	
e132	0.2390	21.70(0.05)	0.92(0.02)	0.19(0.04)	40.47(0.19)	13	
e136	0.3520	22.80(0.06)	0.82(0.05)	0.19(0.06)	41.44(0.22)	13	
e138	0.6120	24.05(0.19)	1.37(0.19)	0.68(0.31)	42.26(0.82)	13	
e140	0.6310	23.39(0.07)	0.99(0.10)	0.05(0.07)	42.57(0.27)	13	
e147	0.6450	23.38(0.07)	0.96(0.04)	-0.09(0.06)	42.83(0.23)	13	
e148	0.4290	22.65(0.05)	0.87(0.03)	-0.02(0.05)	41.83(0.22)	13	
e149	0.4970	22.90(0.07)	0.92(0.03)	0.01(0.07)	42.09(0.23)	13	
f011	0.5390	23.29(0.07)	0.88(0.05)	0.03(0.07)	42.36(0.24)	13	
f041	0.5610	23.09(0.06)	1.07(0.07)	-0.05(0.07)	42.60(0.25)	13	
f076	0.4100	22.37(0.05)	0.90(0.03)	0.09(0.06)	41.35(0.22)	13	

TABLE C2
SNe of the Union compilation

f096	0.4120	23.06(0.11)	1.21(0.10)	0.37(0.12)	41.78(0.30)	13	
f216	0.5990	23.75(0.09)	0.71(0.06)	-0.07(0.09)	42.85(0.29)	13	
f231	0.6190	23.45(0.08)	1.01(0.07)	-0.07(0.07)	42.92(0.25)	13	
f235	0.4220	22.45(0.07)	0.88(0.05)	-0.03(0.08)	41.67(0.24)	13	
f244	0.5400	23.30(0.06)	0.94(0.11)	-0.02(0.06)	42.57(0.25)	13	
f308	0.4010	23.07(0.08)	0.88(0.14)	0.07(0.10)	42.07(0.31)	13	
g005	0.2180	21.32(0.07)	1.17(0.06)	0.23(0.05)	40.32(0.20)	13	
g050	0.6330	23.18(0.09)	0.96(0.07)	0.09(0.09)	42.23(0.30)	13	
g052	0.3830	22.33(0.08)	0.78(0.03)	-0.10(0.08)	41.59(0.23)	13	
g055	0.3020	23.28(0.14)	1.23(0.13)	0.57(0.11)	41.57(0.26)	13	
g097	0.3400	22.27(0.06)	1.00(0.03)	0.19(0.04)	41.14(0.20)	13	
g120	0.5100	22.79(0.07)	0.96(0.06)	0.06(0.08)	41.92(0.26)	13	
g133	0.4210	23.17(0.12)	1.15(0.11)	0.30(0.06)	41.97(0.23)	13	
g142	0.3990	23.46(0.11)	0.75(0.09)	0.32(0.11)	41.71(0.28)	13	
g160	0.4930	22.92(0.06)	1.06(0.04)	0.08(0.07)	42.12(0.23)	13	
g240	0.6870	23.40(0.09)	0.92(0.07)	-0.10(0.08)	42.83(0.28)	13	
h283	0.5020	23.45(0.13)	0.65(0.10)	0.18(0.16)	41.90(0.31)	13	
h300	0.6870	23.52(0.08)	1.04(0.05)	0.02(0.06)	42.82(0.25)	13	
h319	0.4950	22.90(0.06)	1.09(0.08)	0.05(0.06)	42.20(0.25)	13	
h323	0.6030	23.48(0.07)	0.92(0.05)	0.02(0.08)	42.64(0.27)	13	
h342	0.4210	22.44(0.08)	1.15(0.11)	-0.05(0.09)	42.04(0.28)	13	
h359	0.3480	22.65(0.05)	0.95(0.03)	0.15(0.04)	41.55(0.20)	13	
h363	0.2130	22.01(0.09)	0.88(0.03)	0.36(0.07)	40.34(0.20)	13	
h364	0.3440	21.71(0.05)	0.90(0.02)	-0.08(0.04)	41.07(0.20)	13	
k396	0.2710	21.84(0.07)	0.81(0.06)	0.15(0.06)	40.55(0.21)	13	
k411	0.5640	22.89(0.13)	0.93(0.16)	-0.12(0.10)	42.38(0.40)	13	
k425	0.2740	21.94(0.09)	0.91(0.04)	0.15(0.07)	40.77(0.22)	13	
k430	0.5820	23.81(0.07)	0.94(0.06)	-0.08(0.08)	43.21(0.28)	13	
k441	0.6800	23.73(0.07)	1.13(0.10)	0.16(0.06)	42.83(0.25)	13	
k448	0.4010	23.34(0.07)	0.97(0.06)	0.29(0.07)	41.93(0.24)	13	
k485	0.4160	23.93(0.11)	0.92(0.12)	0.61(0.11)	41.75(0.30)	13	
m027	0.2860	22.52(0.12)	1.10(0.19)	0.24(0.10)	41.39(0.33)	13	
m062	0.3140	21.99(0.11)	0.83(0.13)	0.03(0.08)	41.02(0.29)	13	
m138	0.5810	23.28(0.09)	1.20(0.11)	-0.34(0.09)	43.60(0.38)	13	
m158	0.4630	23.09(0.07)	1.00(0.05)	0.19(0.08)	41.95(0.27)	13	
m193	0.3410	21.66(0.08)	0.98(0.03)	-0.07(0.05)	41.09(0.21)	13	
m226	0.6710	23.64(0.09)	1.07(0.15)	0.37(0.14)	42.19(0.33)	13	
n256	0.6310	23.41(0.07)	1.07(0.08)	-0.06(0.05)	42.93(0.23)	13	
n258	0.5220	23.29(0.07)	0.91(0.05)	-0.08(0.11)	42.67(0.30)	13	
n263	0.3680	22.04(0.05)	0.97(0.03)	-0.05(0.04)	41.41(0.20)	13	
n278	0.3090	21.87(0.05)	0.89(0.04)	0.08(0.05)	40.85(0.21)	13	
n285	0.5280	23.27(0.09)	1.14(0.22)	0.11(0.10)	42.48(0.31)	13	
n326	0.2680	22.11(0.06)	0.66(0.02)	0.09(0.05)	40.77(0.20)	13	
n404	0.2160	21.85(0.07)	0.92(0.02)	0.19(0.06)	40.61(0.20)	13	o
p454	0.6950	23.93(0.11)	0.71(0.16)	-0.02(0.15)	42.92(0.41)	13	
p455	0.2840	21.66(0.06)	0.85(0.02)	-0.01(0.05)	40.79(0.20)	13	
p524	0.5080	22.91(0.06)	1.02(0.03)	0.04(0.04)	42.14(0.21)	13	
p528	0.7810	24.12(0.11)	0.96(0.16)	-0.00(0.16)	43.38(0.34)	13	
p534	0.6130	23.40(0.11)	0.63(0.32)	-0.08(0.18)	42.43(0.33)	13	
b020	0.4250	22.47(0.18)	0.84(0.11)	0.07(0.18)	41.41(0.29)	13	d
d086	0.2050	20.94(0.03)	0.94(0.02)	0.00(0.00)	40.16(0.05)	13	c
d099	0.2110	20.88(0.10)	0.92(0.04)	-0.06(0.06)	40.22(0.08)	13	p
e020	0.1590	20.65(0.03)	1.03(0.06)	0.00(0.00)	39.99(0.09)	13	c
k429	0.1810	20.34(0.03)	0.95(0.04)	0.00(0.00)	39.58(0.07)	13	c
m026	0.6530	22.90(0.25)	1.38(0.23)	-0.08(0.18)	42.85(0.46)	13	p
m032	0.1550	20.21(0.14)	0.96(0.06)	0.00(0.00)	39.46(0.09)	13	p,c,d
m034	0.5620	22.90(0.15)	1.25(0.11)	-0.30(0.12)	43.18(0.25)	13	p
m039	0.2490	22.01(0.24)	1.01(0.18)	0.30(0.14)	40.63(0.19)	13	p
m057	0.1840	21.01(0.10)	1.35(0.18)	0.00(0.00)	40.75(0.32)	13	p,c,d
h311	0.7500	-	-	-	-	13	f
m022	0.2400	-	-	-	-	13	f
m043	0.2660	-	-	-	-	13	f
m075	0.1020	-	-	-	-	13	f
n346	0.2660	-	-	-	-	13	f
n368	0.3440	-	-	-	-	13	f
n395	0.4620	-	-	-	-	13	f
p425	0.4530	-	-	-	-	13	f
p429	0.5480	-	-	-	-	13	f

References. — [1]Hamuy et al. (1996), [2]Krisciunas et al. (2005), [3]Riess et al. (1996), [4]Jha et al. (2006), [5]this work, [6]Riess et al. (1998) + HZT, [7]Perlmutter et al. (1999), [8]Tonry et al. (2003), [9]Barris et al. (2003), [10]Knop et al. (2003), [11]Riess et al. (2006), [12]Astier et al. (2006), [13]Miknaitis et al. (2007).

Note. — Explanation of cuts: o: 3σ outlier, p: insufficient early data, c: no color, d: too few data points, f: fit not converged

LIGHTCURVE DATA FROM PERLMUTTER ET AL. (1999)

TABLE D1
THE PHOTOMETRIC LIGHTCURVE DATA FROM THE 42 SNE OF PERLMUTTER ET AL. (1999). IT CONSISTS OF BESSELL R AND I BAND DATA AND IS PRESENTED AS FLUX, WITH A COMMON ZERO-POINT OF $zp = 30$ MAGNITUDES. MULTIPLE DATA POINTS FOR A GIVEN NIGHT WERE COMBINED INTO A SINGLE DATA POINT. SINCE REFERENCE IMAGES WHERE USED TO SUBTRACT THE HOST GALAXY LIGHT, THE DATA POINTS ARE CORRELATED. WE RECOMMEND USING THE DATA FROM THE WEB-LINK "HTTP://SUPERNOVA.LBL.GOV/UNION", WHICH INCLUDES THE COVARIANCE MATRIX. MORE INFORMATION ABOUT THE SNE CAN BE FOUND IN PERLMUTTER ET AL. (1999).

	R			I	
MJD	flux ($zp = 30$ mag)	σ(flux)	MJD	flux ($zp = 30$ mag)	σ(flux)
		SN 1997s ($z = 0.612$)			
50431.85	9.89e+01	5.71e+01	50459.04	5.84e+02	2.20e+02
50432.82	1.11e+02	5.85e+01	50465.96	3.68e+02	3.64e+02
50454.82	6.49e+02	4.05e+01	50466.92	7.34e+02	2.29e+02
50459.01	5.49e+02	4.47e+01	50480.86	4.28e+02	9.23e+01
50462.82	6.82e+02	4.05e+01	50489.79	9.54e+02	1.16e+02
50465.82	5.92e+02	7.19e+01	50513.78	4.54e+02	1.85e+02
50480.83	2.18e+02	3.04e+01	50514.77	6.36e+02	1.06e+02
50489.76	2.37e+02	3.30e+01	50518.77	3.95e+02	1.51e+02
50513.74	4.10e+01	2.98e+01			
50514.73	6.83e+01	6.09e+01			
50517.76	4.12e+01	3.52e+01			
50518.82	5.07e+01	4.58e+01			
50573.67	8.88e+01	4.52e+01			
50574.56	7.71e+01	5.64e+01			
50872.56	3.30e+00	5.91e+01			
50873.56	1.65e+01	6.60e+01			
50895.54	6.63e+01	5.88e+01			
50896.59	1.06e+02	5.42e+01			
		SN 1997r ($z = 0.657$)			
50431.84	4.11e+01	5.26e+01	50480.82	3.69e+02	5.65e+01
50432.82	-7.37e+01	4.82e+01	50489.83	8.53e+01	9.77e+01
50454.81	2.37e+02	3.54e+01	50513.76	-2.51e+02	1.35e+02
50459.89	3.88e+02	2.73e+01	50514.76	9.04e-01	7.16e+01
50462.84	4.10e+02	3.44e+01	50518.75	-2.90e+02	1.21e+02
50464.99	3.82e+02	4.12e+01			
50467.94	5.19e+02	4.63e+01			
50480.80	3.60e+02	2.65e+01			
50489.86	2.01e+02	2.73e+01			
50513.73	1.94e+01	2.50e+01			
50514.71	-2.29e+00	4.54e+01			
50517.75	-1.73e+01	3.61e+01			
50518.80	-1.08e+01	4.23e+01			
50574.68	3.16e+01	3.28e+01			
50872.57	-4.18e+01	4.74e+01			
50873.74	1.44e+01	3.30e+01			
50895.62	-1.53e+01	3.53e+01			
50896.59	-4.52e+01	3.69e+01			
50899.69	2.03e+01	4.77e+01			
50904.65	6.30e+00	2.10e+01			
		SN 1997q ($z = 0.43$)			
50431.84	1.40e+02	5.56e+01	50480.82	6.17e+02	6.04e+01
50432.82	1.68e+02	4.87e+01	50489.83	1.82e+02	8.41e+01
50454.81	1.62e+03	4.04e+01	50513.76	5.27e+01	1.35e+02
50459.82	1.42e+03	3.84e+01	50514.76	-1.09e-01	7.27e+01
50461.83	1.23e+03	6.42e+01	50518.75	-1.01e+02	1.19e+02
50462.79	1.30e+03	4.03e+01	50573.60	2.54e+01	2.13e+02
50467.91	9.60e+02	7.10e+01			
50480.80	4.41e+02	2.87e+01			
50489.86	2.51e+02	2.97e+01			
50513.73	1.65e+02	2.69e+01			
50514.71	1.81e+02	4.88e+01			
50517.75	1.44e+02	3.59e+01			
50518.80	1.52e+02	4.11e+01			
50573.60	2.08e+02	6.76e+01			
50872.57	1.25e+01	4.95e+01			
50873.73	2.03e+01	3.58e+01			
50895.62	5.65e+01	3.69e+01			
50896.59	1.27e+01	3.74e+01			
50899.69	-3.98e+01	4.89e+01			
50904.65	4.48e+01	2.22e+01			
		SN 1997p ($z = 0.472$)			

TABLE D1 — *Continued*

MJD	R flux ($zp = 30$ mag)	σ(flux)	MJD	I flux ($zp = 30$ mag)	σ(flux)
50431.86	8.28e+01	1.72e+02	50458.98	1.39e+03	1.76e+02
50432.84	1.06e+02	3.52e+01	50465.69	1.57e+03	1.15e+03
50454.80	9.74e+02	4.02e+01	50482.94	4.29e+02	1.07e+02
50458.02	9.25e+02	3.28e+01	50489.83	3.74e+02	1.10e+02
50462.76	7.71e+02	4.50e+01	50513.76	5.59e+02	1.91e+02
50465.68	8.64e+02	7.94e+01	50514.75	2.19e+02	1.31e+02
50467.88	6.02e+02	5.94e+01	50518.75	2.95e+02	1.50e+02
50482.90	1.64e+02	3.01e+01	50521.82	2.12e+02	1.38e+02
50489.86	2.05e+02	3.48e+01	50573.48	3.00e+02	1.90e+02
50513.73	7.12e+01	3.39e+01	50845.94	-2.15e+02	2.02e+02
50514.71	4.58e+01	5.62e+01			
50517.75	1.14e+02	4.25e+01			
50518.80	1.29e+02	5.64e+01			
50521.79	5.45e+01	7.06e+01			
50550.53	2.17e+01	3.09e+01			
50568.51	6.03e+01	3.34e+01			
50573.46	-2.63e+01	6.07e+01			
50575.67	-4.93e-01	2.58e+01			
50873.73	9.29e+01	6.74e+01			
50895.62	-1.24e+01	5.19e+01			
50896.59	1.03e+01	4.91e+01			
50899.69	3.67e+01	5.87e+01			
50904.65	1.05e+02	3.05e+01			
		SN 1997o ($z = 0.374$)			
50432.76	8.62e+00	4.15e+01	50458.95	2.32e+02	1.60e+02
50454.76	3.41e+02	3.82e+01	50466.55	4.00e+02	7.16e+02
50458.92	4.86e+02	4.81e+01	50480.76	8.01e+02	9.12e+01
50465.90	6.24e+02	6.89e+01	50489.68	4.13e+02	9.35e+01
50467.83	7.03e+02	7.68e+01	50513.63	5.24e+02	1.50e+02
50480.73	5.30e+02	3.18e+01	50514.61	3.83e+02	1.07e+02
50489.65	3.52e+02	3.25e+01	50518.62	2.85e+02	9.73e+01
50490.70	2.59e+02	4.72e+01	50521.75	1.15e+02	2.10e+02
50513.63	9.68e+01	3.42e+01	50537.69	6.90e+01	2.21e+02
50514.63	1.16e+02	3.30e+01	50573.52	-1.53e+01	1.24e+02
50517.63	9.37e+01	4.09e+01	50816.74	9.05e+01	6.86e+01
50518.62	9.74e+01	3.84e+01	50835.79	7.49e+01	8.18e+01
50521.72	1.15e+02	5.22e+01			
50537.69	4.86e+01	7.72e+01			
50545.52	8.47e+01	6.80e+01			
50550.39	9.98e+01	3.58e+01			
50573.51	2.91e+01	4.54e+01			
50780.79	3.91e+01	2.71e+01			
50781.82	2.02e+01	2.66e+01			
50810.81	3.23e+01	1.90e+01			
50811.83	6.20e+01	4.50e+01			
50835.75	3.34e+01	2.34e+01			
		SN 1997n ($z = 0.18$)			
50020.86	-1.33e+02	5.63e+01	50160.56	-1.46e+02	1.02e+02
50137.56	-1.01e+01	6.13e+01	50168.54	-4.47e+00	7.27e+01
50138.54	9.56e+00	6.97e+01	50459.94	3.52e+03	2.30e+02
50159.54	2.74e+01	5.37e+01	50466.50	3.42e+03	2.53e+02
50160.53	-1.67e+01	3.80e+01	50482.87	2.41e+03	2.15e+02
50168.54	1.83e+00	4.13e+01	50490.70	2.05e+03	1.82e+02
50431.81	3.67e+03	8.03e+01	50513.64	9.16e+02	1.94e+02
50432.76	4.17e+03	5.93e+01	50514.62	9.58e+02	1.19e+02
50453.79	6.31e+03	8.44e+01	50573.50	2.09e+02	2.31e+02
50454.71	5.89e+03	7.11e+01			
50457.99	5.26e+03	6.23e+01			
50459.79	4.74e+03	6.23e+01			
50461.80	4.50e+03	9.12e+01			
50466.54	3.95e+03	1.74e+02			
50467.79	3.53e+03	8.67e+01			
50482.85	1.76e+03	5.38e+01			
50490.72	1.40e+03	5.08e+01			
50513.63	7.77e+02	5.06e+01			
50514.62	7.54e+02	4.04e+01			
50517.62	8.20e+02	5.97e+01			
50573.50	3.39e+02	8.00e+01			
50780.84	1.85e+01	4.65e+01			
50781.79	2.52e+01	3.35e+01			
50811.78	-4.63e+00	3.39e+01			
		SN 1997l ($z = 0.55$)			
50432.75	3.66e+01	4.52e+01	50490.69	3.63e+02	1.12e+02
50453.76	4.66e+02	4.75e+01	50513.62	1.27e+02	1.33e+02
50454.73	4.65e+02	4.63e+01			

TABLE D1 — *Continued*

MJD	*R* flux ($zp = 30$ mag)	σ(flux)	MJD	*I* flux ($zp = 30$ mag)	σ(flux)
50457.94	6.16e+02	5.17e+01			
50459.89	6.63e+02	3.49e+01			
50461.69	6.91e+02	5.87e+01			
50462.74	7.96e+02	3.99e+01			
50464.89	6.28e+02	8.59e+01			
50480.68	4.63e+02	2.69e+01			
50489.71	3.03e+02	2.96e+01			
50508.46	2.67e+02	3.01e+01			
50513.62	1.59e+02	3.57e+01			
50514.60	1.52e+02	4.89e+01			
50517.62	1.53e+02	3.66e+01			
50573.48	6.99e+01	7.41e+01			
50780.83	4.44e+01	4.98e+01			
		SN 1997k ($z = 0.592$)			
50454.67	3.75e+02	6.02e+01	50458.76	5.47e+02	1.19e+02
50458.76	3.83e+02	5.29e+01	50459.70	3.71e+02	9.49e+01
50459.70	3.48e+02	4.02e+01	50483.84	1.96e+02	1.64e+02
50462.71	2.90e+02	5.33e+01	50490.65	1.84e+02	8.55e+01
50465.79	2.66e+02	6.51e+01	50514.54	1.35e+02	1.78e+02
50483.80	1.59e+02	5.37e+01	50517.56	1.85e+02	1.88e+02
50490.63	1.40e+02	3.90e+01	50518.57	6.74e+01	9.15e+01
50513.57	4.09e+01	5.05e+01			
50514.55	2.07e+01	4.74e+01			
50517.59	1.09e+02	5.29e+01			
50518.54	7.45e+01	4.64e+01			
		SN 1997j ($z = 0.619$)			
50020.84	1.26e+02	7.96e+01	50457.91	4.63e+02	1.54e+02
50040.83	1.42e+02	8.66e+01	50458.90	4.58e+02	1.58e+02
50431.77	1.09e+02	6.64e+01	50464.85	6.31e+02	1.38e+02
50453.72	6.14e+02	5.23e+01	50489.60	2.84e+02	1.10e+02
50454.64	6.59e+02	5.59e+01	50514.55	2.39e+02	1.84e+02
50457.88	5.25e+02	4.34e+01			
50458.84	5.38e+02	4.50e+01			
50462.63	5.86e+02	5.75e+01			
50464.82	5.43e+02	5.22e+01			
50482.73	1.63e+02	4.37e+01			
50489.63	2.33e+02	4.22e+01			
50513.56	1.55e+02	5.68e+01			
50514.54	1.79e+02	5.06e+01			
50517.54	2.13e+02	5.86e+01			
50867.70	1.93e-01	3.42e+01			
		SN 1997i ($z = 0.172$)			
50432.65	1.72e+02	5.00e+01	50458.84	8.39e+03	2.52e+02
50453.67	4.04e+03	5.67e+01	50464.79	9.01e+03	3.35e+02
50454.60	4.69e+03	4.25e+01	50480.65	5.08e+03	1.68e+02
50458.82	7.02e+03	6.28e+01	50486.64	4.82e+03	1.75e+02
50461.58	8.32e+03	9.03e+01	50490.57	5.30e+03	2.33e+02
50462.60	8.50e+03	8.23e+01	50545.50	1.39e+03	1.81e+02
50464.78	8.72e+03	1.20e+02	50757.89	3.17e+00	5.52e+01
50480.63	5.74e+03	6.45e+01			
50490.56	3.62e+03	6.00e+01			
50545.49	7.61e+02	7.25e+01			
50752.93	-1.40e+00	3.10e+01			
50781.71	-5.10e+00	5.52e+01			
50811.62	3.78e-01	4.03e+01			
		SN 1997h ($z = 0.526$)			
50432.65	1.58e+02	5.63e+01	50458.84	1.11e+03	1.72e+02
50453.67	8.75e+02	4.46e+01	50464.79	1.03e+03	2.28e+02
50454.60	8.17e+02	3.08e+01	50480.65	4.62e+02	1.09e+02
50458.82	7.76e+02	3.82e+01	50486.64	4.74e+02	1.22e+02
50461.58	6.94e+02	6.34e+01	50490.57	4.91e+02	1.34e+02
50462.60	6.02e+02	4.17e+01	50545.50	4.84e+02	1.85e+02
50464.78	6.35e+02	1.19e+02	50757.89	4.80e+00	5.92e+01
50480.63	1.70e+02	3.33e+01			
50490.57	1.93e+02	4.61e+01			
50545.49	9.60e+01	7.54e+01			
50752.93	4.90e-01	3.16e+01			
50781.71	7.95e+00	5.91e+01			
50811.62	2.50e+01	4.24e+01			
		SN 1997g ($z = 0.763$)			
50431.69	6.16e+01	5.13e+01	50458.73	4.42e+02	1.37e+02
50432.64	1.10e+02	4.43e+01	50464.74	1.96e+02	1.48e+02
50453.66	3.87e+02	3.63e+01	50482.69	1.32e+02	1.47e+02
50454.61	3.84e+02	3.52e+01	50483.63	2.03e+02	9.46e+01
50458.70	2.33e+02	3.26e+01	50490.56	1.76e+02	1.56e+02

TABLE D1 — *Continued*

MJD	R flux ($zp = 30$ mag)	σ(flux)	MJD	I flux ($zp = 30$ mag)	σ(flux)
50462.57	2.95e+02	3.25e+01	50775.87	1.15e+00	9.22e+01
50465.72	2.34e+02	6.68e+01			
50482.64	4.27e+01	3.35e+01			
50490.56	6.65e+01	3.09e+01			
50752.96	1.17e+02	9.65e+01			
50781.70	5.46e+00	2.59e+01			
50810.70	3.23e+00	3.01e+01			
		SN 1997f ($z = 0.58$)			
50431.63	1.41e+02	4.90e+01	50458.63	6.00e+02	1.80e+02
50432.60	5.70e+01	6.34e+01	50459.83	3.93e+02	1.61e+02
50453.61	2.41e+02	3.91e+01	50480.60	8.00e+02	1.43e+02
50454.61	3.96e+02	3.98e+01	50485.64	8.64e+02	1.24e+02
50458.59	5.41e+02	3.56e+01	50489.57	7.07e+02	1.52e+02
50459.76	5.57e+02	6.37e+01	50755.85	3.77e+00	8.84e+01
50462.55	6.71e+02	4.27e+01			
50465.75	7.67e+02	6.99e+01			
50480.57	6.02e+02	3.07e+01			
50489.54	5.09e+02	4.23e+01			
50508.40	1.69e+02	4.43e+01			
50752.87	1.90e-01	3.13e+01			
		SN 1997ap ($z = 0.83$)			
50137.81	-1.63e+01	6.93e+01	50168.80	-1.06e+02	7.63e+01
50138.82	4.19e+01	6.28e+01	50514.86	3.97e+02	8.39e+01
50168.81	6.91e+00	3.76e+01	50518.85	3.70e+02	6.70e+01
50490.87	1.33e+01	3.01e+01	50521.97	3.65e+02	7.91e+01
50513.83	2.24e+02	2.89e+01	50522.89	3.00e+02	7.55e+01
50514.85	2.68e+02	3.14e+01	50545.82	2.23e+02	5.92e+01
50517.89	2.40e+02	2.39e+01	50547.24	2.47e+02	1.46e+01
50518.87	3.44e+02	3.41e+01	50550.68	9.64e+01	9.37e+01
50521.94	3.04e+02	3.72e+01	50552.88	9.38e+01	4.81e+01
50522.87	2.44e+02	3.16e+01	50553.91	1.24e+02	6.99e+01
50545.78	1.15e+02	3.00e+01	50555.03	1.44e+02	8.20e+00
50547.23	9.17e+01	9.79e+00	50565.04	8.63e+01	7.29e+00
50550.60	1.82e+02	3.37e+01	50573.68	5.37e+01	8.93e+01
50552.85	9.47e+01	2.74e+01	50574.77	-1.06e+00	7.86e+01
50573.79	5.92e+01	2.10e+01	50592.07	1.97e+01	6.12e+00
50574.73	8.23e+01	2.61e+01	50608.72	5.51e+01	4.64e+01
50872.89	7.99e+01	6.89e+01	50609.74	2.80e+01	6.72e+01
50873.87	-6.33e+00	4.07e+01	51280.66	-5.39e+00	3.36e+01
50895.80	2.32e+01	4.03e+01			
50899.78	3.52e+01	3.75e+01			
50900.76	5.10e+01	4.53e+01			
50904.76	3.49e+00	2.04e+01			
		SN 1997am ($z = 0.416$)			
50490.79	6.96e+02	3.18e+01	50490.82	-2.63e+00	9.52e+01
50513.73	1.58e+03	5.58e+01	50513.77	9.38e+02	2.10e+02
50514.72	1.38e+03	8.93e+01	50514.76	8.43e+02	1.05e+02
50517.75	1.35e+03	6.88e+01	50518.76	7.27e+02	1.92e+02
50518.81	1.33e+03	6.75e+01	50520.60	3.78e+02	1.21e+02
50519.62	1.29e+03	6.06e+01	50521.87	2.14e+02	2.02e+02
50521.86	1.06e+03	5.74e+01	50545.71	-3.09e+02	1.30e+02
50545.73	2.80e+02	4.58e+01	50573.53	-5.20e+02	2.44e+02
50550.47	2.55e+02	2.75e+01	50574.60	-5.50e+02	1.04e+02
50573.51	1.18e+02	8.87e+01			
50574.64	1.21e+02	2.97e+01			
50872.55	6.22e+01	6.16e+01			
50895.63	7.64e+00	4.52e+01			
50900.70	-5.52e+01	4.06e+01			
50904.61	2.26e+00	2.08e+01			
		SN 1997aj ($z = 0.581$)			
50431.86	2.66e+02	1.82e+02	50458.98	4.40e+02	2.03e+02
50432.84	-9.50e+01	4.33e+01	50482.94	2.65e+02	1.54e+02
50454.81	1.11e+01	4.71e+01	50489.83	1.64e+02	1.71e+02
50458.02	-8.60e+01	3.72e+01	50513.76	7.88e+02	2.82e+02
50482.90	8.62e+00	3.36e+01	50514.76	8.80e+02	1.64e+02
50489.86	1.24e+02	3.09e+01	50518.75	1.15e+03	1.95e+02
50513.73	5.45e+02	3.52e+01	50521.82	1.06e+03	1.82e+02
50514.71	6.76e+02	6.13e+01	50573.48	7.17e+02	1.91e+02
50517.75	8.00e+02	4.66e+01	50845.94	0.00e+00	2.11e+02
50518.80	7.81e+02	5.85e+01			
50521.79	7.92e+02	9.33e+01			
50550.53	3.14e+02	3.22e+01			
50568.51	1.25e+02	2.88e+01			
50573.46	1.63e+02	6.28e+01			
50575.67	3.05e+01	3.73e+01			

TABLE D1 — *Continued*

MJD	*R* flux ($zp = 30$ mag)	σ(flux)	MJD	*I* flux ($zp = 30$ mag)	σ(flux)
50873.74	1.22e+02	4.31e+01			
50896.59	-1.18e+02	4.60e+01			
50899.69	-4.59e+01	5.76e+01			
50904.64	-1.66e+00	3.32e+01			
		SN 1997ai ($z = 0.45$)			
50490.77	-4.18e-01	2.49e+01	50490.75	-2.55e+00	8.56e+01
50513.69	1.18e+03	4.17e+01	50513.70	1.36e+03	2.27e+02
50514.69	1.15e+03	4.46e+01	50514.69	1.47e+03	1.25e+02
50517.71	1.09e+03	4.01e+01	50517.73	1.32e+03	2.14e+02
50518.70	1.02e+03	5.10e+01	50518.72	1.27e+03	1.52e+02
50519.55	9.83e+02	3.98e+01	50520.54	1.11e+03	1.68e+02
50521.78	9.05e+02	5.15e+01	50521.76	1.41e+03	1.76e+02
50537.79	3.49e+02	8.70e+01	50537.77	6.59e+02	1.47e+02
50545.66	1.08e+02	4.03e+01	50545.68	2.64e+02	1.22e+02
		SN 1997af ($z = 0.579$)			
50432.76	-2.30e+01	4.26e+01	50458.95	-4.49e+00	1.18e+02
50453.79	1.04e+02	9.62e+01	50480.76	2.62e+01	1.27e+02
50454.76	4.27e+01	3.67e+01	50489.68	1.05e+02	1.24e+02
50458.92	5.93e+00	4.22e+01	50513.63	3.62e+02	2.14e+02
50465.90	1.08e+02	6.26e+01	50514.61	2.24e+02	1.67e+02
50467.83	-1.55e+01	7.01e+01	50517.67	-2.69e+02	4.76e+02
50480.73	5.38e+01	2.87e+01	50518.62	3.91e+02	1.46e+02
50489.65	-1.88e+00	3.01e+01	50521.75	5.87e+02	2.68e+02
50490.69	3.50e+01	4.29e+01	50537.69	8.03e+02	2.13e+02
50508.54	-7.05e+01	1.08e+02	50545.54	6.45e+02	2.08e+02
50513.63	2.19e+02	3.58e+01	50573.52	2.54e+01	1.72e+02
50514.63	3.48e+02	3.14e+01	50816.77	1.81e+01	1.77e+02
50517.62	3.99e+02	4.10e+01	50817.87	1.97e+03	1.61e+03
50518.62	4.15e+02	3.82e+01	50835.78	-3.99e+01	1.75e+02
50521.72	6.66e+02	4.53e+01			
50537.69	5.54e+02	6.81e+01			
50545.52	3.14e+02	4.77e+01			
50550.40	2.77e+02	3.42e+01			
50573.56	4.18e+01	4.87e+01			
50780.79	2.74e+01	3.62e+01			
50781.81	6.45e+01	3.43e+01			
50810.80	3.33e+01	3.36e+01			
50811.83	2.75e+01	5.44e+01			
50817.80	2.43e+00	3.97e+01			
50835.76	4.22e+01	4.10e+01			
		SN 1997ac ($z = 0.32$)			
50432.76	-8.22e+00	4.47e+01	50480.76	5.56e+01	1.02e+02
50453.79	-3.16e+01	7.15e+01	50489.68	4.06e+02	1.07e+02
50454.76	-2.64e+01	3.49e+01	50513.63	3.01e+03	2.22e+02
50480.73	-5.03e+01	2.66e+01	50514.60	3.07e+03	1.59e+02
50489.65	3.49e+02	3.42e+01	50518.62	2.69e+03	1.34e+02
50490.69	4.94e+02	4.69e+01	50521.75	2.34e+03	2.38e+02
50508.54	2.60e+03	1.24e+02	50537.69	1.31e+03	2.06e+02
50513.63	2.58e+03	5.34e+01	50545.54	1.28e+03	1.54e+02
50514.62	2.49e+03	5.26e+01	50573.52	4.82e+02	1.46e+02
50517.63	2.23e+03	5.24e+01	50816.77	-1.16e+02	1.24e+02
50518.62	2.15e+03	5.22e+01	50835.79	1.67e+02	1.14e+02
50521.73	2.02e+03	4.76e+01			
50537.69	9.11e+02	6.63e+01			
50545.52	5.76e+02	4.62e+01			
50550.39	4.64e+02	3.68e+01			
50573.51	1.43e+02	4.05e+01			
50780.79	-5.25e+01	3.45e+01			
50781.82	-9.01e+00	3.28e+01			
50810.80	-1.86e+01	3.34e+01			
50817.82	-8.26e+01	3.75e+01			
50835.77	-8.00e+01	3.99e+01			
		SN 1996cn ($z = 0.43$)			
50137.80	5.14e+01	6.00e+01	50167.88	1.41e+03	1.36e+02
50138.81	2.23e+01	4.90e+01	50168.83	1.25e+03	1.14e+02
50160.82	8.67e+02	4.26e+01	50514.85	-9.61e+01	9.22e+01
50163.88	8.89e+02	5.67e+01	50518.89	1.03e+02	9.03e+01
50167.86	9.18e+02	3.56e+01	50573.77	-6.04e+01	2.10e+02
50168.83	9.93e+02	4.06e+01			
50192.57	2.69e+02	2.95e+01			
50223.80	1.16e+02	2.59e+01			
50490.87	5.24e+01	3.33e+01			
50513.84	-1.75e+00	3.18e+01			
50514.84	2.54e+00	3.37e+01			
50518.85	6.03e+01	3.86e+01			

TABLE D1 — *Continued*

MJD	R flux ($zp = 30$ mag)	σ(flux)	MJD	I flux ($zp = 30$ mag)	σ(flux)
50573.76	8.07e+01	8.20e+01			
		SN 1996cm ($z = 0.45$)			
50137.84	9.47e+01	5.02e+01	50168.89	9.90e+02	1.79e+02
50138.85	1.67e+02	5.17e+01	50187.96	4.43e+02	7.53e+01
50160.85	8.64e+02	4.07e+01	50513.89	9.00e-01	5.63e+01
50163.89	7.70e+02	7.35e+01	50573.70	6.91e+01	6.75e+01
50167.91	6.31e+02	5.48e+01			
50168.88	6.47e+02	4.91e+01			
50169.88	5.50e+02	5.87e+01			
50184.96	2.99e+02	8.04e+01			
50192.69	1.82e+02	3.72e+01			
50211.84	8.68e+01	3.29e+01			
50513.86	1.22e+01	2.49e+01			
50514.89	3.09e+01	2.52e+01			
50573.78	5.91e+01	6.75e+01			
		SN 1996cl ($z = 0.828$)			
50138.66	1.63e+01	5.73e+01	49365.00	-4.15e+01	6.84e+01
50159.65	3.08e+02	4.35e+01	50160.80	4.85e+02	1.66e+02
50160.68	3.62e+02	4.49e+01	50168.64	4.65e+02	6.98e+01
50162.73	2.18e+02	5.30e+01	50169.66	2.37e+02	1.54e+02
50164.72	2.51e+01	7.58e+01	50432.84	9.52e+01	8.77e+01
50168.62	2.99e+02	4.05e+01	50453.85	-7.98e+00	1.86e+02
50169.66	2.30e+02	5.64e+01	50454.78	1.57e+01	1.21e+02
50192.42	1.50e+02	6.43e+01	50458.85	-1.60e+02	1.70e+02
50223.67	-4.05e+01	3.40e+01	50459.85	-2.31e+01	7.51e+01
50426.99	-6.15e+01	4.42e+01	50490.82	7.22e+01	6.85e+01
50431.83	-2.63e+01	5.46e+01	50513.77	-1.18e+02	1.39e+02
50432.83	-4.06e+01	5.32e+01	50514.76	-7.52e+01	8.02e+01
50453.84	-6.29e+01	4.91e+01	50518.76	4.51e+01	1.15e+02
50454.80	6.02e+00	3.49e+01	50573.61	-2.19e+02	2.02e+02
50459.83	1.51e+01	2.49e+01			
50490.79	4.16e+01	2.99e+01			
50513.73	5.04e+01	3.29e+01			
50514.72	5.60e+01	6.24e+01			
50517.75	5.99e+01	4.42e+01			
50518.81	-4.54e+00	5.00e+01			
50573.61	3.67e+00	8.05e+01			
		SN 1996ck ($z = 0.656$)			
50138.75	4.58e+01	4.53e+01	50160.74	5.35e+02	1.56e+02
50159.75	6.13e+02	4.21e+01	50168.74	7.59e+02	1.25e+02
50160.74	5.76e+02	4.54e+01			
50162.88	4.91e+02	5.27e+01			
50163.92	4.54e+02	7.17e+01			
50168.73	4.70e+02	3.54e+01			
50169.76	4.89e+02	8.47e+01			
50192.45	6.07e+01	5.50e+01			
50210.77	2.03e+01	4.94e+01			
50513.81	4.02e+01	2.96e+01			
50573.72	4.35e+00	6.65e+01			
		SN 1996ci ($z = 0.495$)			
50137.78	6.72e+01	6.88e+01	50160.80	1.41e+03	9.73e+01
50138.80	4.70e+00	5.15e+01	50168.77	1.47e+03	1.04e+02
50159.80	1.30e+03	4.83e+01	50187.91	5.09e+02	1.13e+02
50160.79	1.34e+03	5.45e+01	50514.86	-6.70e+01	1.01e+02
50162.90	1.24e+03	5.25e+01	50518.85	1.32e+01	8.85e+01
50168.77	1.16e+03	4.93e+01	50573.73	1.34e+02	1.86e+02
50184.84	5.37e+02	4.64e+01			
50199.90	1.36e+02	3.08e+01			
50212.72	1.17e+01	4.08e+01			
50223.76	1.72e+01	2.79e+01			
50257.44	-1.18e+01	3.08e+01			
50490.87	1.38e+01	3.45e+01			
50513.83	-1.20e+00	3.33e+01			
50514.85	-3.29e+01	3.60e+01			
50517.89	-4.91e+01	2.81e+01			
50518.86	-5.81e+00	4.17e+01			
50519.69	-9.32e+00	3.80e+01			
50573.73	5.69e+00	6.70e+01			
		SN 1996cg ($z = 0.49$)			
50020.86	6.50e+00	5.79e+01	50160.56	1.41e+03	1.19e+02
50137.56	1.51e+02	6.81e+01	50168.54	1.40e+03	1.01e+02
50138.54	1.05e+02	7.13e+01	50426.92	1.64e+02	1.00e+02
50159.54	1.09e+03	6.06e+01	50457.85	-1.96e+01	8.60e+01
50160.54	1.05e+03	3.85e+01	50490.70	4.48e+01	1.93e+02
50162.69	9.58e+02	4.33e+01	50513.64	1.06e+01	1.89e+02

TABLE D1 — *Continued*

MJD	R flux ($zp = 30$ mag)	σ(flux)	MJD	I flux ($zp = 30$ mag)	σ(flux)
50168.54	9.15e+02	4.37e+01	50514.62	1.52e+00	1.23e+02
50187.65	2.94e+02	2.87e+01	50573.42	4.82e+02	2.20e+02
50211.66	4.26e+01	4.04e+01			
50429.00	6.15e+01	3.75e+01			
50431.81	-8.37e+00	7.16e+01			
50432.78	2.05e+01	3.28e+01			
50453.79	-6.84e-01	5.56e+01			
50454.71	1.01e+01	3.68e+01			
50457.81	-3.60e+00	2.75e+01			
50490.72	-6.26e+01	4.55e+01			
50513.63	5.28e+01	4.99e+01			
50514.63	7.90e+00	3.98e+01			
50517.62	5.32e+01	5.52e+01			
50573.42	-5.27e+01	6.36e+01			
50574.54	4.38e+01	1.39e+02			
50780.81	-2.58e+01	2.95e+01			
50781.78	-4.93e+01	2.86e+01			
50811.76	2.84e+01	2.04e+01			
		SN 1996cf ($z = 0.57$)			
50138.65	-3.96e+01	5.15e+01	50160.66	1.03e+03	8.63e+01
50159.64	8.05e+02	4.10e+01	50168.62	8.92e+02	8.38e+01
50160.67	7.28e+02	5.50e+01	50490.75	4.42e+01	6.71e+01
50162.71	8.28e+02	5.49e+01	50513.70	5.89e+01	1.53e+02
50164.70	8.31e+02	4.97e+01	50514.68	-1.87e+01	7.73e+01
50168.60	7.88e+02	3.47e+01	50517.73	3.63e+01	1.61e+02
50187.69	3.41e+02	2.60e+01	50518.72	5.81e+01	1.21e+02
50199.70	1.33e+02	5.03e+01			
50223.71	-2.79e+01	3.12e+01			
50432.01	-1.82e+01	7.00e+01			
50490.77	1.49e+01	2.30e+01			
50513.68	-2.04e+01	2.75e+01			
50514.70	1.19e+01	3.11e+01			
50517.71	3.78e+01	2.83e+01			
50518.70	-1.09e-01	4.25e+01			
50573.60	7.86e+00	6.53e+01			
		SN 1995ba ($z = 0.388$)			
50020.85	5.41e+02	6.69e+01	50043.85	1.34e+03	2.34e+02
50041.84	1.36e+03	5.64e+01	50045.91	1.35e+03	1.56e+02
50043.84	1.25e+03	6.51e+01	50049.03	1.28e+03	1.57e+02
50045.90	1.17e+03	4.88e+01	50052.84	7.46e+02	1.61e+02
50048.92	1.00e+03	4.17e+01	50075.64	5.40e+02	1.07e+02
50052.83	8.16e+02	4.66e+01	50169.53	-2.09e+02	1.55e+02
50069.88	2.28e+02	3.53e+01	50394.99	-1.90e+02	2.03e+02
50070.69	3.15e+02	7.06e+01	50395.98	2.14e+00	9.09e+01
50074.58	2.12e+02	2.41e+01			
50081.99	2.42e+02	4.72e+01			
50137.55	-4.97e+01	6.18e+01			
50138.54	-8.71e+01	6.78e+01			
50159.53	-9.24e+00	5.55e+01			
50169.52	-9.79e+01	6.86e+01			
50394.99	9.59e+01	6.75e+01			
50407.00	-7.43e-02	2.06e+01			
50431.79	-1.70e+01	4.75e+01			
50453.75	7.76e+01	4.51e+01			
50454.69	-4.26e+01	6.75e+01			
		SN 1995az ($z = 0.45$)			
50019.84	4.20e+01	7.47e+01	50047.81	8.16e+02	1.61e+02
50041.80	3.82e+02	8.02e+01	50052.80	1.01e+03	1.24e+02
50045.88	7.10e+02	7.71e+01	50071.80	8.82e+02	2.04e+02
50047.80	7.46e+02	6.25e+01	50394.92	-2.52e+02	2.80e+02
50048.84	8.08e+02	6.13e+01	50396.87	8.70e+00	1.01e+02
50052.79	1.05e+03	6.68e+01			
50069.86	7.05e+02	8.17e+01			
50081.81	3.46e+02	5.31e+01			
50091.81	2.17e+02	6.82e+01			
50092.75	1.95e+02	6.23e+01			
50394.93	-1.64e+02	1.31e+02			
50395.94	3.79e-01	4.35e+01			
		SN 1995ay ($z = 0.48$)			
49601.87	-1.90e+01	1.83e+01	50052.78	1.19e+03	1.51e+02
49634.73	6.33e+01	8.56e+01	50067.74	6.20e+02	1.69e+02
49657.69	-2.68e+01	5.92e+01	50075.56	3.86e+02	7.57e+01
50020.73	-5.03e+01	7.16e+01	50394.92	-8.84e+01	3.24e+02
50041.72	6.99e+02	5.05e+01	50407.72	-6.58e+00	8.77e+01
50043.66	8.17e+02	4.63e+01			

TABLE D1 — *Continued*

MJD	R flux ($zp = 30$ mag)	σ(flux)	MJD	I flux ($zp = 30$ mag)	σ(flux)
50045.86	8.50e+02	3.67e+01			
50052.75	7.81e+02	5.39e+01			
50071.75	2.76e+02	8.05e+01			
50074.52	2.06e+02	2.74e+01			
50093.45	1.46e+00	4.08e+01			
50394.91	-1.24e+02	9.13e+01			
50406.85	9.02e-02	2.31e+01			
		SN 1995ax ($z = 0.615$)			
50020.64	3.06e+01	6.47e+01	50052.76	4.72e+02	2.83e+02
50040.72	8.22e+02	7.73e+01	50067.72	9.66e+02	1.42e+02
50045.84	1.02e+03	8.35e+01	50075.53	1.04e+03	1.80e+02
50049.70	9.21e+02	8.76e+01	50394.90	1.34e+01	3.61e+02
50052.70	8.07e+02	7.73e+01	50396.83	6.23e+00	1.55e+02
50067.69	5.35e+02	6.20e+01			
50074.48	3.23e+02	4.49e+01			
50092.70	-4.58e+01	7.46e+01			
50429.79	-7.70e-01	4.83e+01			
		SN 1995aw ($z = 0.4$)			
50020.63	2.67e+01	5.81e+01	50047.71	1.88e+03	1.71e+02
50040.70	8.81e+02	5.14e+01	50052.74	2.16e+03	2.60e+02
50041.70	9.81e+02	6.12e+01	50075.50	1.26e+03	9.70e+01
50043.69	1.35e+03	7.55e+01	50394.89	-4.13e+02	3.11e+02
50045.79	1.49e+03	5.23e+01	50395.88	7.35e+01	1.56e+02
50047.69	1.60e+03	4.11e+01			
50049.68	1.62e+03	7.65e+01			
50052.67	1.95e+03	8.17e+01			
50067.65	1.61e+03	5.41e+01			
50071.77	1.21e+03	9.25e+01			
50075.46	1.40e+03	4.15e+01			
50394.89	-3.58e+00	8.03e+01			
50395.82	8.03e-01	3.10e+01			
		SN 1995at ($z = 0.655$)			
50041.57	8.01e+02	4.94e+01	50045.77	1.26e+03	1.10e+02
50043.67	9.14e+02	5.92e+01	50432.56	1.80e+02	1.10e+02
50044.32	7.84e+02	7.76e+01	50713.82	3.13e+00	8.49e+01
50045.74	9.22e+02	4.33e+01			
50047.63	8.68e+02	3.01e+01			
50049.67	9.76e+02	1.16e+02			
50053.39	7.58e+02	1.16e+02			
50071.73	3.75e+02	1.34e+02			
50074.44	4.23e+02	5.06e+01			
50075.43	3.16e+02	2.57e+01			
50092.67	5.47e+01	3.70e+01			
50093.36	1.90e+02	4.39e+01			
50429.67	4.53e-01	1.83e+01			
50713.80	9.70e+00	5.05e+01			
		SN 1995as ($z = 0.498$)			
50020.55	7.85e+01	6.07e+01	50045.73	7.04e+02	1.12e+02
50040.63	5.72e+02	6.60e+01	50394.84	5.80e+01	2.53e+02
50041.60	6.53e+02	6.19e+01	50417.69	-4.99e+00	8.62e+01
50045.70	6.09e+02	4.45e+01			
50048.73	5.21e+02	9.75e+01			
50067.67	2.19e+02	4.32e+01			
50075.34	1.41e+02	4.04e+01			
50092.64	2.51e+01	5.29e+01			
50093.41	6.73e+01	9.70e+01			
50394.83	-1.04e+02	9.24e+01			
50417.63	1.16e+01	3.22e+01			
		SN 1995ar ($z = 0.465$)			
50020.55	4.72e+01	6.50e+01	50045.68	1.21e+03	1.78e+02
50040.61	7.07e+02	6.25e+01	50394.82	2.25e+00	2.41e+02
50041.58	7.57e+02	5.84e+01			
50043.66	1.10e+03	8.11e+01			
50045.66	7.43e+02	4.19e+01			
50067.63	4.49e+02	4.22e+01			
50074.44	1.80e+02	2.52e+01			
50092.61	7.82e+01	3.17e+01			
50394.83	3.56e+01	6.75e+01			
50397.74	-6.02e-02	1.81e+01			
		SN 1995aq ($z = 0.453$)			
50019.62	7.69e+01	1.24e+02	50045.63	8.64e+02	9.11e+01
50040.56	9.63e+02	6.17e+01	50755.72	4.09e+01	9.04e+01
50041.60	8.88e+02	5.07e+01			
50043.34	8.68e+02	7.38e+01			
50045.61	7.48e+02	4.87e+01			

TABLE D1 — *Continued*

MJD	R flux ($zp = 30$ mag)	σ(flux)	MJD	I flux ($zp = 30$ mag)	σ(flux)
50048.69	7.52e+02	9.37e+01			
50053.35	6.62e+02	2.66e+02			
50071.69	1.54e+02	5.83e+01			
50074.36	1.39e+02	2.35e+01			
50082.60	7.46e+01	9.63e+01			
50362.40	3.41e+01	3.62e+01			
50394.80	4.22e+01	7.51e+01			
50395.67	7.27e+01	5.23e+01			
		SN 1994h ($z = 0.374$)			
49343.37	1.09e+02	1.16e+02			
49361.36	2.19e+03	1.21e+02			
49363.32	2.79e+03	1.03e+02			
49365.41	2.87e+03	5.54e+01			
49369.66	2.91e+03	6.49e+01			
49387.63	1.70e+03	5.84e+01			
49396.62	8.24e+02	5.49e+01			
49568.65	2.68e+02	6.86e+01			
49623.96	2.33e+01	5.99e+01			
49634.70	8.81e+01	5.86e+01			
49636.81	1.02e+02	3.07e+01			
49657.67	1.21e+02	6.64e+01			
49693.03	2.02e+02	9.66e+01			
50041.71	4.35e+01	5.45e+01			
		SN 1994g ($z = 0.425$)			
49420.94	1.14e+03	5.31e+01	49396.80	1.87e+03	2.39e+02
49421.91	1.08e+03	5.12e+01	49403.81	2.45e+03	2.28e+02
49425.51	7.69e+02	9.34e+01	49420.99	1.83e+03	1.43e+02
49429.69	7.42e+02	1.57e+02	49425.48	9.73e+02	3.14e+02
49432.87	4.46e+02	1.95e+02	49429.71	1.24e+03	3.95e+02
49452.80	1.48e+02	5.04e+01	49431.36	1.40e+03	2.55e+02
49505.44	2.14e+00	4.26e+01	49432.88	1.09e+03	4.02e+02
		SN 1994f ($z = 0.354$)			
48735.45	6.63e+01	1.44e+02			
49361.78	1.11e+03	2.99e+02			
49365.67	1.43e+03	1.10e+02			
49386.80	4.92e+02	4.75e+01			
49396.95	1.86e+02	6.11e+01			
49399.79	2.28e+02	5.39e+01			
49809.55	4.45e+01	6.76e+01			
50138.68	3.31e+01	1.03e+02			
		SN 1994an ($z = 0.378$)			
49657.42	1.31e+03	9.27e+01			
49662.60	1.22e+03	1.11e+02			
49683.01	6.27e+02	3.24e+02			
49685.41	4.31e+02	5.45e+01			
49688.96	1.43e+02	2.28e+02			
49691.55	2.13e+01	1.10e+02			
49692.96	1.09e+01	1.40e+02			
49872.69	7.25e+01	1.18e+02			
		SN 1994am ($z = 0.372$)			
49361.36	1.91e+02	1.11e+02			
49363.32	2.63e+02	9.19e+01			
49365.33	2.51e+02	7.35e+01			
49369.66	5.97e+02	6.53e+01			
49387.63	1.90e+03	5.38e+01			
49396.62	1.24e+03	5.74e+01			
49399.63	1.09e+03	7.65e+01			
49568.65	1.39e+02	5.93e+01			
49607.97	1.31e+02	4.77e+01			
49623.96	7.46e+01	6.77e+01			
49625.82	1.02e+02	1.22e+02			
49634.70	8.22e+01	5.66e+01			
49636.90	9.05e+01	3.32e+01			
49657.67	1.14e+02	6.65e+01			
		SN 1994al ($z = 0.42$)			
49341.41	1.55e+02	8.19e+01			
49361.38	9.33e+02	9.44e+01			
49363.35	1.18e+03	7.83e+01			
49365.36	1.21e+03	7.53e+01			
49369.67	1.15e+03	6.32e+01			
49371.65	1.08e+03	1.02e+02			
49386.72	5.17e+02	3.32e+01			
49395.68	1.75e+01	1.59e+02			
49396.68	2.76e+02	3.29e+01			
49607.97	1.00e+02	5.18e+01			

TABLE D1 — *Continued*

MJD	R flux ($zp = 30$ mag)	σ(flux)	MJD	I flux ($zp = 30$ mag)	σ(flux)
49624.86	5.77e+01	5.85e+01			
49625.81	7.09e+01	7.81e+01			
49636.97	7.63e+00	4.01e+01			
49637.70	4.35e+01	5.33e+01			
49657.71	5.83e+01	6.40e+01			
50020.71	2.73e+01	6.59e+01			
50041.72	5.60e+01	7.12e+01			
		SN 1992bi ($z = 0.458$)			
48707.76	5.25e+01	3.61e+02			
48709.75	1.62e+02	2.70e+02			
48737.62	1.32e+03	1.33e+02			
48740.67	1.14e+03	4.33e+02			
48741.64	1.37e+03	1.44e+02			
48745.67	1.38e+03	1.94e+02			
48749.71	1.11e+03	1.22e+02			
48751.71	1.09e+03	2.07e+02			
48753.71	1.08e+03	2.45e+02			
48783.84	2.70e+02	1.55e+02			